

# Guides and bumpers

Energy transfer between guides and bumpers due to impulse loads

S. L. Tielens

Master of Science Thesis





# GUIDES AND BUMPERS

## ENERGY TRANSFER BETWEEN GUIDES AND BUMPERS DUE TO IMPULSE LOADS

in partial fulfillment of the requirements for the degree of the degree of

**Master of Science**

in Offshore and Dredging Engineering

**S. L. Tielens**

At the Delft University of Technology,

to be defended on Thursday March 22, 2018 at 14:30 AM.

Student number: 4038282  
Project duration: May 15, 2018 – March 22, 2018  
Chairman: Prof. dr. A. V. Metrikine  
Thesis committee: Ir. J. S. Hoving, TU Delft  
Ir. S. Sánchez Gómez, TU Delft  
Ir. P. Meeuws, Heerema Marine Contractors  
Ir. J. Zwartveld, Heerema Marine Contractors

*This thesis is confidential and cannot be made public until December 31, 2023.*

An electronic version of this thesis is available at <http://repository.tudelft.nl/>.



# PREFACE

This report contains the thesis study "Energy transfer between guides and bumpers". This thesis is the result of 10 months of research that was conducted to fulfill the requirements for the degree of Master of Science in Offshore Engineering at Delft University of Technology. The work has been performed at and in cooperation with Heerema Marine Contractors (HMC) in Leiden and Delft University of Technology. The research has been performed at the Innovation department of HMC in collaboration with the structural and marine department at HMC with Pim Meeuws and Jim Zwartveld as main supervisors. At the TU Delft Sergio Sánchez Gómez, Jeroen Hoving and Dominik Fallais have supervised me during the process.

I want to express my gratitude to the people that have supported me during the past ten months. First of all I would like to thank my daily supervisors, Pim and Jim for sharing their expertises and insights and especially their patience. They have really guided me through this process, helping me every step on the way. I also want to thank Radboud van Dijk for keeping me on track and making time whenever I needed guidance. I want to thank HMC for giving me this opportunity and making me feel part of the company. I have enjoyed my time here and it was a great learning environment.

In addition I would like to thank Jeroen for helping me decide on the subject and always making time when needed, Sergio for the numerous meetings and the explanation of the energy balance, Dominik for his hard work on the FE model that had to be finished in such short notice and off course Kees van Beek, Fred Schilperoort and John for guiding and helping me with all the details during my experiment. I would also like to express my gratitude to prof. Metrikine for his supervision.

Finally I want to thank my fellow graduate students at HMC for their support and for keeping my spirit high.

*S. L. Tielens  
Delft, March 2018*



# ABSTRACT

During reverse installation for executing platform decommissioning and removal projects, heavy modules such as the topside of an offshore platform are cut off their substructures and lifted back on the deck of crane vessels or onto cargo barges. To assure that the modules are placed on the intended location and to prevent the modules from moving during transportation, a guide and bumper system is used.

During set-down, it is possible that the module bumps into one of the guides. The relative motions between the vessel and the barge can cause significant impulse loads when the module and guide make contact. To prevent the module from being damaged, bumpers are welded onto the module to protect the module during the contact phase. Both the guide and bumpers are designed to only deform elastically and to cope with the expected impulse loads. The designs are based on internal standard criteria that state that the guide and bumper system will be designed for a maximum horizontal load that is 10% of the designed weight of the lifted module. During the design state, this load is statically applied on the weakest spot of the guide and bumper system. In reality, the loads are not applied statically but dynamically and it is still unknown how to correctly estimate the magnitude of the impact. The estimated loads might differ from the actual loads due to unaccounted forms of energy transfer that occur during the impact, such as the rotation of the module, motions of the bumper and guides or deformations in the guides and bumpers.

To analyze the energy transfer during impact and to say something about the magnitude of the impact an experiment was conducted with a model. The model consists of two standard steel guides clamped to steel plates and a squared module with a bumper that with the motions of a pendulum. The module is pulled back to a magnet, from where it is let go to hit both the guides once, after which the module is pulled back again. The impact location on the guides and bumpers is enclosed with sensors that measure the potential energy in the form of strain and the kinetic energy in the form of accelerations. The sensors are situated so that they enclose the energy flow in every possible direction. For each of the enclosed segments, an energy balance was set-up. The guides were tested as a guide with an inclined brace and as a simple cantilever beam. A number of case studies were tested to analyze the energy transfer as a result of impulse loads and to estimate the magnitude of the loads; impact location on the guides, bumper height of the module (at the CoG of the module, above and below), weight of the module, deviation of the module and different damping materials around the guides. The energy balance comprises of the external energy that enters the segment, which should be equal to the energy flux, the energy that exits or enters the segment through the cross-section of its boundaries, the energy rate of the segment and the energy that is dissipated. Both the externally applied load which was needed to calculate the external energy that enters the system, as well as the rotational velocity that was needed to determine the energy flux, are computed with an analytical model.

This model compares the response of a unit load of 1 to the responses of the experiment. The difference between the two is computed as the applied load on the system. The computed energy balance shows the energy flow through the structure as a result of the impulse load. From the results, it is possible to conclude that the impulse loads in this experiment can be assumed to be linear elastic. Based on these experiments a more accurate description of impulse loads can be used as an input for models, for both duration and shape. The second one is that based on these experiments, at least 97% of the energy is transferred back into motions of the module, the effect of energy transfer in a linear elastic response has little to no effect on the magnitude of the loads.



# CONTENTS

<b>Abstract</b>	<b>v</b>
<b>List of Figures</b>	<b>xi</b>
<b>List of Tables</b>	<b>xv</b>
<b>Abbreviations</b>	<b>xvii</b>
0.1 List of Abbreviations . . . . .	xvii
0.2 List of Symbols . . . . .	xvii
<b>1 Introduction</b>	<b>1</b>
1.1 Introduction . . . . .	1
1.2 Problem Definition . . . . .	2
1.3 Current situation . . . . .	3
1.3.1 Bentley SACS. . . . .	3
1.4 Scope and objective. . . . .	3
1.5 Thesis structure. . . . .	3
<b>2 Literature study</b>	<b>5</b>
2.1 Guide and bumpers . . . . .	5
2.1.1 Dimensions guide system . . . . .	5
2.1.2 Topside movements . . . . .	6
2.1.3 Impact Loads . . . . .	6
2.1.4 Conclusion. . . . .	7
2.2 Possible causes for energy transfer during set-down . . . . .	7
2.3 Theory Impact Loads . . . . .	8
2.3.1 Dynamic response . . . . .	8
2.4 Potential energy . . . . .	8
2.5 Kinetic energy . . . . .	8
2.6 Coefficient of Restitution . . . . .	9
<b>3 Experimental set-up</b>	<b>11</b>
3.1 Test Design . . . . .	11
3.2 Material. . . . .	11
3.3 Scaling . . . . .	11
3.4 Module and Bumper . . . . .	12
3.5 Guides . . . . .	12
<b>4 Numerical model: SACS</b>	<b>15</b>
4.1 Introduction SACS . . . . .	15
4.2 Model SACS. . . . .	15
4.2.1 Module . . . . .	15
4.2.2 Guide With Brace . . . . .	15
4.2.3 Guide Without Brace. . . . .	16
4.3 Natural frequencies and mode shapes . . . . .	16
4.4 Impact analysis . . . . .	17
4.5 Acceleration. . . . .	18
4.6 Displacement . . . . .	19
4.7 Strain . . . . .	19
4.8 Conclusion . . . . .	19

<b>5</b>	<b>Experimental tests</b>	<b>21</b>
5.1	Case studies . . . . .	21
5.2	Sensors . . . . .	22
5.2.1	location Sensors . . . . .	23
5.2.2	Module and bumper . . . . .	23
5.3	Instrumental set-up . . . . .	25
5.4	Measurements . . . . .	25
5.4.1	Strain . . . . .	26
5.4.2	Accelerations . . . . .	27
5.5	Conclusion . . . . .	28
<b>6</b>	<b>Results</b>	<b>29</b>
6.1	Natural Frequencies . . . . .	29
6.2	Linear elastic deformation . . . . .	31
6.3	Magnitude of Impulse Loads . . . . .	32
6.4	Calculations . . . . .	36
6.4.1	Curvature . . . . .	36
6.4.2	Rotational velocity . . . . .	38
6.4.3	Velocity . . . . .	38
6.5	Energy Balance . . . . .	39
6.5.1	External energy . . . . .	39
6.5.2	Energy rate . . . . .	40
6.5.3	Energy flux . . . . .	40
6.5.4	Energy dissipated . . . . .	41
6.5.5	Energy Balance . . . . .	42
6.5.6	Results . . . . .	42
6.6	Coefficient of Restitution . . . . .	43
6.6.1	Results CoR and Load, variation in impact location . . . . .	44
6.6.2	Conclusion CoR . . . . .	45
<b>7</b>	<b>Conclusions and Recommendations</b>	<b>47</b>
7.1	Conclusions . . . . .	47
7.2	Recommendations . . . . .	48
<b>8</b>	<b>Discussion</b>	<b>49</b>
<b>A</b>	<b>Experimental set-up</b>	<b>51</b>
A.1	Material . . . . .	51
A.2	Load curve . . . . .	51
A.3	Unity Check . . . . .	51
<b>B</b>	<b>Experimental tests</b>	<b>55</b>
B.1	Measurements . . . . .	55
B.2	Case studies . . . . .	57
<b>C</b>	<b>Analytical Model</b>	<b>59</b>
C.1	Modal Analysis Guide in Python . . . . .	59
C.1.1	General . . . . .	59
C.1.2	Model description . . . . .	60
C.1.3	Model properties . . . . .	60
C.1.4	General expressions . . . . .	61
C.1.5	Boundary conditions . . . . .	62
<b>D</b>	<b>Results</b>	<b>65</b>
D.1	Frequencies . . . . .	65
D.2	Load results . . . . .	66
D.3	Energy balance results . . . . .	67
D.4	CoR . . . . .	68
D.4.1	Results CoR and Load, variation in impact location . . . . .	68
D.4.2	Results CoR and Load, variation in bumper height module . . . . .	68
D.4.3	Results CoR and Load, variation in deviation module . . . . .	69
D.4.4	Results CoR and Load, variation in added weight and CoG of module . . . . .	69

---

D.4.5 Results CoR and Load, variation in added material on the guides . . . . .	70
<b>Bibliography</b>	<b>71</b>



# LIST OF FIGURES

1.1	Example of reverse installation module on barge with guides . . . . .	1
1.2	Example of damaged bumper . . . . .	2
2.1	A schematic view of the vertical guide and horizontal bumper system . . . . .	5
2.2	Topsides Movement criteria for Guide and Bumper Design (SC-251) . . . . .	6
2.3	Compression of a Rod . . . . .	8
2.4	Deflection curve beam . . . . .	9
3.1	Clamping system of bumper on module . . . . .	12
3.2	Attachment module to roof . . . . .	12
3.3	Picture of one of the guides . . . . .	13
3.4	The Test setup of the scaled experiment . . . . .	13
4.1	Module in SACS . . . . .	16
4.2	Guide with brace in SACS . . . . .	16
4.3	Guide without brace in SACS . . . . .	16
4.4	Natural frequencies and modal shapes of beams with constant $EI\rho A$ [1] . . . . .	16
4.5	Impact locations on guide . . . . .	18
4.6	Acceleration at top guide without brace . . . . .	18
4.7	Displacement at top guide without brace . . . . .	19
5.1	Case study 1: Impact Location Top/Brace/Low . . . . .	21
5.2	Case study 2: Bumper height on module Top/Middle/Low . . . . .	21
5.3	Case study 3: Displacement module 9.3/12/15.5 cm . . . . .	22
5.4	Case study 4: Weight and moment of inertia 4/8 kg . . . . .	22
5.5	Case study 5: Damping of guide . . . . .	22
5.6	Cross-section guide/bumper with locations of strain gauges and accelerometer. Yellow dots are strain gauges, green line is accelerometer and red arrow shows the location of the impact . . . . .	23
5.7	Sensor locations at Module and Bumper . . . . .	23
5.8	Sensors around impact location Top . . . . .	24
5.9	Sensors around impact location Brace Height . . . . .	24
5.10	Sensors around impact location Low . . . . .	25
5.11	Schematic view of measuring equipment . . . . .	25
5.12	Measurements strain at the top of guide 2 with brace . . . . .	26
5.13	Measurements strain at the top of guide 2 without brace . . . . .	26
5.14	Measurements strain at guide 2, above brace, below brace and on brace . . . . .	27
5.15	Measurements strain at the brace of guide 2 . . . . .	27
5.16	Measurements strain at guide 2, below brace and near bottom of guide . . . . .	27
5.17	Measurements acceleration at the top of guide 2 with brace . . . . .	28
5.18	Measurements acceleration at the top of guide 2 without brace . . . . .	28
5.19	Measurements acceleration at guide 2, above brace, below brace and on brace . . . . .	28
5.20	Measurements acceleration at guide 2, below brace and near bottom of guide . . . . .	28
6.1	Frequency spectrum measured strain, impact at the top of guide . . . . .	29
6.2	Frequency spectrum measured acceleration, impact at the top of guide . . . . .	29
6.3	Frequency spectrum measured strain, impact at the top of guide, logarithmic scale . . . . .	30
6.4	Frequency spectrum measured acceleration, impact at the top of guide, logarithmic scale . . . . .	30
6.5	Example of non-linear elastic response of bumper due to impact . . . . .	31
6.6	Example of linear elastic response of guide due to impact . . . . .	31
6.7	Fitting of strain measurements . . . . .	32
6.8	Mirrored frequency spectrum of accelerations . . . . .	34

6.9	Mirrored frequency spectrum of response to a unit load 1	34
6.10	Frequency spectrum calculated load based on accelerations	34
6.11	Example of computed loads by using accelerations, guide 1	35
6.12	Example of computed loads curve zoomed in at impact Guide 1	35
6.13	Frequency spectrum calculated load based on accelerations filtered	35
6.14	Example of computed loads based on filtered accelerations	35
6.15	Example of computed loads based on filtered accelerations zoomed in at impact	35
6.16	Example of computed loads, guide 1, zoomed in at impact	36
6.17	Example of computed loads, guide 1, zoomed in at impact	36
6.18	Example of computed loads curve only during impact Guide 1	36
6.19	Schematic drawing curvature	37
6.20	Curvature z, y vs x-direction	37
6.21	Rotational velocity at the location of impact (V5)	38
6.22	Filtered acceleration vs non-filtered acceleration V5	38
6.23	Integrated Accelerations V5	38
6.24	Schematic drawing of Energy balance	39
6.25	External energy rate entering guide 1 at the top of the guide	40
6.26	Energy rate in the top segment of guide 1	40
6.27	Example of beam segment, only bending is assumed	41
6.28	Example of Rod segment, both bending and axial compression is assumed	41
6.29	Energy flux through the cross-section at the location of the sensors of guide 1	41
6.30	Dissipated energy guide 1	42
6.31	Impact location at the Top	42
6.32	Impact location below at brace height	42
6.33	Impact location below the brace	42
6.34	A combination of the internal energy rate, energy flux and external energy of guide 1, module deviation 12 cm	43
6.35	A combination of the energy dissipated, energy flux, internal energy rate and external energy of guide 1, module deviation 12 cm	43
6.36	CoR of the variation in impact location of guide with brace vs. guide without brace	45
6.37	Load of the variation in impact location of guide with brace vs. guide without brace	45
A.1	Clamping system of cable to adjust length of cable between test variations	51
A.2	Turnbuckle used to adjust cable length	51
A.3	Load and clearance curve Thialf	52
A.4	Unity check for the guides and bumper	53
B.1	Measurements of the three strains at the top of the guide without brace	55
B.2	Measurements of the three strains at the top of the guide with brace	55
B.3	Strain in the lowest sensors at the guide with impact at the lowest impact location, guide with brace	56
B.4	Strain in the lowest sensors at the guide with impact at the lowest impact location, guide without brace	56
B.5	Comparison maximum strain above and below impact at lowest impact location, G1R4 is below, G1R9 is above	56
B.6	Comparison maximum strain above, below and at brace for impact at brace height. G1R3 is at brace height, G1R9 is below and G1R12 is above.	57
B.7	All cases studies for guide with and guide without brace	58
D.1	Frequencies of the accelerations at V5	65
D.2	Frequencies of the response function for accelerations	65
D.3	Frequency spectrum of measured strain	65
D.4	Frequency spectrum of Response function for strains based on unit load 1	65
D.5	Load in frequency spectrum based on curvature	66
D.6	Example of computed loads based on curvature non filtered	66
D.7	Example of computed loads non filtered, zoomed in on impact	66
D.8	Computed load case B1U2G1W1 at accelerometer V5, impact location top of guide 1	66
D.9	Computed load case B1U3G1W1 at accelerometer V5, impact location top of guide 1	66
D.10	Computed load case B1U2G1W1 at accelerometer V6, impact location top of guide 1	67

---

D.11 Computed load case B1U3G1W1 at accelerometer V6, impact location top of guide 1 . . . . .	67
D.12 Computed load case B1U2G1W1 at accelerometer V7, impact location top of guide 1 . . . . .	67
D.13 Computed load case B1U2G1W1 at accelerometer V8, impact location top of guide 1 . . . . .	67
D.14A combination of the energy dissipated, energy flux and external energy of guide 1, module deviation 15.5 <i>cm</i> . . . . .	67
D.15A combination of the energy dissipated, energy flux, external energy and dissipated energy of guide 1, module deviation 15.5 <i>cm</i> . . . . .	67
D.16 CoR of the variation in impact location of guide with brace vs. guide without brace . . . . .	68
D.17 Load of the variation in impact location of guide with brace vs. guide without brace . . . . .	68
D.18 CoR of the variation in bumper height of guide with brace vs. guide whithout brace . . . . .	69
D.19 Load of the variation in bumper height on guide with brace vs. guide without brace . . . . .	69
D.20 CoR of the variation in deviation, guide with brace vs. guide whithout brace . . . . .	69
D.21 Load of the variation in deviation on guide with brace vs. guide whithout brace . . . . .	69
D.22 CoR of the variation in added weight on the module on guide with brace vs. guide without brace	70
D.23 Load of the variation in added weight on the module on guide with brace vs. guide without brace	70
D.24 CoR of the variation in adjusted material on guide with brace vs. guide without brace . . . . .	70
D.25 Load of the variation in adjusted material on guide with brace vs. guide without brace . . . . .	70



# LIST OF TABLES

4.1 Theoretical natural frequencies . . . . .	17
4.2 SACS frequencies guide without brace in x-direction only . . . . .	17
4.3 SACS frequencies of guide with brace in x-direction only . . . . .	17
4.4 SACS frequencies of module in x-direction only . . . . .	17
4.5 Maximum accelerations (1G is $9.81 \text{ m/s}^2$ ) . . . . .	18
4.6 Maximum Displacement ( $mm$ ) due to impact . . . . .	19
4.7 Maximum expected strains during impact ( $\mu\epsilon$ ) . . . . .	19
6.1 Frequency spectrum measured acceleration and strain if impact is at top of the guide . . . . .	30
6.2 Frequency spectrum measured acceleration and strain if impact is at top of the guide . . . . .	30
6.3 Natural frequencies analytical model . . . . .	31
6.4 Correlation to polynomial curves of the second order per case study . . . . .	32
6.5 All CoR values and equivalent loads for all case studies . . . . .	44
6.6 Calculated load and CoR for the variations in impact location; top, brace height and low for the guide with and without brace . . . . .	44
D.1 Calculated load and CoR for the variations in impact location; top, brace height and low for the guide with and without brace . . . . .	68
D.2 Calculated load and CoR for the variation in bumper height; middle, low and high for the guide with and without brace . . . . .	68
D.3 Calculated load and CoR for the variations in deviation; 9.3, 12 and 15.5 $cm$ for the guide with and without brace . . . . .	69
D.4 Calculated load and CoR for the variations in added weight and it's locations (variation of CoG of module) . . . . .	69
D.5 Calculated load and CoR for the variations in damping material; tape and pipe insulation for the guide with and without brace . . . . .	70



# ABBREVIATIONS

## 0.1. LIST OF ABBREVIATIONS

CoG	Centre of Gravity
CoR	Coefficient of Restitution
DAQ	Data Acquisition
HMC	Heerema Marine Contractors
OHS	Occupational Safety and Health law
TU Delft	Technical University Delft

## 0.2. LIST OF SYMBOLS

$\alpha$	Damping ratio [%]
$\beta$	Roots axial space response
$\gamma$	Roots tranverse space response
$\epsilon$	Strain
$\theta$	Angle [ $rad/s$ ]
$\kappa$	Curvature [ $rad/m$ ]
$\pi$	3.14
$\rho$	Density [ $kg/m^3$ ]
$\phi$	Angle of Rotation [ $rad$ ]
$\omega$	Frequency [ $rad/s$ ]
$\omega_n$	Natural Frequency [ $rad/s$ ]
$A$	Area [ $m^2$ ]
$\tilde{A}$	Matrix of measured accelerations [ $m/s$ ]
$C$	Damping coefficient
$E$	Youngs Modulus [ $Pa$ ]
$E_k$	Kinetic Energy [ $kg * m^2/s^2$ ]
$E_p$	Potential Energy [ $kg * m^2/s^2$ ]
$F$	Force [ $N$ ]
$f$	Frequency [ $Hz$ ]
$g$	Gravitational constant [ $9.81m/s^2$ ]
$G$	Gravitational constant [ $9.81m/s^2$ ]
$i$	Imaginary number
$I$	Area Moment of Inertia [ $m^4$ ]
$\tilde{K}$	Matrix of measured curvatures [ $m^{-1}$ ]
$k$	Stiffness [ $N/m$ ]
$L$	Length [ $m$ ]
$m$	Mass [ $kg$ ]
$P$	Impact [ $kg * m/s$ ]
$Q$	Shear force [ $N$ ]
$r$	Radius in [ $m$ ]
$T$	Period [ $s$ ]
$t$	Time [ $s$ ]
$u$	Displacement in x-direction [ $m$ ]
$v$	Velocity [ $m/s^2$ ]
$w$	Displacement in y-direction [ $m$ ]



# 1

## INTRODUCTION

### 1.1. INTRODUCTION

Heerema Marine Contractors (HMC) is a world leading marine construction company for the oil and gas industry and specializes in design, transportation, installation and removal of all types of fixed and floating offshore structures, subsea pipelines and infrastructures in shallow and deep water. HMC offers turnkey platform decommissioning and removal services with the world's largest crane vessels: semi-submersible crane vessel (SSCV) Thialf and the Sleipnir (currently under construction in Jurong Shipyard, Singapore) and Deepwater Construction vessels (DCV) Balder and Aegir (monohull).

Due to the aging of offshore oil and gas facilities, there is a rapid increase in the demand for removal of offshore facilities. Over 600 facilities are expected to be decommissioned in the next 5 years with 2000 more to follow through the year 2040 [11].

Reverse installation has been the main method for executing platform decommissioning and removal projects: Heavy modules such as the topside of an offshore platform are cut off their substructures and lifted back on the deck of crane vessels or onto cargo barges. These modules can weight up to 43,000 tonnes [13]. To assure that the modules are placed on the intended location and to prevent the modules from moving during transportation, a guide and bumper system is used. During the set down of the modules, the modules are carefully lowered to the correct position which is demarcated by guides.



Figure 1.1: Example of reverse installation module on barge with guides

Due to the motions of the crane vessel and the cargo barge, it is possible that the module bumps into one of the guides. The relative motions between the vessel and the barge can cause considerable impulse loads when

the module and guide make contact. To prevent the module from being damaged (see figure 1.2), bumpers are welded onto the module to protect the module during the contact phase.



Figure 1.2: Example of damaged bumper

The Guide and bumper system is normally designed as a set of horizontal steel beams welded on the lifted module (purple arrow in figure 1.1) that makes impact onto a set of vertical steel beams (the green arrow in 1.1) that are welded onto a barge that serves as the new site of the module. In this thesis, the guide will always be the beam mounted onto the barge and the bumper will be the beam welded onto the module.

## 1.2. PROBLEM DEFINITION

Both the guide and bumper are designed to only deform elastically. To ensure that the guides and bumpers are designed to cope with impulse loads that result from the contact between guides and bumpers, the designs of the guides and bumpers are based on internal standard criteria [4]. These standard criteria state that the guide and bumper system will be designed for a maximum horizontal load that is 10% of the designed weight of the lifted module. This load is statically applied on the weakest spot of the guide and bumper system (often the top of the guide and the center of the bumper).

The subject of guides and bumpers is a well researched subject. P.J. Maas showed in 2006 that both the design where only elastic deformation is allowed and the high stiffness of the currently used guides at HMC, increase the impulse loads. He also showed that the LiFSiM models inaccurately predict impulse loads if damping is taken into account[10]. Both P.J. Maas and Pistidda [2] investigated the SC-251[4] guidelines of HMC for guides and bumpers assuming static loading, E. de Boer described in 2012 that the peak forces are highly dependent on the stiffness and damping of the guides and bumpers and that the upper segment of the peak forces is caused by the bouncing of a module between guides[5]. He compared the displacement of a guide with static stiffness to the displacement of a guide with dynamic stiffness and concluded that the dynamic calculations consistently show a larger deformation at the upper part of the guide. The loads on guides can therefore not be assumed to be quasi-static. In 2013 N.P. Autar found, using a finite element model, that the force time history shows great resemblance with a half sine pulse load and that the forcing frequency is much lower compared to the first natural frequency and that the dynamic problem therefore can be simplified to a static one[3]. He also concluded that impulse load reduces once rotations of the module are taken into account and that the location of impact has a great influence on the magnitude of the impulse load due to the change in stiffness. Nevertheless it is still unknown how to correctly estimate the magnitude of the impulse loads. The calculated loads might differ from the actual loads due to unaccounted forms of energy transfer that occur during the impact, such as the rotation of the module [3].

This gives the following research question:

*What is the effect of energy transfer between guides and bumpers on the magnitude of the impulse loads during offshore set-down?*

To solve this question, the guide and bumper system during the set-down of an offshore platform will be analyzed. The following step is to design a model that has resemblance to the collision between guides a lifted module to conduct an experiment and to see how energy is transferred during the impact between guides and bumpers. The experiment will be compared with a finite element model (FEM) to validate the results and the models. Based on these results a recommendation will follow.

### 1.3. CURRENT SITUATION

HMC uses a combination of two computer programs to determine the dimensions of the guide and bumper system and compute the loads during impact between guides and bumpers; Bentley SACS and either Orcaflex or LifSim. Since this research only focuses on the structural dynamic behavior of the guides and bumpers and the motions of the vessel and barge will not be taken into account, Orcaflex and LifSim will not be discussed any further in this report.

#### 1.3.1. BENTLEY SACS

SACS is an integrated finite element structural analysis program. It is a program that provides in design, fabrication, installation, operations, and maintenance of offshore structures.

One of the functions of Bentley SACS at HMC is to determine the behavior of steel guides and bumpers as a reaction to static forces. The stiffness of the guide and bumper system is determined by applying 10% of the designed weight of the module as a static load to different locations on the guide and bumper system. The resulting stiffness is used as an input in the computer program Orcaflex or LifSim to determine the motions and reactions of the whole process including the motions of the barge and vessel.

### 1.4. SCOPE AND OBJECTIVE

This master thesis study focuses on energy transfer between guides and bumpers and the effect of this energy transfer on the magnitude of impulse loads. In this thesis only the elastic deformation of the guide and bumper will be taken into account since the guides and bumpers at HMC are designed to only deform elastically. The energy transfer will be computed by doing a scaled experiment, where a module with bumper will hit against two guides. The difference in potential and kinetic energy of the module before and after the impulse load will be analyzed and compared to the energy that has been transferred in the form of strains and accelerations in the guides and bumpers. Since the module will only hit the guides horizontally, friction is negligible in this experiment and will therefore not be taken into account. The results will be used to analyze the energy transfer, to compare the standard coefficient of restitution (CoR) of steel to the measured values and to estimate the magnitude of the pulse loads.

### 1.5. THESIS STRUCTURE

The literature that was used for this research will be discussed in chapter 2. In chapter 3 the design of the experiment will be discussed, this will be followed by the model analyses of the experiment in chapter 4. Here the expected values of the experiment will be discussed. Based on these results, the sensors to measure the strains and accelerations and their locations on the structures will be determined. This, the equipment that was used for the experiments and the measurements will be discussed in chapter 5. In chapter 6, the results will be shown, the energy transfer; the magnitude of the impulse loads and the energy loss during the collision between guides and bumpers. The conclusions and recommendations will be discussed in chapter 7 and the discussion follows in chapter ??.



# 2

## LITERATURE STUDY

In this chapter the preliminary research of the thesis will be discussed. The first step (2.1) was to investigate the currently used guide and bumper system of HMC. After this, the different possible forms of energy transfer will be discussed in section 2.2. The theory of impact loads and the chosen values for the impulse load in this research will be discussed in section 2.3. The use of the rod-theory and the bending of a beam will be shortly discussed in section 2.5. The last step of the preliminary research is the coefficient of restitution and this will be discussed in section 2.6.

### 2.1. GUIDE AND BUMPERS

At HMC there is a standard criteria for Engineering design of Guides and bumpers ([4]). The relevant information for this research will be discussed in this section. At HMC there are three different guidance system types which are generally used for lift operations. For the installation of topside modules supported from one side (hang-off modules) onto base support arrangements, a horizontal cow-horn bumper and a vertical guide system are preferred. Since the goal of this research is to conduct a scaled experiment, the guide system will be a simplified version of the most simple guide system; the vertical guide and horizontal bumper system. A schematic view of this system is shown in figure 2.1.

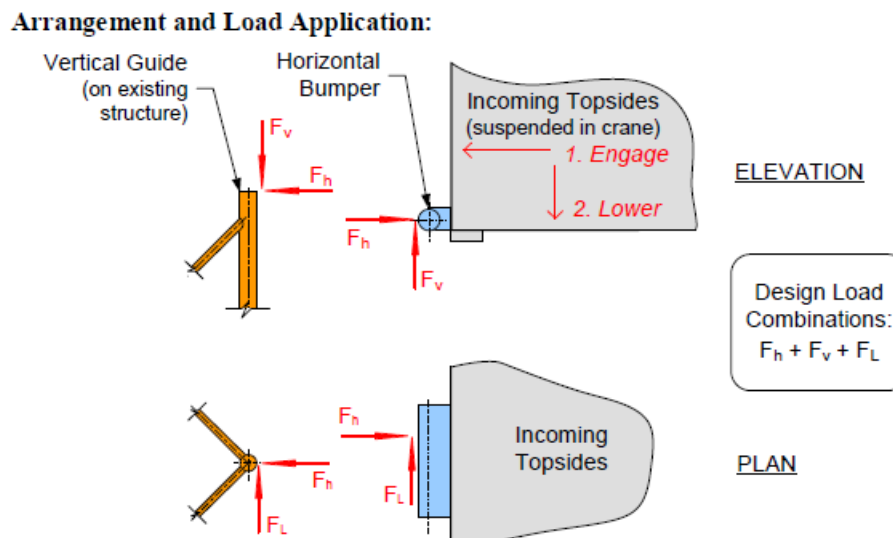


Figure 2.1: A schematic view of the vertical guide and horizontal bumper system

#### 2.1.1. DIMENSIONS GUIDE SYSTEM

Normally the dimensions for a vertical guide and horizontal bumper system are:

Height Guide = 3.0 - 4.5 m

Length Bumper = 3.0 m

But the guides and bumpers should allow for the topside movements that are discussed in the section below and they should allow for the incoming topside to be moved into position 3 meters above major obstacles. After comparing 44 guide designs, the average guides have a length of 3.0-3.5 m with the first brace at  $\frac{2}{3}$  of the height of the guide with a slope of approximately  $40^\circ$ .

### 2.1.2. TOPSIDE MOVEMENTS

The guide and bumper system have to be designed such that no other part of the topside than the supports or bumpers will make contact with the guide or other parts of the structure. The movement of the module should satisfy the following criteria for the three axes:

Vertical movement	=	$\pm 0.75 \text{ m}$
Longitudinal movement	=	$\pm 1.50 \text{ m}$
Transverse movement	=	$\pm 1.50 \text{ m}$

Further cases with regard to tilt and rotation of the topside shall also be included, these are:

Longitudinal tilt	=	4 %
Transverse tilt	=	4 %
Plan rotation	=	4 %

The plan rotation limit is only applicable when the topside has been orientated close to its final position.

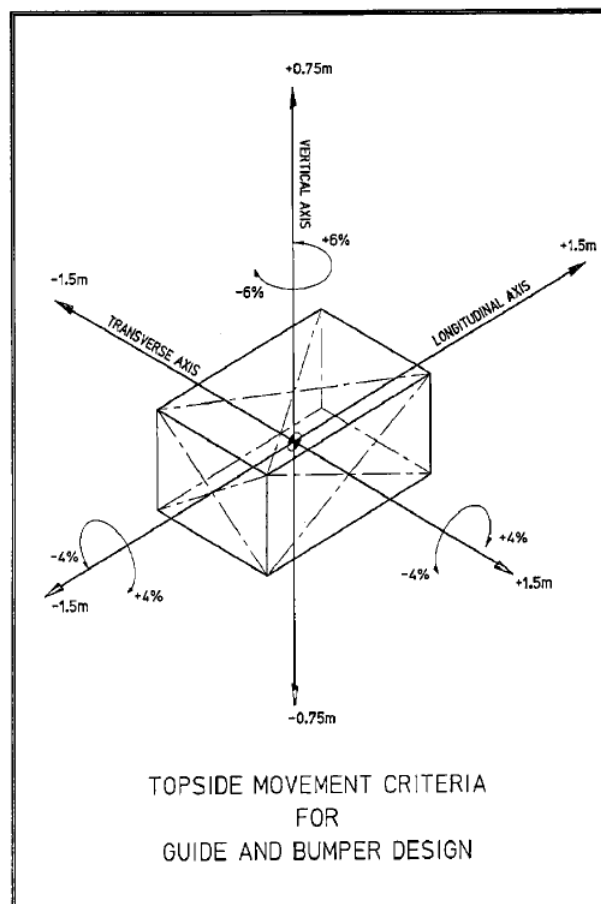


Figure 2.2: Topsides Movement criteria for Guide and Bumper Design (SC-251)

### 2.1.3. IMPACT LOADS

The primary impact loads for which the guides and bumpers are designed, are based on the following criteria:

Fh	=	10 % of topside design weight
Fv	=	1% of topside design weight (applied along vertical face)
Fl	=	1% of topside design weight (applied along vertical face)

#### 2.1.4. CONCLUSION

During the offshore set-down of a heavy module, the movement of the module may not be larger than 1.50 m and the module cannot rotate more than 4 % . The guides need to be designed for a maximum horizontal static load of 10% of the dry weight of the module, and should allow the topside to be moved into a position, 3 meters above major obstacles on the new site of the module.

## 2.2. POSSIBLE CAUSES FOR ENERGY TRANSFER DURING SET-DOWN

This research focuses on the effect of energy transfer between steel structures. Therefore it is important to discuss the possible causes for energy transfer during set-down. After a number of internal discussions at HMC and literature research, the following list of possible forms for energy transfers was set-up;

- Plastic local deformation guide/bumper
- Elastic local deformation guide/bumper/module
- Vibrations through guide/bumper/module
- Design (flexibility) guide/bumper
- Friction between guide and bumper
- Friction of rotation around hinge of crane
- Mass of guide/bumper
- Location guide/bumper
- Rotation of module horizontally
- Rotation of module vertically
- Motions of the crane ship/barge
- Human factor

Of this list, the horizontal and vertical rotation of the module are already taken into account in the currently used models at HMC, as well as the motions of the crane ship/barge. Therefore these will not be taken into the scope of this research. The human factor will not be taken into account since this will be an entirely different research by itself and this research only focuses on the structural behavior of the guides and bumpers. Currently the guides and bumpers at HMC are designed to only deform elastically. This means that the experiment for this research will be designed in a similar way where plastic deformation will not be assumed to occur. In the experiment the loads will be applied horizontally on the the guides and bumpers and thus the friction will be assumed to be so small that they can be neglected. No measurement equipment will be used to analyze the friction during the collision. The experiment will be conducted without the use of a hinge. The module will hang from the ceiling through two holes where the friction is so small that it can be assumed to be zero. This will be tested by the displacement of the module in its stationary position before and after the collision. A previous research on the location of the impact on guides and bumpers was conducted at HMC by P.J.Maas in 2006 ([10]). In this research the impact was only applied statically, therefore the location of the impact on the guides and bumpers will be taken into account since the results might differ due to the static versus dynamic analyses or due to the model versus experimental analyses. This leaves the following causes of energy transfer that will be analyzed during this research;

- Elastic local deformation guide/bumper/module
- Vibrations through guide/bumper/module
- Design (flexibility) guide/bumper
- Mass of guide/bumper
- Location of impact on guide/bumper

## 2.3. THEORY IMPACT LOADS

In mechanics, an impact is a force or shock applied over a short time period where two or more bodies collide [7]. The physics of impact necessarily involve conservation of energy and momentum. When a moving object strikes a structure, the force which decelerates the mass satisfies the conservation of momentum [6]. Impact loads are described by a short impulse with a certain force;  $F\Delta t = m\Delta v = \Delta p$ . Where  $F\Delta t$  describes how long and hard one 'pushes'.  $m\Delta v$  describes the change in velocity of a certain mass.  $F$  is the force in newtons (N),  $t$  the time in seconds (s),  $m$  the mass in  $kg/m^3$ ,  $v$  the velocity in  $m/s$  and  $P$  the impulse in  $kgm/s$  or  $Ns$ .

At least one of the bodies that collide is in motion. All the colliding bodies have a certain amount of potential energy ( $E_p$ ) and if not in stationary position, also a kinetic energy ( $E_k$ ). The kinetic energy of the moving body will partially be converted to strain energy and vibrations in the target and partly dissipated through friction, local plastic deformation and strain energy radiate away as stress waves. In structures the deceleration of a body is limited by elastic and plastic deformation, which 'cushions' the blow. To be able to say anything about this 'cushion effect', it is important to make a reasonable estimate on the stiffness ( $k$ ) at the point of the impact.

### 2.3.1. DYNAMIC RESPONSE

Since this research looks at the response of a dynamic system, the loads applied to the system will only last for a short amount of time. Since it is still unknown what the force time history of the impact will be at different locations on the guides and bumper due to the variance in stiffness over the length, the force time history will assumed to be as described by N.P. Autar in his thesis ([3]); a half sine pulse load. In the thesis of E. de Boer, the pulse load has a duration of approximately 0.1 seconds ([5]). In the thesis of N.P. Autar, the pulse load has a duration of approximately 0.7 seconds, the force time history that will be used to test the reactions of the test set-up will lie between 0.1 and 0.7 seconds and has the form of a half sine pulse load.

## 2.4. POTENTIAL ENERGY

One of the forms of energy transfer will be measured by strain gauges. Elastic potential energy is energy that is stored as a result of the elastic deformation of an object. The elastic deformation will be measured in the form of strain ( $\epsilon$ ). Parts of the guides will deform as a result of bending and other parts will deform as a result of longitudinal motions. Strain is formulated as  $\epsilon = \frac{L-L_0}{L_0}$ , where  $L$  is the length in meters.

## 2.5. KINETIC ENERGY

The other form of energy transfer that will be measured is the transfer of kinetic energy in the form of accelerations. The accelerations will be measured with accelerometers. Kinetic energy is the energy in an object or a particle due to its motions in the form of accelerations or velocities. During this experiment, the accelerations of the structure will be measured in  $G$ . One  $G$  is  $9.81 m/s^2$ .

### AXIAL DEFORMATION OF A ROD

A part of the guides (the brace) will deform as a result of longitudinal motions. The strains will measure this deformation as a result of compression or tension in the beam segments. For this compression, the compression and tension of the beam in the longitudinal direction ( $\frac{du}{dx}$ ) is the measured strain, see figure 2.3. The  $du$  here is the change in length of the segment, and the  $dx$  is the length of the segment, which is similar to the explained strain in section 2.5.

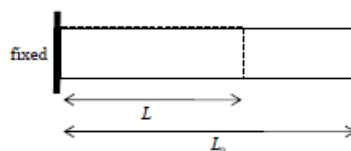


Figure 2.3: Compression of a Rod

Using the assumptions from rod-theory, the equation of motion of the guide in  $x$ -direction is assumed to be [12]:

$$EA \frac{\partial^2 u(x, t)}{\partial x^2} - \rho A \frac{\partial^2 u(x, t)}{\partial t^2} = q(x, t) \quad (2.1)$$

$E$  is the Young's Modulus in  $N/m^2$ ,  $A$  the cross-section of the segment in  $m^2$ ,  $\rho$  the density in  $kg/m^3$  and  $q$  the load depended on time and space as well as  $u$ .

### BENDING OF A BEAM

A part of the guides will bend as a result of the impact loads and the the strains will measure the deformation of the guides as a result of this bending. When a beam with a longitudinal axis is loaded by lateral forces (which is the case with the guides during the experiment), the axis is deformed in a curve which is the deflection curve of the beam (figure 2.4). The deflection  $w$  is the displacement in the  $y$  direction. Following the Euler-Bernoulli

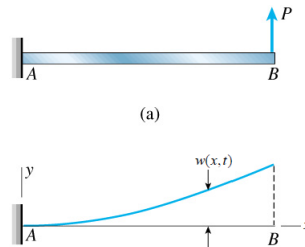


Figure 2.4: Deflection curve beam

model, the following equations apply[1]:

$$\phi = \frac{dw}{dx}; \quad \kappa = \frac{d\phi}{dx}; \quad \epsilon(y) = y\kappa \quad (2.2)$$

Where  $y$  is the distance from the center of the beam within the material.  $\phi$  is the angle of rotation which is a ratio and  $k$  is the curvature in  $m^{-1}$ . The moments ( $M$ ) and shear forces ( $Q$ ) are calculated with the following formula's:

$$M = EI \frac{d^2w}{dx^2} \quad Q = EI \frac{d^3w}{dx^3} \quad (2.3)$$

With the expression  $M = EI\kappa$  and the assumption that  $EI$  is constant, the following force balance for Euler-Bernoulli beam can be derived:

$$EI \frac{\partial^4 w(x, t)}{\partial x^4} + \rho A \frac{\partial^2 w(x, t)}{\partial t^2} = f(x, t) \quad (2.4)$$

## 2.6. COEFFICIENT OF RESTITUTION

Damping in a structure is often referred to as the energy dissipated internally or energy dissipated beyond the boundaries of the system. In this research the structure is only assumed to deform elastically, meaning that no energy will be dissipated internally due to deformations. The energy dissipated beyond the boundaries of the system, effectively decreases the motions of the system. This damping can reduce the magnitude of the impact loads on a system. A clear example of damping is when a tennis ball is dropped from a certain height. When the tennis ball bounces back, it will not reach its initial height, showing that a certain amount of energy was dissipated. This effect can be described with the coefficient of restitution (CoR). Y. Hurmuzlu described the CoR in 1998 [9] as the ratio between impulse  $I$  before and after impact (2.5). Since impact is described as  $m\Delta v$  and the mass of the object does not change, the CoF depends on the change of velocity. If energy is dissipated during an impact, the velocity out will be lower than the velocity in.

$$CoR = \frac{I_{after}}{I_{before}} = \frac{v_{out}}{v_{in}} \quad (2.5)$$

For steel the CoR is estimated to lie between 0.63 and 0.93.



# 3

## EXPERIMENTAL SET-UP

In this chapter the base test set-up will be discussed. The design will be discussed in section 3.1 where after the materials will be discussed in section 3.2. In section 3.3 the scaling of the experiment will be explained and in sections 3.4 and 3.5 the design of the guides and bumpers will be discussed.

### 3.1. TEST DESIGN

The test setup will suffice as the base experiment to analyze the structural behavior of guides and bumpers due to impact loads. To get comprehensible results, the test will be simplified in comparison to reality. The test will be controlled and clearly demarcated to see what the structural reactions of the guides are to a short pulse load as a result of the module bumping into the guides. The motions of the barge and crane ship will not be taken into account. This is because the motions of the vessels and barges are already well researched and modeled within HMC and also to prevent the occurrence of inexplicable phenomena. Since scaling is difficult and never completely accurate (quote Kaminski), a model-the-model technique will be applied. First a scaled experiment will be designed, this design will be modeled within SACS Bentley to determine the magnitude of the reaction of the design and to decide which sensors will be needed to measure these reactions. This will be discussed in chapter 4. With this information the test set-up for a scaled experiment will be finalized. The results of this scaled experiment can be used to verify the SACS Bentley model and to compare the results of a full scale test. The experimental model will be modeled for comparison and for further research, this model can be scaled and compared to full scale test.

### 3.2. MATERIAL

The material that is used for offshore platforms and guides is steel. The guides consist of a steel pipe with braces and the platforms consist of a complex structure of steel pipes, beams and plates. The experimental model will therefore be built with steel as well. The guides and bumpers are designed to deform only elastically at HMC. This means that the loads on the guides and bumpers will have to be small enough for the stresses of the guides and bumpers to remain below the yield stress. Due to the lack of available S355 steel (steel with a minimal yield stress of  $355 \text{ N/mm}^2$ ) at the company where the module and guides were built, the setup was built with s235 steel.

### 3.3. SCALING

The first step of the design was to scale the dimensions of the module and guides. The weight of the lifted topsides in the HMC database varies between 57 and 2510 tonnes. The height of the guides that HMC has used varies between 2 and 8.6 meters, the diameter between 0.14 and 0.762 meters and the wall thickness between 12.5 and 38.1 mm. For the scaling of an offshore platform, the standard dry weight of a platform is assumed to be 1000 tonnes and a guide to have a height of 3.5 meters, a diameter of 0.35 meters and a wall thickness of 15 mm. The OHS act (Occupational Health and Safety act) demands that a person cannot lift more than 25 kg for professional purposes. To ensure that the module can be lifted by two professionals or by one non-professional, the weight should remain below 35-40 kg. This means that the scaling factor for weight according to Froude scaling will be:  $\lambda^3 = \frac{m_f}{m_m}$  where  $\lambda$  is the scaling factor,  $m_f$  is the mass of the full scale model and  $m_m$  the mass of the scaled model. Assuming a standard platform of 1000 tonnes and a scaled model of 35-40 kg the scaling factor varies between 15.6 and 23.3. The length of the wire that hangs the module from

the ceiling was scaled to the maximum lifting height of the Thialf. The maximum lifting height is based on the load capacity curves of the Thialf (A.A.3). The lifting height for a weight of 1000 tonnes is approximately 92 *m*. Scaled this lifting height of the module should be between 3.95 and 5.9 meter. At the test location, the maximum possible height between the module and the ceiling was 2.3 *m*. If the guide would be scaled with the same scaling factor, the guide would have a height of 0.15-0.22 meters and a wall thickness of 0.42-0.38 *mm* which is too small and too thin to attach sensors on the structures. To ensure a number of test variations and the correct attachments of sensors, the guides will have a diameter of 3 *cm* and a height of 1 meter. This mismatch in scaling should be taken into account when the model will be scaled to full scale.

### 3.4. MODULE AND BUMPER

Guide and bumper systems are used for the set-down of a wide spectrum of offshore structures, varying in shape, mass and material; from offshore platforms to jacket-piles. The behavior of these structures depends on the material properties of the structures, such as stiffness, moment of inertia, density, Young's modulus and dimensions. To match the design of an offshore structure to reality, the module should have a higher stiffness than the guides it collides with. To ensure this stiffness, the module will be a square with cross bracing built with square tubular pipes. To conform to the OHS and to provide a surface large enough to attach the needed sensors, the dimensions of the module will be 0.7 *m* \* 0.7 *m* \* 0.7 *m*. The tubular pipes will have a width and height of 0.3 *m* and a wall thickness of 2 *mm*. The bumper will be attached to one side of the module. The bumper will be a tubular pipe with a diameter of 0.3 *m* and a wall thickness of 2.5 *mm*, similar to the guides. The bumper will be attached to the module through a clamping system so that the bumper can move from the top of the module to the bottom of the module. The bumper has a length of 800 *mm* and is clamped at 50 *mm* from each end. The connection between the bumper and the module are two square tubes of 105 *mm* with similar dimensions as the square tubes of the module. An example of the bumper is shown in figure 3.1 below. The module will weight approximately 35 *kg*. The module is fastened with 2 cables through 2 holes in a railing at the roof. The two holes are 120 *cm* apart and the cables go from one corner of the module through a hole to the next corner of the module. The cables were fastened to the corners of the module with a clamp, a hook, a turnbuckle and cable clamps. An example of the cable fastening is shown in figure 3.2. An example of a turnbuckle and a cable clamp are shown in Appendix A in figure A.1 and A.2. The cable clamps and the turnbuckles were used to adjust the cable length between the variations of the tests.



Figure 3.1: Clamping system of bumper on module

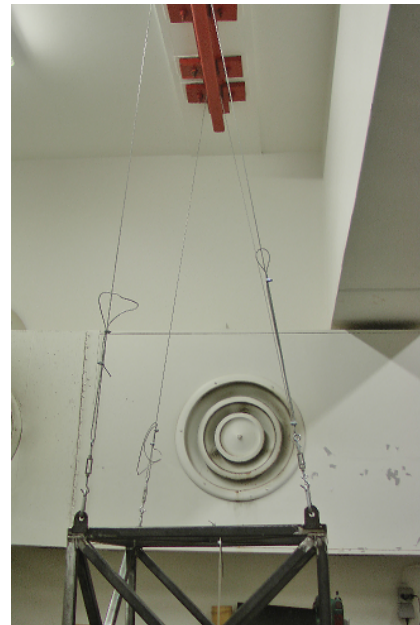


Figure 3.2: Attachment module to roof

### 3.5. GUIDES

The guides have a length of 1 meter as mentioned in the previous section. The guides are tubular pipes with a diameter of 0.3 *m* and a wall thickness of 2.5 *mm*. A unity check was performed to see whether the guides could withstand the assumed horizontal force that the bumper would apply on the guides (10% of the dry

weight of the module). This unity check can be found in [A section A.3](#). On  $\frac{2}{3}$  of the guide a brace is welded to the guide with an angle of  $40^\circ$ . The brace has a length of  $0.877\text{ m}$  to the bottom. Both guides are welded to separate steel plates with a thickness of  $20\text{ mm}$ . Every  $200\text{ mm}$  holes were drilled in these plates so they can be screwed tightly to a  $200\text{ kg}$  structure that suffices as the structure where the guides are normally welded on. Due to the fact that Grimbergen (the company that builds the guides and module) did not have enough tubular pipes with a diameter of  $0.3\text{ m}$  in stock, the braces were steel tubular pipes with a diameter of  $0.269\text{ m}$  and a wall thickness of  $2.85\text{ mm}$ . An example of the guides is shown in [figure 3.3](#) and a picture of the whole set up is shown in [figure 3.4](#). To simplify the results even more, it would be convenient to use guides without braces. Therefore the braces will be cut off after the first round of test are conducted with the guides with braces.



Figure 3.3: Picture of one of the guides

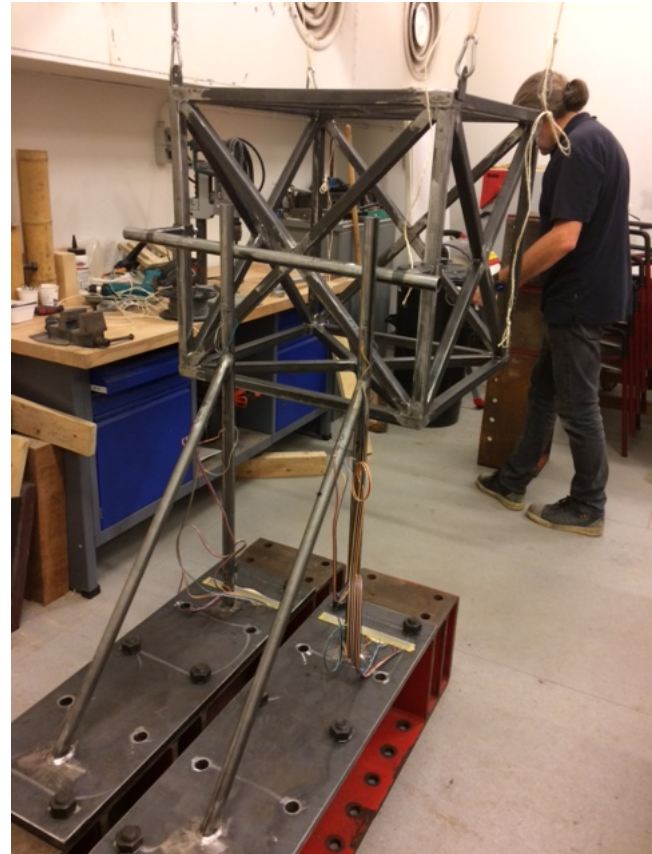


Figure 3.4: The Test setup of the scaled experiment



# 4

## NUMERICAL MODEL: SACS

After the test setup was determined it had to be modelled to gain some knowledge on the magnitude of the reactions of the system. The test setup was therefore modelled in SACS Bentley. As was explained in the introduction, SACS is an integrated finite element structural analysis program. This chapter will explain how this program was used to predict some of the responses of the experiment and how basic information of the setup was gained. First SACS and the models in SACS will be discussed in sections 4.1 and 4.2. Then the natural frequencies of the models will be discussed in section 4.3 and the implementation of the impact loads in the model in 4.4. The results of the model analyses will be discussed in sections 4.5, 4.6 and 4.7.

### 4.1. INTRODUCTION SACS

SACS is a structural analysis program that can also compute the response of structures to impact loads. The first step is to design the model and to give it the correct characteristics. In SACS you choose the location of your nodes and draw lines between them. Per node one can decide how many degrees of freedom it has. The lines between the nodes represent the material between the nodes. Each line can be given its own properties, length, thickness, type of material, strength etc. Once the model is finished forces can be applied to the model. One can choose point loads, uniform distributed loads and pulse loads. Since it is not possible to model two bodies in SACS and make them collide with one another, the models were built separately and point loads were applied on different locations on the three models.

### 4.2. MODEL SACS

Three models were constructed in SACS; The module, a guide with brace and a guide without brace. All three models consist of the same type of steel with the same material properties: S235 steel, a density of  $7849 \text{ kg/m}^3$  and a Young's Modulus of  $200 \text{ GPa}$ .

#### 4.2.1. MODULE

The module consists of a square,  $0.7 \text{ m} \times 0.7 \text{ m} \times 0.7 \text{ m}$  built from steel squared pipes. Each of the planes is cross-braced with squared pipes to increase the stiffness of the module. All the square pipes have a diameter of  $30 \text{ mm}$  and a wall thickness of  $2 \text{ mm}$ . On the front of the module, at the height of the center of gravity (CoG), a steel tubular pipe (the bumper) is attached to the module by two small links. The tubular has a diameter of  $30 \text{ mm}$  and a wall thickness of  $2.5 \text{ mm}$ . The links are  $105 \text{ mm}$  long and are similar to the square pipes. The module hangs from the corner points to a point  $2070 \text{ mm}$  above the module, precisely as the test setup in the previous chapter was described. A picture of the module in SACS can be found below in figure 4.1

#### 4.2.2. GUIDE WITH BRACE

The guide with brace consists of a 1 meter long tubular pipe that is clamped on one side at the bottom. The pipe has a diameter of  $30 \text{ mm}$  and a wall thickness of  $2.5 \text{ mm}$ . On  $\frac{2}{3}$  of the pipe, the brace is attached to the pipe. The brace has a length of  $0.877 \text{ m}$  and has a slope of  $40^\circ$ . The bottom of the brace is fixed as well. The brace has a diameter of  $26.9 \text{ mm}$  and a wall thickness of  $2.85 \text{ mm}$ . A picture of the guide can be found below in figure 4.2



Figure 4.1: Module in SACS

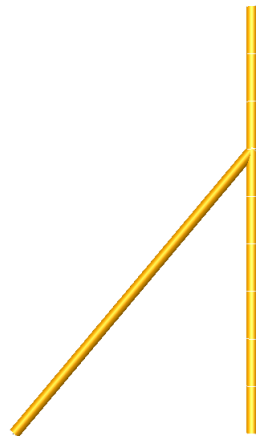


Figure 4.2: Guide with brace in SACS



Figure 4.3: Guide without brace in SACS

### 4.2.3. GUIDE WITHOUT BRACE

The guide without brace is a tubular beam of 1 meter clamped at the bottom. This pipe has a diameter of 30 mm and a wall thickness of 2.5 mm. A picture of the guide can be found below in figure 4.3

### 4.3. NATURAL FREQUENCIES AND MODE SHAPES

The first step of this analysis is to find the natural frequencies and normal modes. These can be used to see whether the experimental model matches the models in SACS and to check whether the models in SACS are adequate. The model of the guide without brace in SACS will be verified by comparing the natural frequencies and normal modes of SACS to the theoretical values. The natural frequencies of the models in SACS will later be used to compare the results of the scaled experimental model to the models in SACS.

The natural frequencies of the guide without brace can easily be calculated by using the following formula;  $\omega_n = \frac{C_n}{L^2} \sqrt{\frac{EI}{\rho * A}}$  where  $C_n$  is taken as the value from the figure below (4.4),  $\rho$  as the density,  $A$  as the cross-sectional area,  $E$  as the Young's modulus and  $I$  as the area moment of inertia. De Eigenmodes will be similar to the clamped modes in the figure below (4.4). The bumper will be assumed to behave like a clamped clamped beam which is shown in the second row of figure 4.4 and the guide with brace will behave like a combination of the two.

		$n = 1$	$n = 2$	$n = 3$	$n = 4$	$n = 5$
clamped	free	 $C = 3.52$	 $C = 22.4$	 $C = 61.7$	 $C = 121.0$	 $C = 200.0$
	clamped	 $C = 22.4$	 $C = 61.7$	 $C = 121.0$	 $C = 200.0$	 $C = 296.0$

Figure 4.4: Natural frequencies and modal shapes of beams with constant  $EI\rho A$  [1]

For the guide without brace this gives the following natural frequencies:

	Freq (Rad/s)
1	173.5
2	1103.9
3	3040.7
4	5963
5	9856.3

Table 4.1: Theoretical natural frequencies

The values from SACS are shown in table 4.2.

	Freq (Rad/s)
1	172.5
2	1066.0
3	2947.5
4	5699.6
5	9288.2

Table 4.2: SACS frequencies guide without brace in x-direction only

This shows that the theoretical natural frequencies almost correspond perfectly to the natural frequencies of SACS. The differences can be explained by the fact that SACS gives the 3D values of the natural frequencies and the theoretical way only looks at the 2D version of the guide and that the SACS model includes structural damping.

The natural frequencies of the guides with brace and the module are displayed in table 4.3 and table 4.4.

	Freq (Rad/s)
2	910.0
3	1509.4
4	2298.1
5	3191.8

Table 4.3: SACS frequencies of guide with brace in x-direction only

	Freq (Rad/s)
1	14.5
2	457.4
3	539.1
4	645.9
5	701.8

Table 4.4: SACS frequencies of module in x-direction only

#### 4.4. IMPACT ANALYSIS

To model the impulse loads in SACS, the dynamic response function was used. The input for this function is a file where the location of input of a load can be chosen as well as the time and magnitude of the load. From the thesis of **N.P. Autar** it shows that the time of the pulse load is approximately 0.02 seconds. The criteria of HMC say that the maximum horizontal load is 10 % of the dry weight of the lifted object. In this case the expected weight of the module is 35 kg so the maximum horizontal load is assumed to be 35 N. To take some extra margins in the experiment, the maximum horizontal load was taken as 70 N. The impulse was designed as a simplified parabola; at 0 seconds the load jumps to 35 N, after 0.01 seconds the load is 70 N and then it decreases linearly again to 35 N and drops back to 0 N at 0.03 seconds. This impulse is modelled to see the reactions of the guides and module to the short impulse. These reactions will be discussed in the following sections. The impact was modelled on three locations on the guides, at the top, at the height of the welding of the brace and in the middle of the bottom and the welding of the brace (figure 4.5). The locations of the impact are similar on the guide with brace as on the guide without brace.

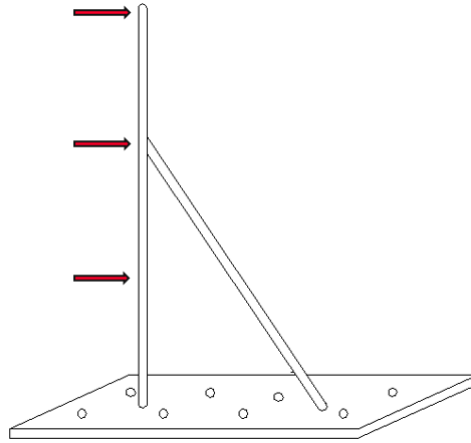


Figure 4.5: Impact locations on guide

For the module, one impact load was modelled on the weakest spot on the bumper, the midpoint.

#### 4.5. ACCELERATION

The maximum acceleration at the location of impact of the module was calculated by SACS as approximately 0.06 G. For the guide with brace, the maximum acceleration for impact on the top (Top) location is approximately 16.6 G and for the top location on the guide without brace, the maximum acceleration is 21.45 (figure 4.6)

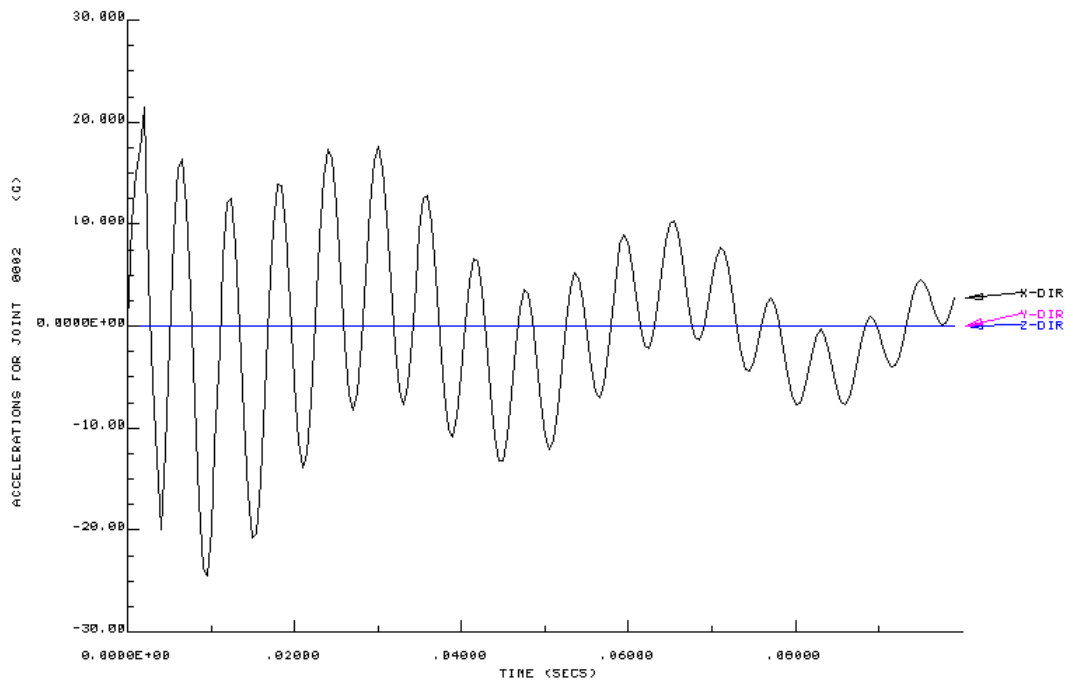


Figure 4.6: Acceleration at top guide without brace

An overview of all the maximum accelerations per model is given in the table below (4.5).

Maximum Accelerations (G)			
	Guide with Brace	Guide No Brace	Module
Top	16.6	24.35	
Middle	10.17	1.14	0.06
Low	14.9	6.72	

Table 4.5: Maximum accelerations (1G is  $9.81 \text{ m/s}^2$ )

The maximum acceleration measured by an impact load of 70 N during 0.02 seconds is 21.45 G, which is  $210 \text{ m/s}^2$ .

#### 4.6. DISPLACEMENT

For the Module, the guide with brace and the guide without brace the displacement at each location was modeled as well. The maximum displacement for the guides is at the top of the guide without brace. The displacement at this location is shown in figure 4.7.

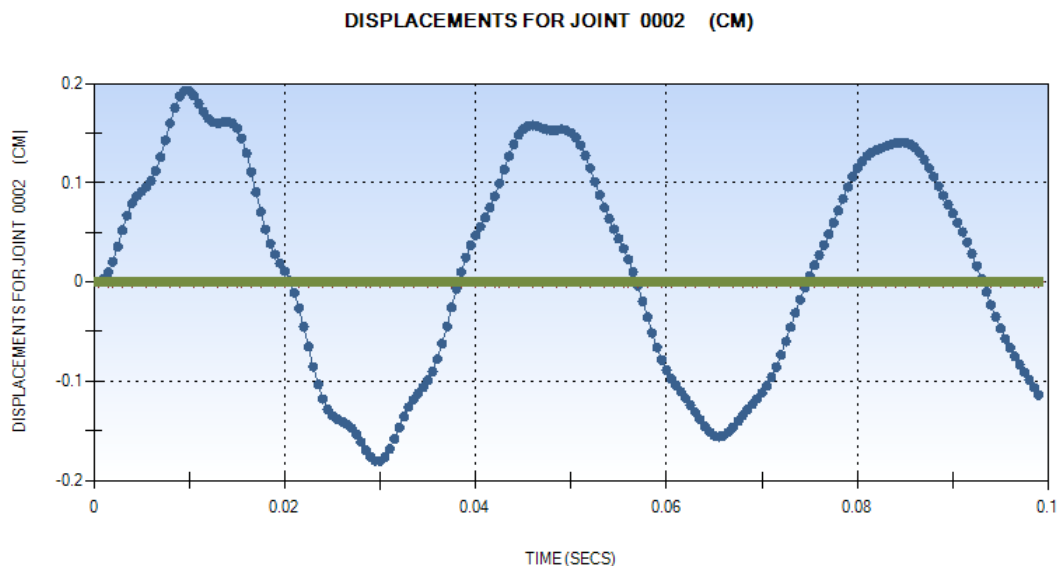


Figure 4.7: Displacement at top guide without brace

An overview of the maximum displacements per model is given below in table 4.6.

Maximum Displacement ( <i>mm</i> )		
	Guide with Brace	Guide No Brace
Top	0.42	1.903
Middle	0.0122	0.1047
Low	0.054	0.604

Table 4.6: Maximum Displacement (*mm*) due to impact

#### 4.7. STRAIN

The maximum strain was checked at all the locations of the sensors. The maximum expected strain from a point load of 70 N is  $73 \mu\epsilon$ . The maximum strains for the module, guide with brace and guide without brace can be found below in table 4.7

Maximum strain ( $\mu\epsilon$ )			
	Guide with Brace	Guide No Brace	Module
Top	73	23.4	
Middle	7.2	17.6	15.2
Low	21.1	62.6	

Table 4.7: Maximum expected strains during impact ( $\mu\epsilon$ )

#### 4.8. CONCLUSION

The sensors used in the experiment should be able to measure accelerations of  $210 \text{ m/s}^2$ , displacements of 2 cm and strains of  $73 \mu\epsilon$ . For the displacement and strain sensors this will be no problem. For the largest accelerations, accelerometers with a higher range have to be ordered. The standard accelerometer of the TU Delft has a maximum range of  $156 \text{ m/s}^2$  (16G).



# 5

## EXPERIMENTAL TESTS

In this chapter the execution of the experiment will be discussed. First the case studies will be discussed in section 5.1. Sensors, their characteristics and their locations will be discussed in section 5.2. The used measuring equipment will be discussed in section 5.3 and some examples and an explanation of the measurements will be shown in section 5.4.

### 5.1. CASE STUDIES

Since the lifted modules differ in shape, size and weight and sometimes hit the guide on the top and sometimes at the bottom, there are a number of case studies to see what the influence of stiffness, weight, location of impact and moment of inertia is on the energy transfer between guide and bumper.

The first case study that has already been discussed in the previous chapter was the location of impact on the guide. The impact location will vary between the top of the guide (2 cm from the top), which will be the most flexible part of the guide, the middle of the guide (at the welding of the brace), which will be the stiffest part of the guide and in between the bottom of the guide and the welding of the brace (22 cm below the welding and 41 cm above the bottom of the guide), see figure 5.1.

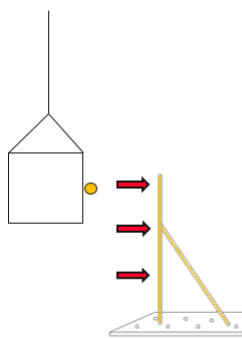


Figure 5.1: Case study 1: Impact Location  
Top/Brace/Low

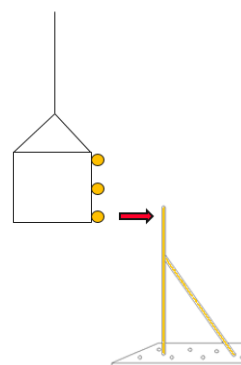


Figure 5.2: Case study 2: Bumper height on module  
Top/Middle/Low

The second case study was the position of the bumper. The bumper can be moved from the middle of the module (at the CoG of the module) to the top and bottom of the bumper, where the top is 7.8 cm from the upper edge of the bumper to the upper edge of the module and the bottom is 8 cm from the bottom of the bumper to the bottom of the module, see figure 5.2

The third case study is the displacement of the module. The module got pulled back to its start position from where it was released at the start of each test. The displacement of the module varied between 9.3, 12 and 15.5 cm. The displacement was based on the scaled criteria of HMC. The SC-251 says that the maximum longitudinal and transverse movement of a lifted module may be  $\pm 1.50 m$ . With a lift height of 100 m,

this gives a movement angle of  $0.859^\circ$ . The maximum lift height of the setup is  $2.3\text{ m}$  which would give a maximum movement of  $3.45\text{ cm}$ . After the first test runs, it showed that the guides could handle a larger impact than calculated, therefore the standard deviation was set to  $12\text{ cm}$  and the other variations in deviation became  $9.3$  and  $15.5\text{ cm}$ , see figure 5.3

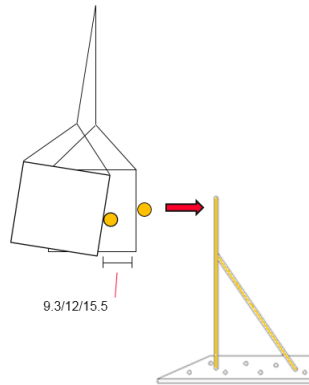


Figure 5.3: Case study 3: Displacement module 9.3/12/15.5  
*cm*

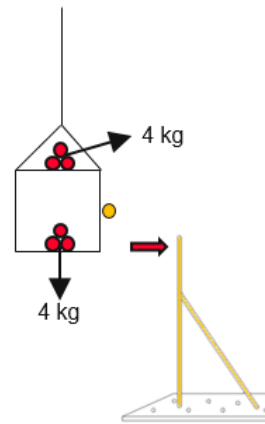


Figure 5.4: Case study 4: Weight and moment of inertia  
 $4/8\text{ kg}$

The fourth case study was the additional weight and thus a change in moment of inertia. Weight blocks of  $4\text{ kg}$  were clamped onto the module. The first variation was to add one weight block in the middle of the bottom left brace, the second to add another weight block in the middle of the bottom right brace. Another variation was one block on the middle of the top left brace, one in the middle on the top back brace and one in the middle of the top left brace together with one in the middle of the bottom left brace, see figure 5.4

The last case study was material on the guide. Two kinds of material were added onto the guide as a damping material; tape and pipe insulation, see picture 5.5

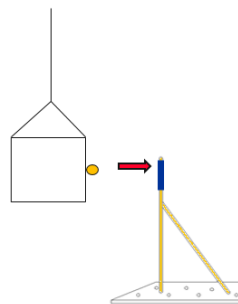


Figure 5.5: Case study 5: Damping of guide

After running all tests for these case studies, the brace was cut off so that only a simple cantilever beam remained. All tests were conducted again with the two guides without brace. The guide without brace is more flexible than the guide with brace at all locations.

## 5.2. SENSORS

To compute the energy and enclose the energy at each location of impact, each location of impact was enclosed by sensors; accelerometers and strain gauges. The energy balance can be set up and calculated by using the information and derived information, gained by these sensors. The sensors that will be used during the experiment are; strain gauges, accelerometers and a laser sensor. There are ten accelerometers with a maximum range of  $16\text{ G}$  and two accelerometers with a maximum range of  $70\text{ G}$  which can only measure  $0.5$  to  $1600\text{ Hz}$ . Thirty strain gauges were used. The strain gauges have a maximum limit of  $30000\text{ }\mu\epsilon$  and a frequency

range of 0-200  $kHz$ . The laser sensor measures over a distance of 100  $mm$  and has a frequency range of 0-10  $kHz$ .

### 5.2.1. LOCATION SENSORS

To enclose the energy that flows through the structures, all possible flow directions should be enclosed by sensors. If the strain gauges would be placed too close to the welding between the brace and the beam part, the sensors could measure peak strains which would give a distorted image of the strain in the members. Therefore the strain gauges had a distance of at least ten centimeters to all the welded parts of the structure. The strain gauges could not be placed at the location of impact, since the strain gauges would break due to the force of the impact. The strain gauges are therefore placed around the guide at the height of the impact load, see figure 5.6. To compute the energy flow at this location, the accelerometers should be placed at the same location as the

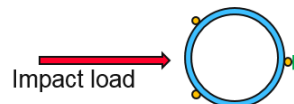


Figure 5.6: Cross-section guide/bumper with locations of strain gauges and accelerometer. Yellow dots are strain gauges, green line is accelerometer and red arrow shows the location of the impact

strain gauges. In the previous section, three different impact locations were discussed; top, brace height and low, the sensors around each of these locations will be discussed in the following sections. The strain gauges on the bumper all start with MR and then their number (MR1, MR2 etc.), the strain gauges on the first guide start with G1R and then their number (G1R1, G1R2 etc.) and the strain gauges on the second guide all start with G2R and then their number. All accelerometers are indicated with a V (V1, V2 etc.). The measuring amplifier that was needed to connect the strain gauges to, only had 16 connection entries. Six strain gauges were installed on the bumper of the module and were connected to the data equipment at all times. For the remaining strain gauges on the guides, combinations of sensors at different locations had to be connected to gather as much information as possible. For each of the guides, five connection entries were available to connect to strain gauges. The laser and accelerometers did not need to be connected to the measuring amplifier, only to a data acquisition system (DAQ). An overview of the sensors per impact location is discussed in the following paragraphs.

### 5.2.2. MODULE AND BUMPER

To measure the movements of the module, its horizontal and rotational motions, 2 accelerometers were installed on the module itself, on top of the module in the middle of the module (V2) and at the middle of one of the right back members (V1). To enclose the energy that flows through the bumper as a result of the impact, the sensors were placed right and left of the impact locations; MR1, MR2, MR3 and V3 on the right and MR4, MR5, MR6 and V4 on the left, see figure 5.7.

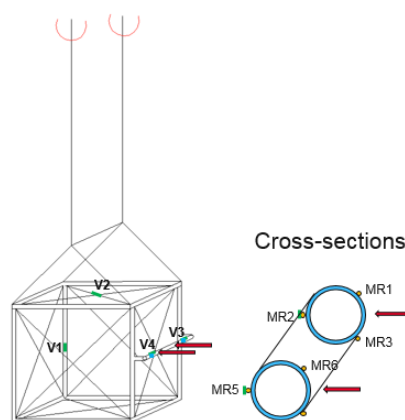


Figure 5.7: Sensor locations at Module and Bumper

### TOP

When the module hits the guides at the top, the energy only has the possibility to flow downwards. Therefore the energy transfer as result of the impact can be computed by taking one single location for the sensors. This location is 21 *cm* from the top and 10 *cm* above the welding of the brace. Since the maximum accelerations are expected to occur at the top, the accelerometers of 70 G were placed at the tip of the guides (2 *cm*) from the top, to measure the maximum accelerations in each test run. At the measurement location for the impact at the top, strain gauges G1R12, G1R11 and G1R10 are placed around the guide, together with accelerometer V5. Accelerometer V7 is placed at the tip for the maximum accelerations, see figure 5.8. For guide 2 the situation is similar, V8 for the maximum accelerations, V6 and G2R1, G2R2 and G2R3 at 21 *cm* from the top which is shown in appendix C.

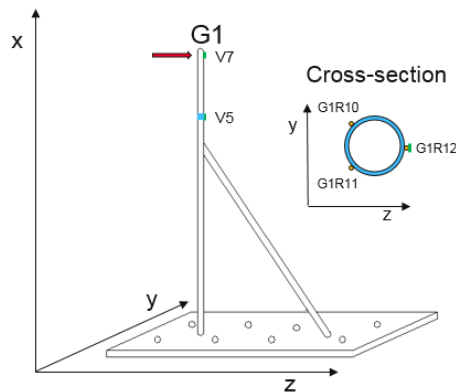


Figure 5.8: Sensors around impact location Top

### BRACE HEIGHT

When the module hits the guides at brace height, the energy has three possible flow directions; up, down and into the brace. Therefore sensors were placed 10 *cm* above the welding, 10 *cm* below the welding and 10 *cm* onto the brace. Since there are only 5 connection entries per guide, the guides were tested separately first to compare the strains in one guide to one another, with these measurements it is possible to estimate the strains that should be measured by each sensor as a relation to the sensors that will be connected in the combined test. Five strain gauges were chosen to measure the strains in both guides during the test runs. The measurements (Appendix C) showed that the strains measured 10 *cm* above the welding are lower compared to the strains measured in the brace and 10 *cm* below the welding. This means that the contribution of strain in the energy balance will be lowest 10 *cm* above the welding of the brace. Therefore only one strain gauge was connected at this location during the combined test, the one that shows the highest strain value at this location (G1R12). For both 10 *cm* below the welding and on the brace, two strain gauges were connected, G1R3 and G1R2 on the brace and G1R9 and G1R8 below the welding. For the second guide this was G2R1 above the welding, G2R4 and G2R5 below the welding and G2R10 and G2R11 on the brace. A schematic overview of the sensors on guide 1 is given in figure 5.9, the schematic overview of the sensors for guide 2 is shown in appendix C.

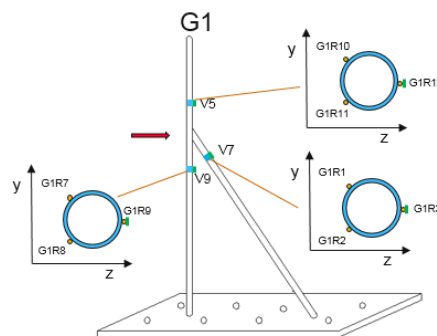


Figure 5.9: Sensors around impact location Brace Height

### Low

When the module hits the guides below the brace, it hits the guides at  $22\text{ cm}$  below the brace and  $41\text{ cm}$  above the bottom of the guides. The energy has the possibility to flow upwards and downwards. Therefore the sensors  $10\text{ cm}$  below the welding will be used to measure the energy flowing up and a set of sensors  $10\text{ cm}$  above the bottom of the guides ( $90\text{ cm}$  from the top) will be used to measure the energy flow going down. Two measuring locations mean 6 strain gauges per guide, which means that one of the six strain gauges cannot be connected. For guide 1 this is G1R9 and for guide 2 this is G2R5. An example of the sensors on guide 1 is given in figure 5.10, the example of guide two can be found in appendix C.

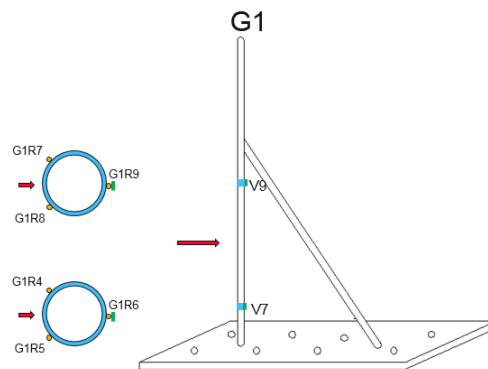


Figure 5.10: Sensors around impact location Low

### 5.3. INSTRUMENTAL SET-UP

To process the data, the strain gauges had to be connected to a measuring amplifier. The measuring amplifier than needed to be connected to a data acquisition (DAQ) device, which in its turn was connected to the computer. The accelerometers and the laser only needed to be connected through the DAQ to the computer. With 16 connection entries for the strain gauges, 10 accelerometers and one laser, 27 sensors in total were connected to the DAQ system. The accelerometers were calibrated in the horizontal direction and measured in G's. The strain gauges were calibrated and set to zero again before each test-run and measured in micro strain. The time difference between each of the connection entries in the DAQ are  $3,7\text{ micro}$ ,  $100\text{ }\mu\text{s}$  between the first and last entry. A schematic overview of the data equipment is given in figure 5.11.

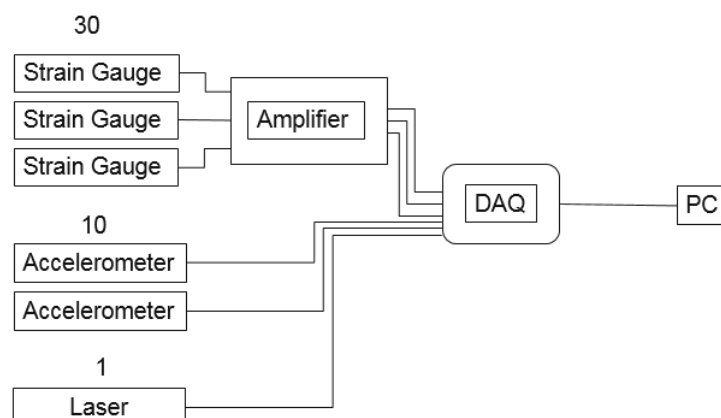


Figure 5.11: Schematic view of measuring equipment

### 5.4. MEASUREMENTS

In this section a number of strain measurements and acceleration measurements are shown. The measurements of five different case studies will be displayed;

- Impact location at the top of the guide with brace

- Impact location at the top of the guide without brace
- Impact location at brace height of the guide with brace with a combination of strains on the guide
- Impact location at brace height with only the strains on the brace
- Impact location below the welding of the brace on a guide with brace

An example of the measurements of each of the case studies is shown in appendix B.

#### 5.4.1. STRAIN

From the strain one can see very clearly when the impact occurs and when the system goes over in its free vibrations. The first figure (5.12) shows that the impact starts at 0.143 s and ends at 0.175 s, a duration of 0.032 seconds. The strain gauge opposite to the impact load (G2R1) measures the highest strains as is expected and during the impact one frequency (31.25 Hz) is clearly stronger than the higher frequencies that can be seen along the line of impact. In the second figure (5.13), where the impact is located at the top of a guide without brace, the duration of the impact is clearly longer (0.112 seconds, from 0.18-0.292 s) and the higher frequencies have a relative stronger presence during the impact. There is also a large difference in measured strain at the guide with brace vs. the guide without brace; -258.717 vs -73.35.

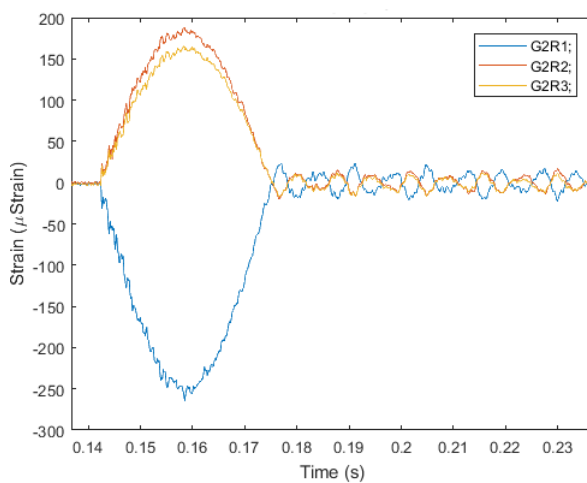


Figure 5.12: Measurements strain at the top of guide 2 with brace

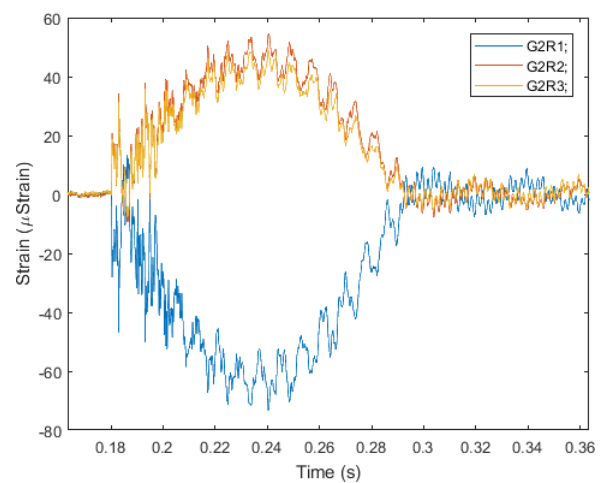


Figure 5.13: Measurements strain at the top of guide 2 without brace

In the following two figures, the impact location at brace height is displayed. The first figure (5.14) shows the strain measurements of a combination of the sensors at three locations as a result of the impact load. G2R1 is the strain gauge above the brace. This sensor shows the lowest peak strains. G2R5 and G2R4 are the strain gauges above the brace and G2R10 and G2R11 are the strain gauges on the brace. The results show that the strain measured below the brace has a slightly higher peak than the strain measured in the brace. The duration of the impact at brace height is smaller than the duration of the impact on the top of the guide. At brace height, the impact starts at 0.1892 seconds and ends at 0.199 seconds giving a duration of 0.0098 seconds. In the second figure (5.15) the measurements at the brace are displayed. The strains all have the same sign, but there is still a difference between the opposite sensors. The difference between these sensors will be discussed in the next chapter to see whether solely compression can be assumed in the brace, or compression and bending combined.

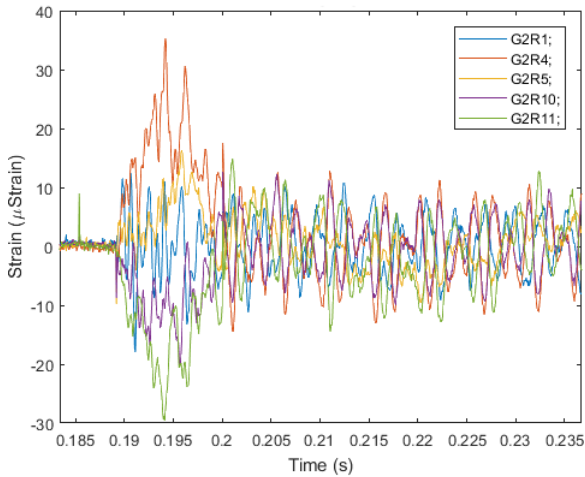


Figure 5.14: Measurements strain at guide 2, above brace, below brace and on brace

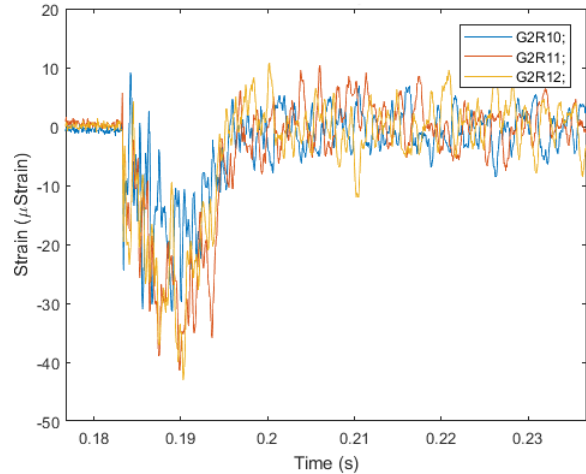


Figure 5.15: Measurements strain at the brace of guide 2

The last figure of the strain measurements is the impact below the brace (figure 5.16). Since it was not possible to measure the impact below the brace with the bumper at CoG height (the module would hit against the plate below the guides instead of against the guides), the bumper was put in its lowest position to run this test. G2R4 and G2R6 represent the strain just below the brace and G2R7, G2R8 and G2R9 represent the strain just above the bottom of the guides. The peak strains just below the brace is higher than the peak strains just above the bottom of the guides, this is probably due to the fact that the impact is closer to the brace than to the bottom. The impact occurs between 0.2010 seconds and 0.2136 seconds (duration is 0.0126 seconds).

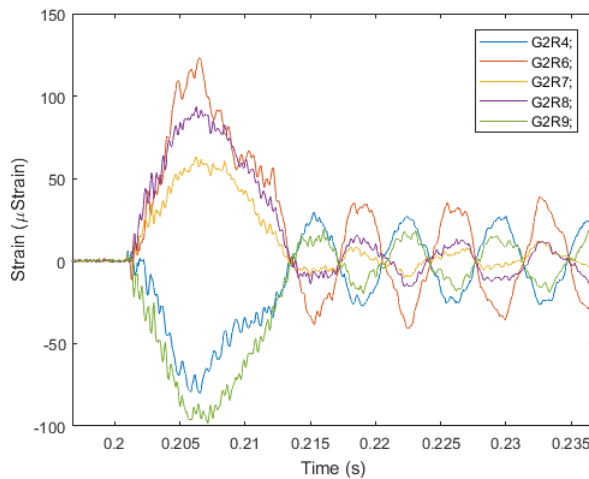


Figure 5.16: Measurements strain at guide 2, below brace and near bottom of guide

### 5.4.2. ACCELERATIONS

The measured accelerations for the same case study as the previous section are displayed below. The difference in duration has been discussed in the previous section. You can see that between the first and the second figure (figure 5.17 and figure 5.18) the accelerations during impact have approximately similar sizes. However, the accelerations after the impact are a lot higher at the top of the guide with brace than the top of the guide without brace. The damping in the second figure seems to be larger than the damping in the first figure.

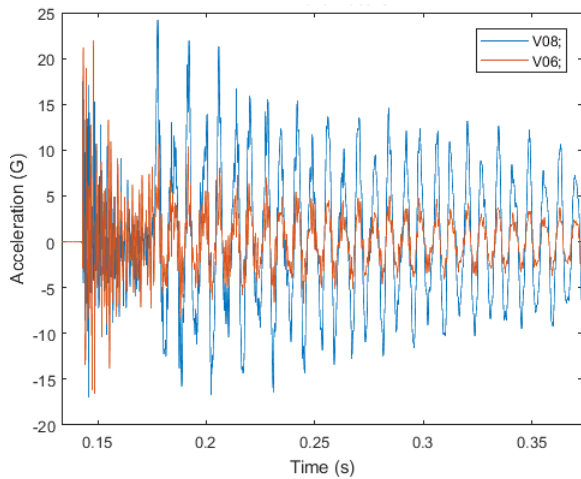


Figure 5.17: Measurements acceleration at the top of guide 2 with brace

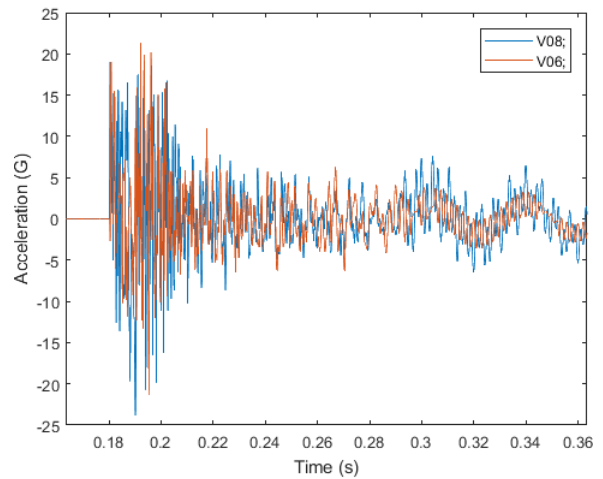


Figure 5.18: Measurements acceleration at the top of guide 2 without brace

The damping and the accelerations as a result of the impact at brace height (figure 5.19) seem to be quit similar to the damping and accelerations as a result of the impact at the top of a guide with brace. The accelerations during impact and after the impact as well as the damping seem to be smaller for the impact below brace height (figure 5.20).

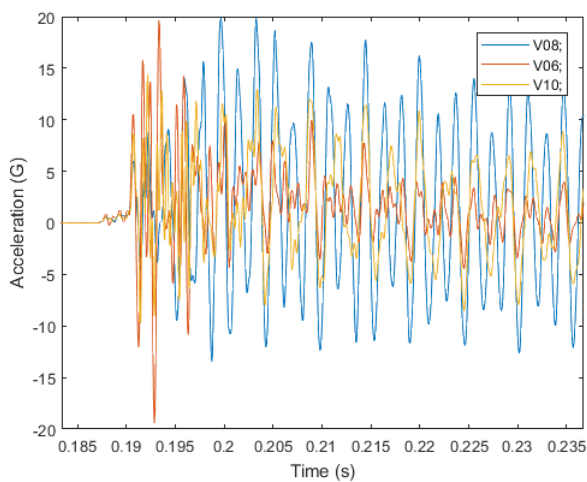


Figure 5.19: Measurements acceleration at guide 2, above brace, below brace and on brace

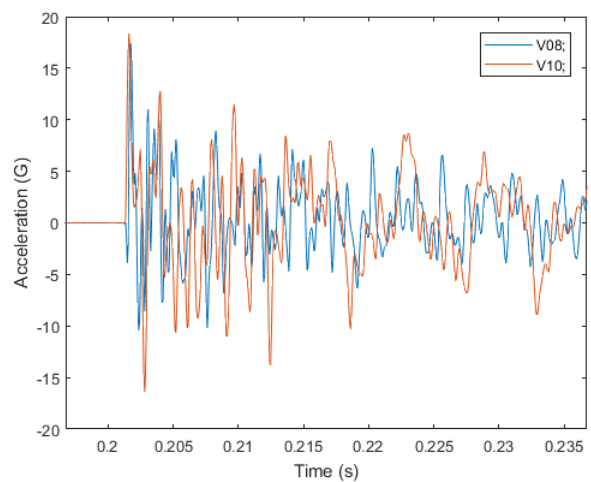


Figure 5.20: Measurements acceleration at guide 2, below brace and near bottom of guide

## 5.5. CONCLUSION

It seems that the location of impact has a large influence on the reactions of the accelerometers and strain gauges. The duration of impact is smaller at stiffer locations, and the accelerations after the impact are larger at the more flexible locations.

# 6

## RESULTS

In this chapter the analyses of the measurements will be discussed. The first step is to check the frequencies of the measurements and to compare these to an analytical model, this will be done in section 6.1. The second section (6.2) will describe the linearity of the elastic deformation and the shape of the impact loads. In the following section (6.3), the loads will be computed using the measurements and an analytical model. Together with the loads and the measurements, an energy balance will be formulated and calculated in section 6.5. The last analyses is the CoR in section 6.6. The velocities before the impact will be compared with the velocities after the impact to establish the energy loss of the module.

### 6.1. NATURAL FREQUENCIES

To determine the natural frequencies of the guides, the Fourier transform was used. The Fourier function transforms data in the time-domain to data in the frequency domain where it shows the extend to which certain time-cycles occur within your data and what the natural frequencies of your system are. The strain gauges could measure up to 200 kHz while the accelerometers could only measure up to 1600 Hz. This means that the accelerometers will not show higher natural frequencies than 1600 Hz (10000 rad/s) in the spectra. Two frequency spectra are displayed below in figure 6.1 and 6.2. These spectra are based on the measured acceleration and strain as a result of an impact at the top of a guide with brace.

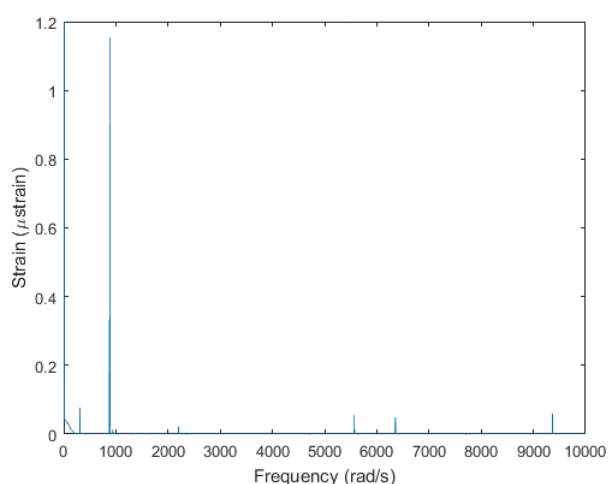


Figure 6.1: Frequency spectrum measured strain, impact at the top of guide

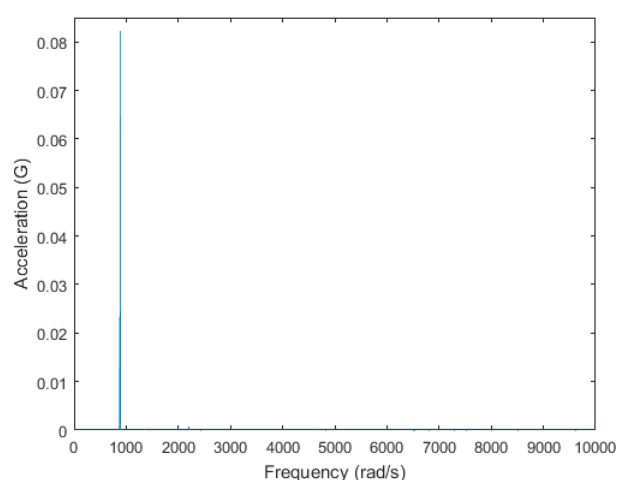


Figure 6.2: Frequency spectrum measured acceleration, impact at the top of guide

One can see that the most dominant frequency is 881.7 rad/s which is approximately 140 Hz. In the frequency spectrum of the strain, one can see that there is a peak below 881.7 at 314 rad/s, this is 50 Hz, which is the frequency of the electricity in Europe. One can also see that there is a peak that goes up, higher than the first mode, at 0. It then goes to zero just before the peak frequency at 314 rad/s. In these values, the frequency of the impact is represented. The impact has the shape of half a sinus, the full sinusoidal wave would have

a frequency between 100 and 300  $rad/s$ . It is assumed that the signal was compromised by putting it in the frequency domain due to the fact that the signal is only half a sinus wave. In the spectrum of the accelerations, the higher natural frequencies are hardly visible. The visibility increases if the y-axis is changed to logarithmic scale, see figure 6.3 and 6.4.

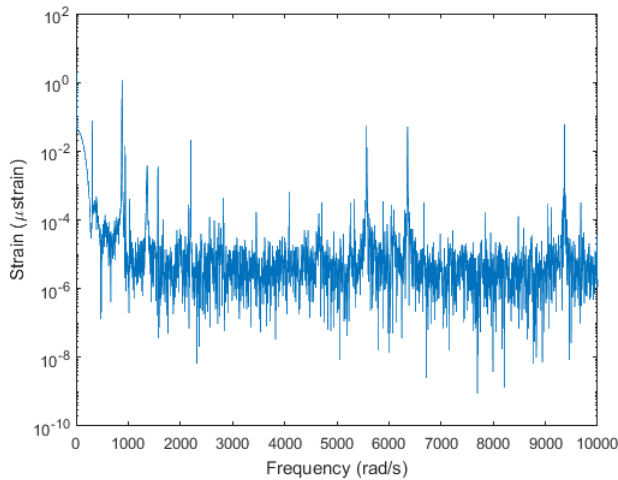


Figure 6.3: Frequency spectrum measured strain, impact at the top of guide, logarithmic scale

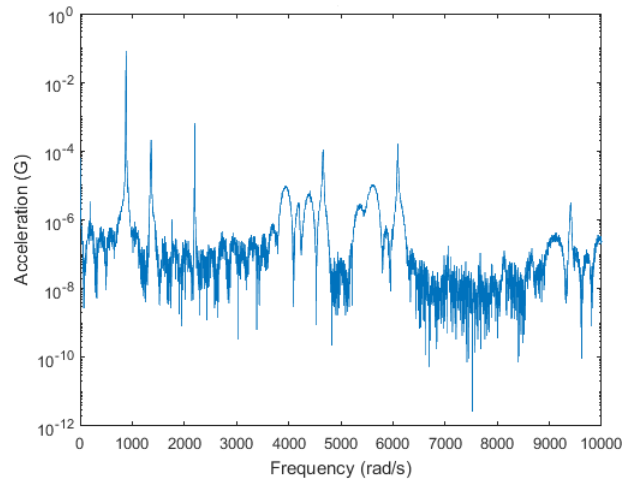


Figure 6.4: Frequency spectrum measured acceleration, impact at the top of guide, logarithmic scale

The table below (6.1) shows all the natural frequencies. Accelerometer V6 shows the natural frequencies measured by the accelerometer V6 which is at the same location as strain gauge G2R1. The differences are caused by the difference in sampling rate of the sensors. The natural frequencies of the strain gauges also contain the natural frequencies of the noise, which are at 314, 941 and 1570  $rad/s$ . If these values are taken out, one can see the similarities more easily, see table 6.2

Natural frequencies		
	Acc V6	G2R1
	$\omega$ (rad/s)	$\omega$ (rad/s)
1	880	314
2	1361	881
3	2196	941
4	4660	1364
5	6093	1570
6		2200
7		5572
8		6356
9		9365

Table 6.1: Frequency spectrum measured acceleration and strain if impact is at top of the guide

Natural frequencies		
	Acc V6	G2R1
	$\omega$ (rad/s)	$\omega$ (rad/s)
1	-	0
2	880	881
3	1361	1364
4	2196	2200
5	4660	5572
6	6093	6356
7		9365

Table 6.2: Frequency spectrum measured acceleration and strain if impact is at top of the guide

An analytical model, written by Jim Zwartveld, computed the frequencies that are shown in table 6.3. This analytical model is written in Python and can be found in appendix D. The analytical model was used to calculate the magnitude of the impact loads. To validate the model, the natural frequencies were compared to the natural frequencies of the measured data. Based on these frequencies the model was assumed valid to determine the external loads that were applied on the guides.

Natural frequencies	
	$\omega$ (rad/s)
<b>1</b>	879
<b>2</b>	1386
<b>3</b>	2298
<b>4</b>	3466
<b>5</b>	5973
<b>6</b>	10110
<b>5</b>	11439
<b>6</b>	13637

Table 6.3: Natural frequencies analytical model

## 6.2. LINEAR ELASTIC DEFORMATION

In the literature, the shape of the impact was described as a half sinus wave. It was unsure whether the impact actually would behave as a half a sinus wave and whether the impact would be a linear elastic process. In almost all the strain measurements, the shape of the impact is a hyperbolic line. In the situations where the response is not dominated by the deformation of the structure, but possibly by the multiple collisions during the impact, this hyperbolic function is not visible. This is because the contact phase is assumed to be constantly interrupted due to the bouncing of steel on steel. This occurs at locations where the structure is stiffer (impact location at brace height) and at locations where the deformation due to the impact is smaller than the effects of the steel on steel interrupted impact. An example of the interrupted pulse load is shown in figure 6.5. This figure show the impact at the bumper of the module. An example of a linear elastic response of the guides due to the impact is shown in figure 6.6.

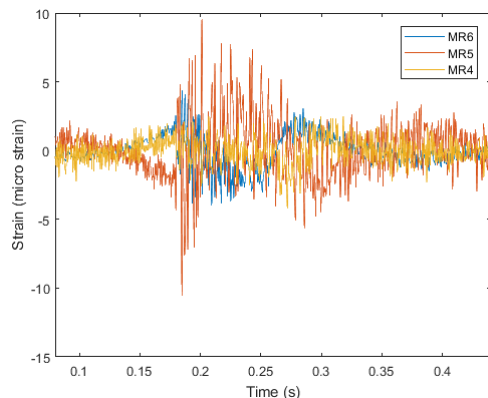


Figure 6.5: Example of non-linear elastic response of bumper due to impact

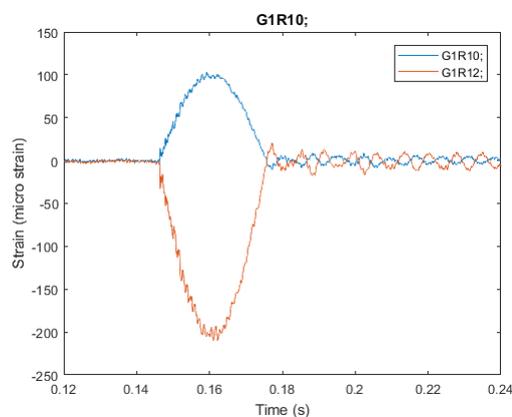


Figure 6.6: Example of linear elastic response of guide due to impact

For every case study except for the once with the impact location at brace height, the measurements of the strains have a hyperbolic shape overall. The energy as a result of strain for linear elastic materials is formulated as

$$E = \frac{1}{2} \epsilon \sigma = \frac{1}{2} E \epsilon^2 \quad (6.1)$$

where  $\sigma$  is equal to  $\epsilon E$ . The strain measurements were fit to a polynomial curve and the correlation between the polynomial fit and the measurements was computed to see whether the impact could be assumed to be linear elastic. An example of this curve is shown in figure 6.7.

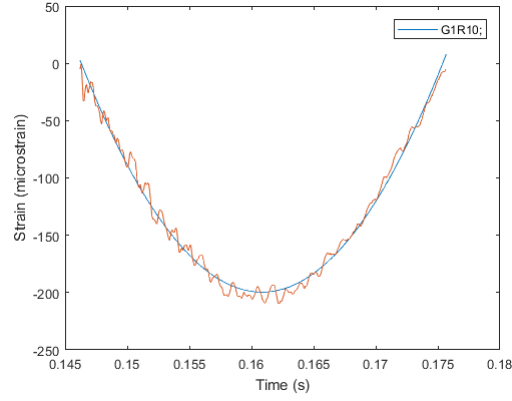


Figure 6.7: Fitting of strain measurements

The correlation between this polynomial fit and the measurements is 0.9947, which is very high and the polynomial fit for this curve is;

$$y = 9.4412e + 05x^2 - 3.0371e + 05x + 2.4226e + 04 \quad (6.2)$$

The correlations between the polynomial fit and the strain measurements is higher than 0.979 for all cases except the ones at the second impact location (at brace height), as you can see in table 6.4. This means that the impact can be assumed to be linearly elastic where the global deformation is dominant to the high frequency deformation based on the results from the strain measurements.

Case study	Correlation
B1U1G1W1	0.9955
B1U2G1W1	0.9947
B1U2G1W2	0.9968
B1U2G1W3	0.9968
B1U2G1W4	0.9961
B1U2G1W5	0.9967
B1U2G1W6	0.9955
B1U2G1W1M1	0.9967
B1U3G1W1	0.9899
B2U2G1W1	0.9963
B2U3G1W1	0.9943
B3U1G1W1	0.9924
B3U2G1W1	0.9905
B3U2G3W1	0.9793
B3U3G3W1	0.9899

Table 6.4: Correlation to polynomial curves of the second order per case study

### 6.3. MAGNITUDE OF IMPULSE LOADS

The magnitude of the impulse loads is analytically determined. The first step was to build an analytical model of the guides. This model can be found in appendix D. The guide was subdivided into three beams; the top section, L2 (from welding point to the top of the guide), the lower section, L1 (from the welding point straight to the bottom of the guide) and the brace, L3 (the inclined part of the guide). Both bending and axial deformations were considered in these beams. For each of these beams, the equations of motions were determined and the boundary conditions (18 boundary conditions) between the beams and at the end of the beams were determined. These can also be found in appendix D. The equation of motion was transposed from the time domain to the frequency domain by using the fourier transform:

$$EI \frac{\partial^4 w(x, t)}{\partial x^4} + \rho A \frac{\partial^2 w(x, t)}{\partial t^2} + \alpha EI \frac{\partial^5 w(x, t)}{\partial x^4 \partial t} = f(x, t) \quad (6.3)$$

after the fourier transform:

$$EI \frac{\partial^4 \tilde{W}(x, w)}{\partial x^4} - \Omega^2 \rho A \tilde{W}(x, w) + \alpha EI(i\omega) \frac{\partial^4 \tilde{W}(x, w)}{\partial x^4} = \tilde{F}(x, w) \quad (6.4)$$

The general solution for the bending in the beam segments is in the following form:

$$\tilde{W}(w, x, F) = C_{11}(\omega)\cos(\gamma x) + C_{12}(\omega)\sin(\gamma x) + C_{13}(\omega)\cosh(\gamma x) + C_{14}(\omega)\sinh(\gamma x) \quad (6.5)$$

and for the axial deformation of the beam segments:

$$\tilde{U}(w, x, F) = C_{15}(\omega)\sin(\beta x) + C_{16}(\omega)\cos(\beta x) \quad (6.6)$$

Where  $\gamma$  is:

$$\gamma = \sqrt[4]{\frac{\rho A}{EI(1 + i\alpha\Omega)}} \sqrt[2]{\Omega} \quad (6.7)$$

The  $\alpha$  is a value for the damping of the structure (in this case 0.00002) and  $\Omega$  is the frequency range.  $\beta$  is equal to  $\Omega/c$ ,  $c$  is equal to  $E/\rho$  and  $x$  is the location of the impact.

The constants can be found by substituting the boundary conditions in the general solutions at the all frequencies. For each frequency a different set of constants was computed. In the boundary conditions, the force was defined as a unit load of 1, to find the constants based on the real part of a unit load of 1 and in the next run, the unit load was defined as 1i to find the constants based on the imaginary part of the unit load. The load will be estimated by comparing the response function to the measurements. The real part of the measurements ( $Re_M$ ) should be equal to real part of the response to the unit load 1 ( $Re_1$ ) times a constant that represents the real part of the load plus the real part of the response to the unit load i ( $Re_i$ ) that represents the imaginary part of the load. Similar for the imaginary part, the imaginary part of the measurements ( $Im_M$ ) should be equal to imaginary part of the response to the unit load 1 ( $Im_1$ ) times the constant that represents the real part of the load plus the imaginary part of the response to the unit load i ( $Im_i$ ) times the constant that represents the imaginary part of the load. The response functions that correspond to the accelerations is the second derivative of equation 6.5 over time:

$$\tilde{\mathbf{R}}_{Accelerations} = -\Omega^2 \tilde{\mathbf{W}} \quad (6.8)$$

The response functions that correspond to the curvature is the second derivative of equation 6.5 over space:

$$\tilde{\mathbf{R}}_{Curvature} = -\gamma^2 \tilde{\mathbf{W}} \quad (6.9)$$

The response functions for a unit load 1 and a unit load i were split up into their real and imaginary to form the following matrix:

$$\begin{bmatrix} Im_1 & Im_i \\ Re_1 & Re_i \end{bmatrix} \begin{bmatrix} a \\ b \end{bmatrix} = \begin{bmatrix} Im_M \\ Re_M \end{bmatrix} \quad (6.10)$$

The load in the frequency domain is then defined by:

$$F = a + ib \quad (6.11)$$

An example is shown below on how the load was calculated. This example shows the base case scenario, case study B1U2G1W1; Bumper at CoG, deviation of 12 cm, impact location at the top and no added weights to the module. For the accelerations, the mirrored frequency spectrum of the measurements is shown below in figure 6.8 and the mirrored frequency spectrum of the response to a unit load of 1 is shown in figure 6.9:

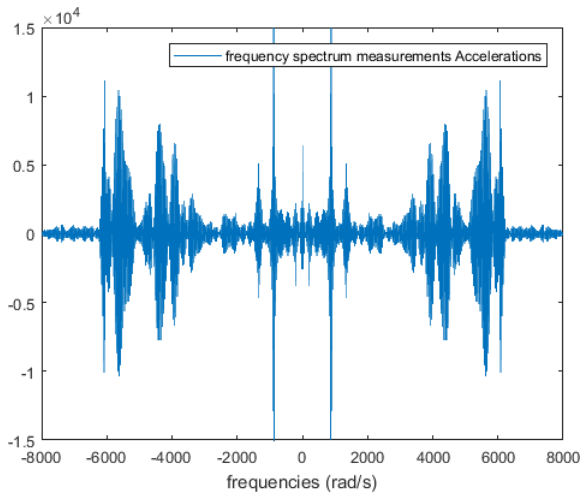


Figure 6.8: Mirrored frequency spectrum of accelerations

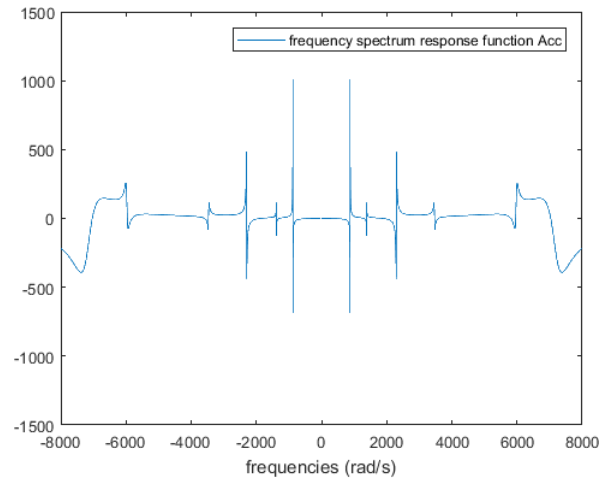


Figure 6.9: Mirrored frequency spectrum of response to a unit load 1

The frequency spectrum of the calculated load is shown below in figure 6.10. The load seems to peak around zero. This means that there is a very dominant peak at a frequency of  $0 \text{ rad/s}$ . This is probably due to the mathematical error of transforming the pulse load into the fourier domain.

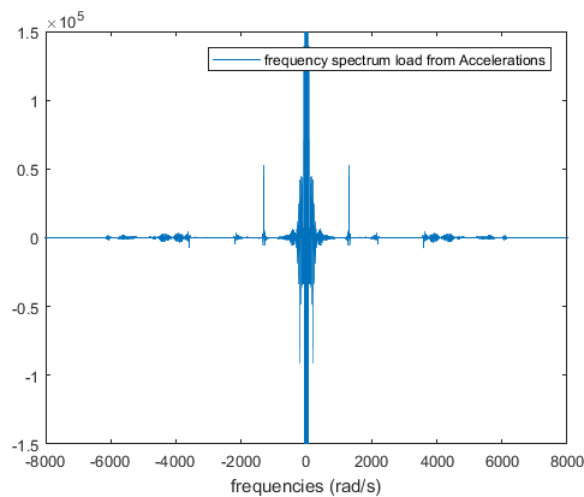


Figure 6.10: Frequency spectrum calculated load based on accelerations

Once the load is transformed back to the time domain, one can see a large curve that dominates the results (figure 6.11). This overall shape is probably the result of the mathematical error. However, if one zooms in at the top during the time of impact (0.145 seconds to 0.175 seconds), the response of the impact becomes visible (figure 6.12). One can see that the load goes over to more stable frequencies after the impact, but the load was assumed to be zero at this point. It is not zero due to the fact that the measurements were used to compute the load (here accelerations). The loads are computed by using the frequencies of these measurements, which means that the load will show a response at all frequencies of the measurements, even after the impact, giving a load based on the free vibrations. Ideally the load would have a similar shape to the shape that was observed in the response of the strain gauges or accelerometers (half sinus shape).

Next the mathematical error was filtered out. Filtering has large influences on the values of the results. Once the frequencies around zero are filtered out, the load curve gives a shape that corresponds more to the expected shape of the pulse load. The filtering was finally based on the duration of impact so that the curve starts around 0.145 seconds and ends at 0.175 seconds. To get these results, the measured data below  $100 \text{ rad/s}$  was filtered out. The frequency spectrum of the calculated loads based on the filtered accelerations are shown in figure 6.13 and the calculated loads in the time domain, based on the filtered accelerations are shown in figure 6.14 and figure...

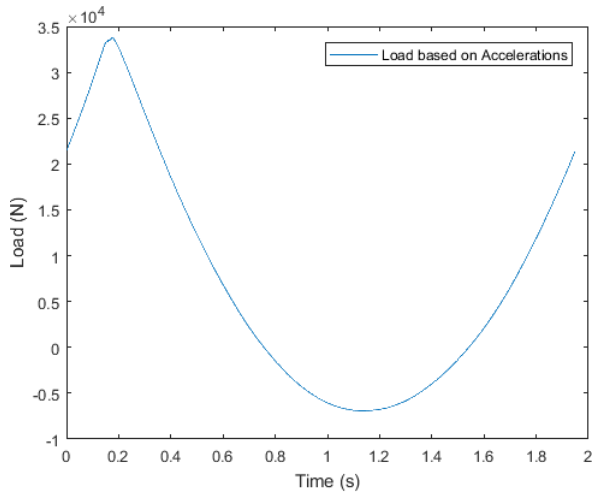


Figure 6.11: Example of computed loads by using accelerations, guide 1

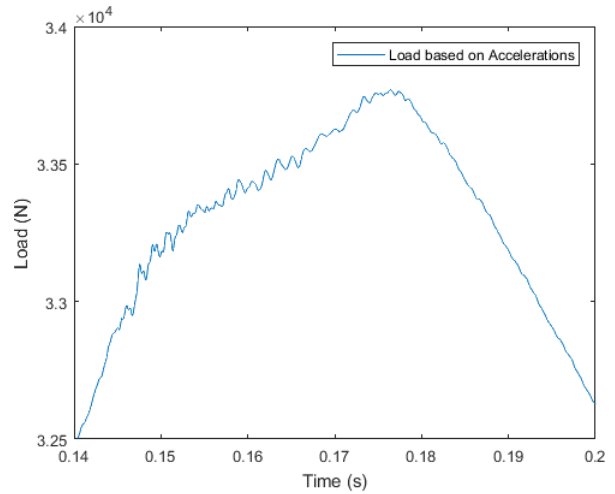


Figure 6.12: Example of computed loads curve zoomed in at impact Guide 1

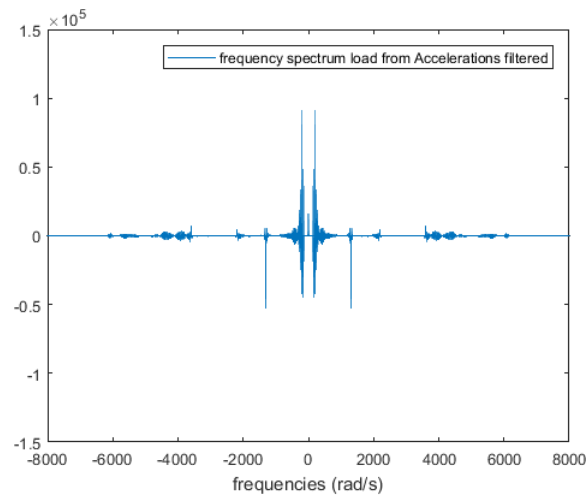


Figure 6.13: Frequency spectrum calculated load based on accelerations filtered

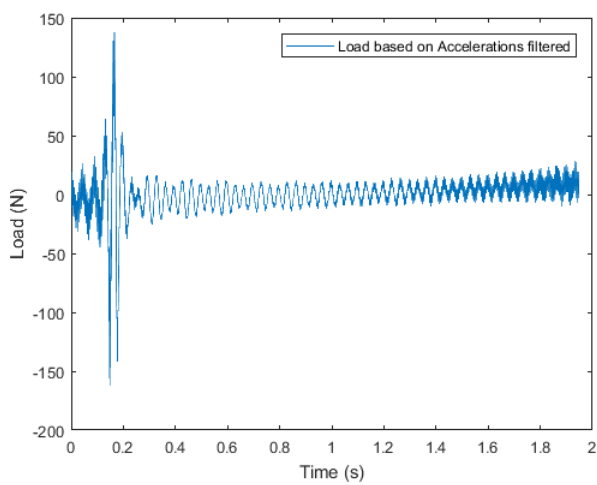


Figure 6.14: Example of computed loads based on filtered accelerations

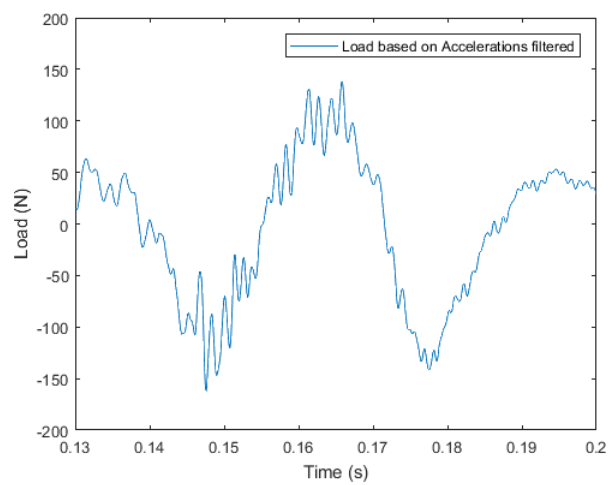


Figure 6.15: Example of computed loads based on filtered accelerations zoomed in at impact

The loads based on the curvature were computed similar to the loads based on the accelerations. The frequencies lower than  $100 \text{ rad/s}$  were filtered out. The filtered results of this method for the strains is shown below. The first figure show the calculated load in the frequency domain based on the filtered curvature (figure 6.16). The second and third show the computed load in the time domain (6.17 and 6.18). Figure 6.18 shows the load zoomed in at the impact.

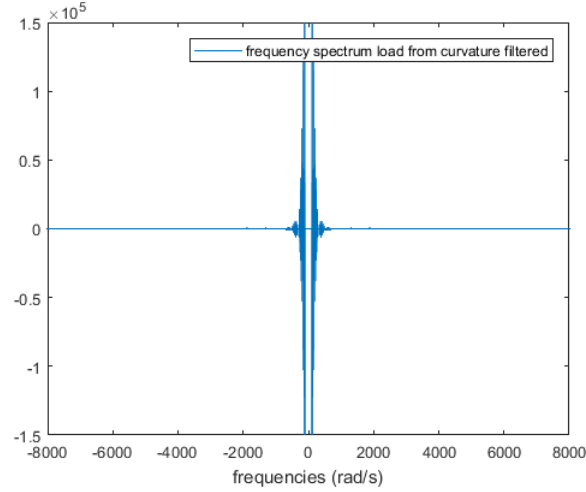


Figure 6.16: Example of computed loads, guide 1, zoomed in at impact

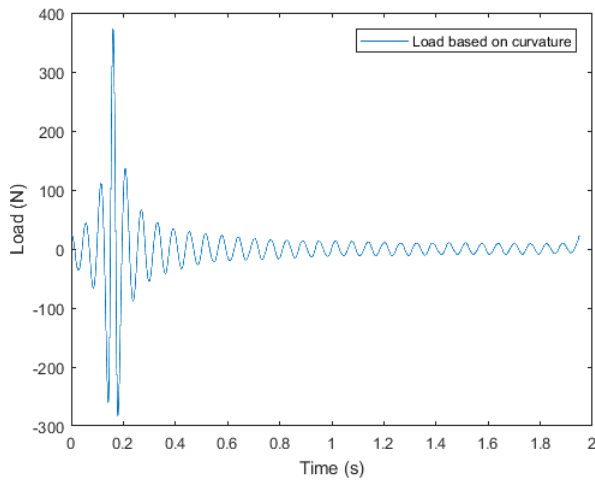


Figure 6.17: Example of computed loads, guide 1, zoomed in at impact

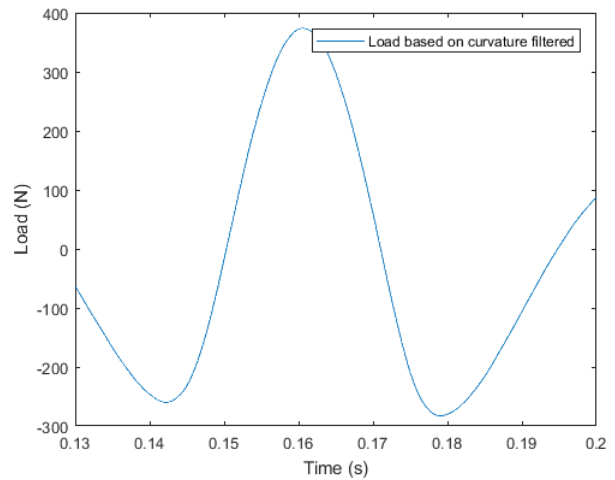


Figure 6.18: Example of computed loads curve only during impact Guide 1

To get the best estimation of the loads with this method, a least-square method should be used to combine the loads based on the accelerations and the loads based on the strains. Due to the large differences in the loads and an assumed error in the loads based on the accelerations, the external loads for the energy balance will only be based on the loads that were calculated with the curvature. More examples of the computed loads are shown in appendix D.

## 6.4. CALCULATIONS

This section will explain how all the needed parameters were extracted from the measurements and from the analytical model.

### 6.4.1. CURVATURE

The curvature

$$\epsilon(y) = y\kappa_y \quad (6.12)$$

$$\epsilon(z) = z\kappa_z \quad (6.13)$$

$$\epsilon(x) = x\sqrt{(\kappa_z^2 + \kappa_y^2)} \quad (6.14)$$

Where  $y$  is the distance from the center of the beam within the material in the  $y$ -direction and  $x$  is the distance from the center of the beam within the material in the  $x$ -direction. The curvature can be calculated with the following formula:

$$\kappa_z = \frac{\epsilon_{z2} - \epsilon_{z1}}{z_2 - z_1} \quad \kappa_y = \frac{\epsilon_{y2} - \epsilon_{y1}}{x_2 - x_1} \quad (6.15)$$

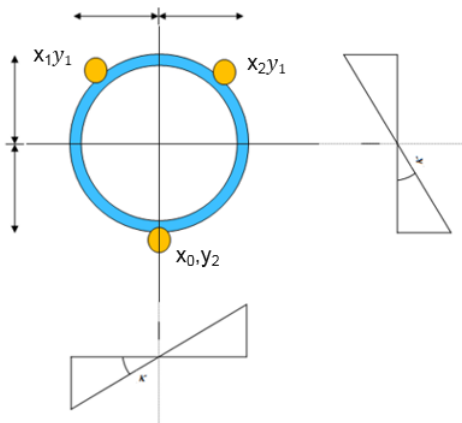


Figure 6.19: Schematic drawing curvature

To calculate the curvature in the  $x$ -direction, the curvature was assumed to be linear between the  $z$  and  $y$ -direction. Therefore the theorem of Pythagoras was used to calculate the curvature in the  $z$ -direction out of the curvature in the  $z$  and  $y$ -direction.

$$\epsilon(x) = x\sqrt{(\kappa_z^2 + \kappa_y^2)} \quad (6.16)$$

The curvature in the  $x$ -direction was compared to the curvature in the  $y$ -direction and the contribution of the curvature in the  $z$ -direction was so small that the curvature in the  $x$ -direction is assumed to be similar to the curvature in the  $y$ -direction, see figure 6.20 where the curvature in the  $y$ -direction lies almost exactly over the curvature in the  $x$ -direction.

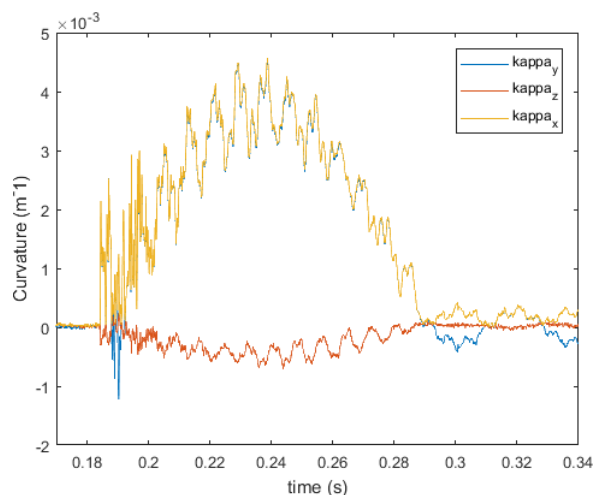


Figure 6.20: Curvature z, y vs x-direction

The moments are simply the curvature multiplied by  $EI$ ;

$$M = EI \frac{\partial^2 w(x, t)}{\partial x^2} \quad (6.17)$$

### 6.4.2. ROTATIONAL VELOCITY

The rotational velocity,  $\phi = \frac{\partial^2 w(x,t)}{\partial x \partial t}$  was computed by using the analytical model. To get the rotational velocity, the first derivative to space and frequency of the general solution was computed in the frequency domain:

$$\tilde{\phi} = -\gamma \omega \tilde{W} \tilde{F} \quad (6.18)$$

After transposing this equation back to the time domain and integrating it over the considered segment, it can be used as an input in the energy balance. The rotational velocity as a result of this method is shown below in figure

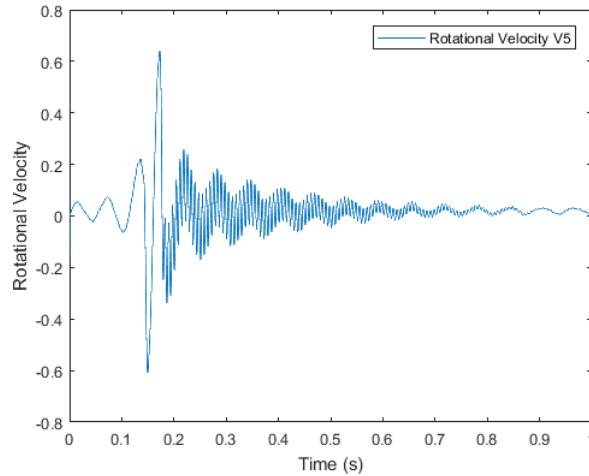


Figure 6.21: Rotational velocity at the location of impact (V5)

During the impact, the rotational velocity should only be positive as a result of the strain, which also occurs only in one direction. After the impact, the rotational velocity should fluctuate above and below zero as a result of free vibrations. Unfortunately the result do not show this.

### 6.4.3. VELOCITY

There are two different directions of the velocity needed to compute the complete energy balance. In the vertical part of the guides where only bending is assumed, only the velocity in the transverse direction of the guide is necessary to calculate the energy balance. This one can be easily calculated by integrating the measured accelerations in the transverse direction. Before integrating, the data should be filtered for lower frequencies. The first natural frequency of the guide without brace is  $182 \text{ rad/s}$ . Only the frequencies below  $100 \text{ rad/s}$  were filtered out to take some margins and the velocities before the impact were set to zero. An example of the data and the filtered and integrated velocity is shown below in figures 6.22 and 6.23.

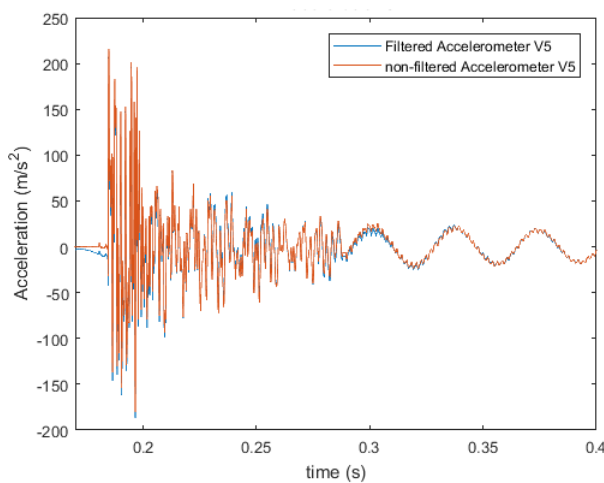


Figure 6.22: Filtered acceleration vs non-filtered acceleration V5

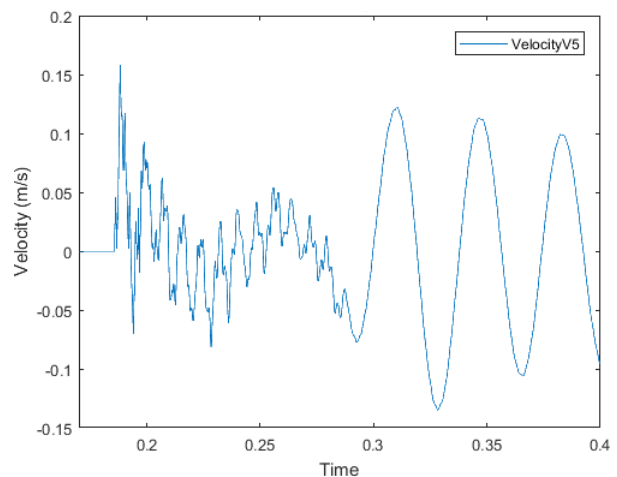


Figure 6.23: Integrated Accelerations V5

If the module hits the guides at brace height, a part of the brace is included in the energy balance. In this brace both bending and compression are assumed. For the bending part of the energy balance, the velocities in the transverse direction of the brace suffice, which can be computed similar to the velocities in the vertical part of the guides. To calculate the energy balance as a result of compression in the brace, the velocity in the axial direction is needed to calculate the internal energy. The velocities in the axial directions were subtracted for the analytical model discussed in section 6.3.

## 6.5. ENERGY BALANCE

The law of conservation of energy states that energy can be neither created nor destroyed. In a closed system, the total energy of the system is conserved, which is one of the basic laws of physics. It means that energy that enters a system minus energy that exits a system always has to be in equilibrium with the energy that is added to the system. Before the impact between the guides and bumpers, the guides are assumed to be in steady state, the behavior of the guides does not change over time. In this steady state, no vibrations nor strains are measured in the guides and bumper. The impulse load caused by the collision between the guides and the moving module, transfers energy into the guides and transforms the energy in the module. The energy transfer as a result of the collision is described as external energy over time ( $W_{extern}(t)$ ). The external energy that enters the system of the guides is equal to the change of internal energy in the system, plus the energy dissipated over time and the energy that flows out of the segment in question over time. The internal energy in the system is the energy in the segment in question of the guide that was enclosed by sensors on which the load was applied. For each of the impact locations a different segment is considered. The schematic example below (figure 6.24) shows the energy flow as a result of the external energy entering the segment on the guides ( $W_{extern}$ ) at brace height. This segment is enclosed by sensors at location  $L_0$  and  $L_1$ , the energy flux represents the energy that flows out of the segment in question through the cross-section at  $L_0$  and  $L_1$  ( $S_1$  and  $S_2$ ), ( $\frac{dE}{dt}$ ) is the change of internal energy inside the segment in question and ( $W_{dissipated}$ ) is the energy dissipated over time .

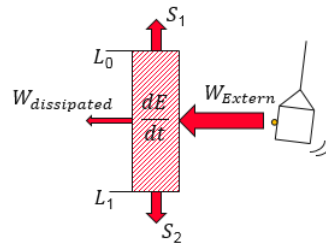


Figure 6.24: Schematic drawing of Energy balance

The energy balance is written in the following form:

$$W_{ext}(t) = \frac{dE(t)}{dt} \pm S(x, t) \Big|_{x=L_0}^{x=L_1} + W_{dis}(t) \quad (6.19)$$

Information about the energy balance and computation of the balance can be found in the paper written by S. S. Gómez ([8]).

### 6.5.1. EXTERNAL ENERGY

The external energy that enters the system over time is described as the magnitude of the load on the system multiplied with the velocity of the system (equation 6.20).

$$W_{ext}(t) = \int_0^L \delta(x) F(t, x) v(x, t) dx \quad (6.20)$$

The external energy that enters the guides is defined as the load from the module times the velocity of the guides, while the external energy that enters the bumper is defined as the load from the guides times the velocity of the module. The computation of the external forces ( $F$ ) are discussed in the previous paragraph. The velocity of the guides and bumper are taken as an average over the segment in question (between  $L_0$  and  $L_1$ ). The velocities are computed by integrating the measured accelerations at the cross-sections over time between  $L_0$  and  $L_1$ . The external energy rate for the base case is shown in figure 6.25.

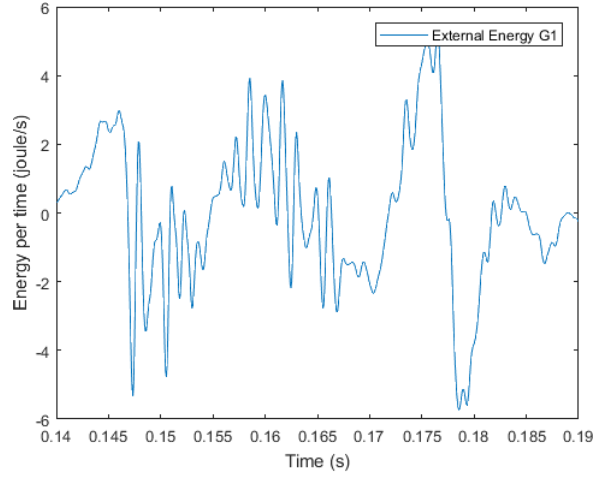


Figure 6.25: External energy rate entering guide 1 at the top of the guide

### 6.5.2. ENERGY RATE

The internal energy is the energy of the considered segment of the system (in the example between  $L_0$  and  $L_1$ ) comprising the kinetic energy and elastic energy stored in the segment over time. This energy is written as follows:

$$E(t) = \int_0^L \frac{1}{2} \rho A \left( \frac{\partial w(x, t)}{\partial t} \right)^2 + \frac{1}{2} EI \left( \frac{\partial^2 w(x, t)}{\partial x^2} \right)^2 dx \quad (6.21)$$

An example of the energy rate for the base case in guide 1 is shown in figure ?? below;

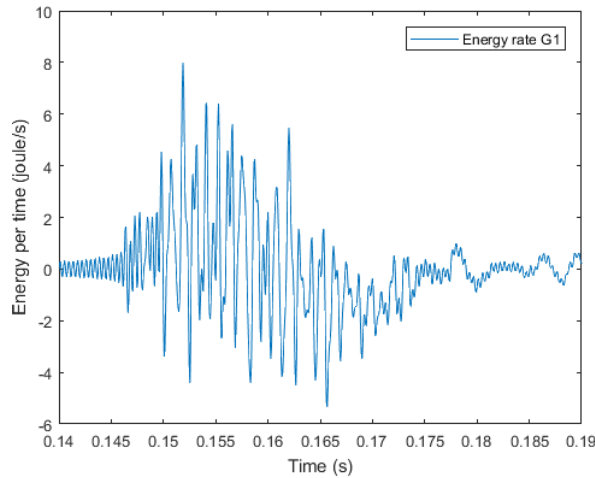


Figure 6.26: Energy rate in the top segment of guide 1

### 6.5.3. ENERGY FLUX

The energy flux is the energy that crosses the boundaries of the segment in question, the energy that flows through the cross-section at  $L_1$  and  $L_0$ . The energy flux is calculated by subtracting the beam and or bar energy from the potential and kinetic energy in the considered segment. This results in the following equation for the energy flux when only bending is assumed:

$$S(x_1, t) = EI \left( \frac{\partial w_1(x_1, t)}{\partial t} \frac{\partial^3 w_1(x_1, t)}{\partial x_1^3} - \frac{\partial^2 w_1(x_1, t)}{\partial t^2} \frac{\partial^2 w_1(x_1, t)}{\partial t \partial x_1} \right) \quad (6.22)$$

This can be simplified to the following equation:

$$S(L_0, t) = Q(L_0, t) \frac{\partial w}{\partial t} - M(L_0, t) \frac{\partial \phi}{\partial t} \Big|_{L_0} = -2 \left( M(L_0, t) \frac{\partial \phi}{\partial t} \right) \quad (6.23)$$

For the part where not only bending can be assumed (the brace), the equation for the energy flux is displayed below;

$$S(L_0, t) = Q(L_0, t) \frac{\partial w}{\partial t} - M \frac{\partial \phi}{\partial t} + Q(L_0, t) \frac{\partial u}{\partial t} = 2(M(L_0, t) \frac{\partial \phi}{\partial t}) + Q(L_0, t) \frac{\partial u}{\partial t} \quad (6.24)$$

The part of the equations with  $w$  considers the bending of the segments, while the equations with  $u$  consider the axial deformation of the segments.

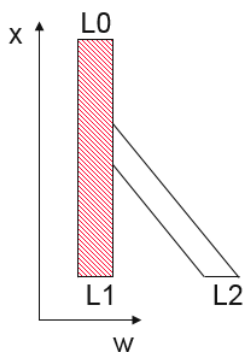


Figure 6.27: Example of beam segment, only bending is assumed

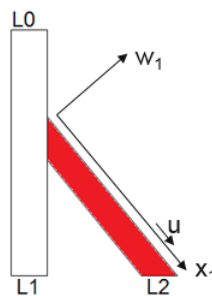


Figure 6.28: Example of Rod segment, both bending and axial compression is assumed

An example of the energy flux for the base case in guide 1 is shown in figure 6.29 below;

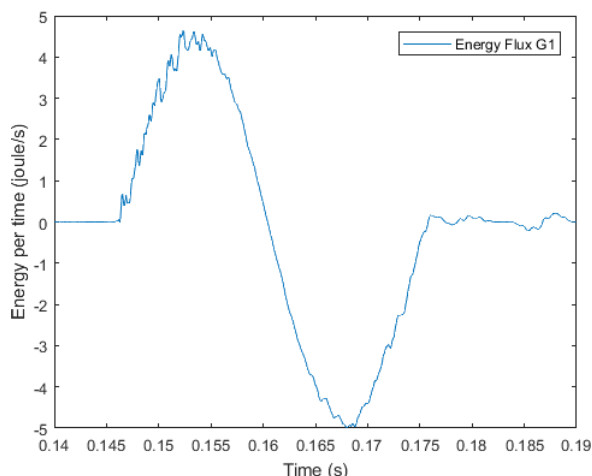


Figure 6.29: Energy flux through the cross-section at the location of the sensors of guide 1

The Energy flux is based on the rotational velocity, which is based on the response function derived to space and time, multiplied with the computed load in its turn. This energy flux shows that energy exits the cross-section and fully comes back during the impact. The negative part of the flux is the returning energy, this is due to the change in sign of the velocity After the impact small vibrations are still visible.

#### 6.5.4. ENERGY DISSIPATED

The energy dissipated is the transferred energy that was not measured with strain gauges and accelerometers during the experiment. This energy can be transferred into rotational energy of the module, friction energy between the bumper and guides, heat and other possible forms of energy dissipation. It is the energy that is 'left over' in the energy balance. Unfortunately due to the used method to calculate the load and rotational energy. The energy rate, energy flux and external energy fluctuate above and below zero at different time-steps due to the different frequency ranges of the strain gauges and accelerometers. The dissipated energy is calculated as a result of the energy balance with the following equation:

$$W_d(t) = W_{ext_3}(x, t) - \frac{dE(t)}{dt} - S(x, t) \quad (6.25)$$

Due to the different time-steps and the fluctuations above and below zero, the dissipated energy seems to be larger than expected, almost as large as the external energy itself.. An example of this dissipated energy is shown below in figure 6.30. Due to

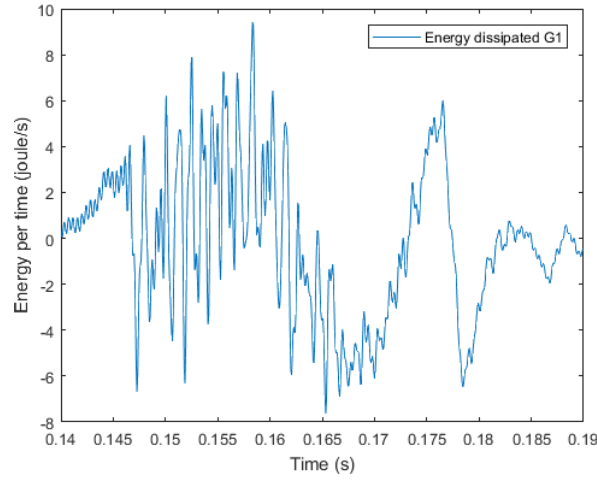


Figure 6.30: Dissipated energy guide 1

### 6.5.5. ENERGY BALANCE

With the three energy terms discussed in the previous sections, the energy balance can be computed. A schematic picture of the energy balance for each of the impact locations are displayed below.

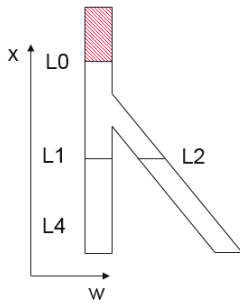


Figure 6.31: Impact location at the Top

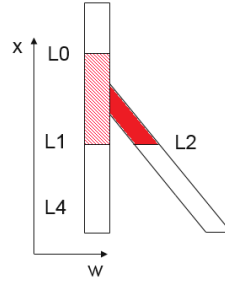


Figure 6.32: Impact location below at brace height

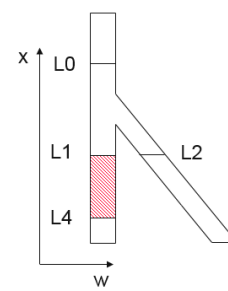


Figure 6.33: Impact location below the brace

The first figure (6.31) shows the segment in question when the bumper hits the guides at the top, the corresponding balance is displayed in equation 6.26(1). The second figure (6.32) shows the segment in question when the bumper hits the guides at brace height with corresponding equation 6.27(2) and the last figure (6.33) shows the segment in question of the impact below the brace. The balance is shown in equation 6.28(3).

$$W_{ext_1}(t) = \frac{dE}{dt} - S(L_0, t) + W_{dissipated_1}(t) \quad (6.26)$$

$$W_{ext_2}(t) = \frac{dE}{dt} \Big|_{L_1}^{L_0} + \frac{dE}{dt} \Big|_{L_2}^{L_0} + S(L_0, t) - S(L_1, t) - S(L_2, t) + W_{dissipated_2}(t) \quad (6.27)$$

$$W_{ext_3}(t) = \frac{\partial E}{\partial t} + S(L_1, t) - S(L_4, t) + W_{dissipated_3}(t) \quad (6.28)$$

### 6.5.6. RESULTS

Below four examples are shown of the energy balance. The first two figures shows the external energy, the energy rate and the energy flux (6.34 and 6.35). The third and fourth figures (?? and ??) show the computed damping as well (the purple line).

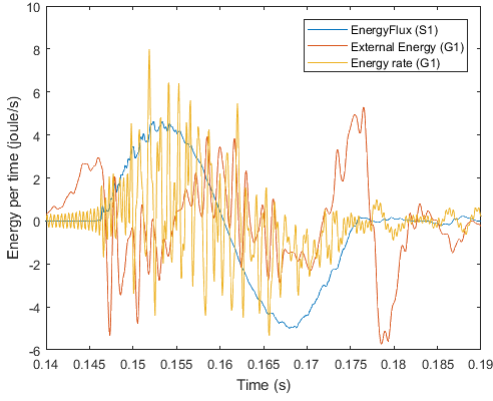


Figure 6.34: A combination of the internal energy rate, energy flux and external energy of guide 1, module deviation 12 cm

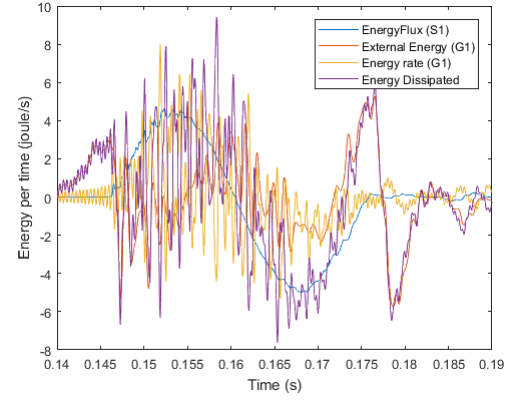


Figure 6.35: A combination of the energy dissipated, energy flux, internal energy rate and external energy of guide 1, module deviation 12 cm

These figures show that the external energy and the internal energy rate have some overlap. The external energy is smaller than the energy flux and energy rate, which is not possible in reality. This is probably due to the fact that the inputs are based on two different sets of sensors, which give different results and that the external load should be based on both accelerations and strain measurements. What one can conclude from these figures, is that almost all energy is transferred into the guide during the impulse, but that almost all energy is transferred back to the module again. After the impact, there is only a small amount of energy left in the form of free vibrations. This shows that this structure does not damp energy and that the energy transfer only occurs very shortly during the impact. This corresponds to an elastic response and to the CoR values that will be discussed in the next section.

## 6.6. COEFFICIENT OF RESTITUTION

The coefficient of Restitution is normally based on the returning height of a dropped object on a similar object of the same material. In this experiment the object is not dropped but horizontally moved to collide with another object. The objects do not have the same shape or weight, so the coefficient based on this experiment cannot be compared directly to the CoR based on dropped objects. With this experiment the energy before and after the collision are compared to one another. This has been done for the case studies of the guide with brace as well as the case studies of the guide without brace. The duration of the impact was based on the shape of the strains where one can easily determine the duration of the impact. The velocity before the impact was calculated by taking the displacement of the laser on 120 time-steps before the impact until 20 time-steps before the impact and dividing them by the time. For the velocity after the impact the displacement of the laser was taken 20 steps after the impact until 120 steps after the impact and divided by the time. The velocity before the impact was then divided by the velocity after the impact to determine the loss of energy during the impact, see equations 6.29, 6.30 and 6.31.

$$v_{before\_impact} = (Laser(tbI - 120) - Laser(tbI - 20)) / (T(tbI - 120) - T(tbI - 20)) \quad (6.29)$$

$$v_{after\_impact} = (Laser(tbE + 20) - Laser(tbE + 120)) / (T(tbE + 20) - T(tbE + 120)) \quad (6.30)$$

$$Cor = \frac{v_{before\_impact}}{v_{after\_impact}} \quad (6.31)$$

$tbI$  here is the starting moment of the impact,  $tbE$  is the end of the impact and  $laser(tbI - 120)$  is the displacement of the laser at 120 time-steps before the impact as well as  $T(tbI - 120)$  is the time at 120 time-steps before the impact.

By determining the start of the impact and the end of the impact, the duration of the impact can be calculated. With the known change in velocity (before and after the collision), the known mass of the module and the calculated duration of the impact, it is possible to estimate the equivalent load that was applied on the guides during the collision, with the following formula:

$$I = F\Delta t = m\Delta v \quad (6.32)$$

giving;

$$F = \frac{m\Delta v}{\Delta t} \quad (6.33)$$

Where  $\Delta t$  is the duration of the impact and  $\Delta v$  is the difference in velocity before and after the impact. The following section will show the results of the CoR and the estimated equivalent load for one case study for the guide with and without brace. The results are the averages taken over the ten runs per case study. The results of the other case studies can be found in appendix D. An overview of the values for all case studies is given below in table 6.5:

With Brace	CoR	F (N)		Without Brace	CoR	F (N)
B1U1G1W1	0.973	8.468		B1U1G1W1	0.986	1.497
B1U2G1W1	0.946	12.873		B1U2G1W1	0.971	2.171
B1U3G1W1	0.916	14.789		B1U3G1W1	0.948	2.770
B1U2G1W1	0.946	12.873		B1U2G1W1	0.971	2.171
B2U2G1W1	0.767	58.052		B2U2G1W1	0.924	6.424
B3U2G1W1	0.555	104.936		B3U2G1W1	0.924	4.843
B1U2G1W1	0.946	12.873		B1U2G1W1	0.971	2.171
B1U2G2W1	0.815	108.970		B1U2G2W1	0.742	30.374
B3U2G3W1	0.555	145.903		B3U2G3W1	0.924	90.675
B1U2G1W1	0.946	12.873		B1U2G1W1	0.971	2.171
B1U2G1W2	0.931	15.197		B1U2G1W2	0.974	1.973
B1U2G1W3	0.953	12.171		B1U2G1W3	0.962	3.197
B1U2G1W4	0.961	14.065		B1U2G1W4	0.983	1.851
B1U2G1W5	0.862	34.558		B1U2G1W5	0.969	2.462
B1U2G1W6	0.810	47.269		B1U2G1W6	0.940	4.793
B1U2G1W1	0.946	12.873		B1U2G1W1	0.971	2.171
B1U2G1W1M1	0.981	4.124		B1U2G1W1M1	0.968	2.300
B1U2G1W1M2	0.000	0.000		B1U2G1W1M2	0.946	2.908

Table 6.5: All CoR values and equivalent loads for all case studies

### 6.6.1. RESULTS COR AND LOAD, VARIATION IN IMPACT LOCATION

The first case study was the location of the impact on the guides; the top of the guide, at brace height and below the brace height and the bottom of the guide. Due to the limitations of the set-up, the impact location below the brace height and the bottom of the guide had to be combined with the bumper at its lowest position. The variation in impact location has effect on both magnitude of the load for the guide with brace as well as for the guide without brace. It was expected that the load at the brace height would be higher than the load between the brace and the bottom. The increase in load in relation to a lower stiffness at the lower impact location is expected to be caused by the different position of the bumper. This is probably the reason for the higher CoR at the lowest impact location. Based on these results the CoR depends on the stiffness of the structures as expected. The load increases if the stiffness increases as well, as was expected.

Case study: Impact Location	With Brace		No Brace	
	CoR	F (N)	CoR	F (N)
B1U2G1W1	0.95	11.05	0.97	2.17
B1U2G2W1	0.81	108.97	0.74	30.37
B3U2G3W1	0.73	145.90	0.53	90.68

Table 6.6: Calculated load and CoR for the variations in impact location; top, brace height and low for the guide with and without brace

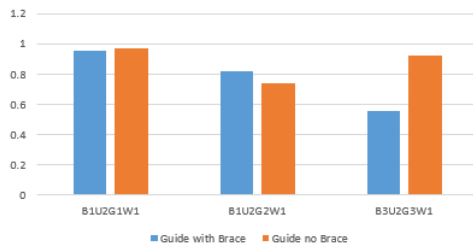


Figure 6.36: CoR of the variation in impact location of guide with brace vs. guide without brace

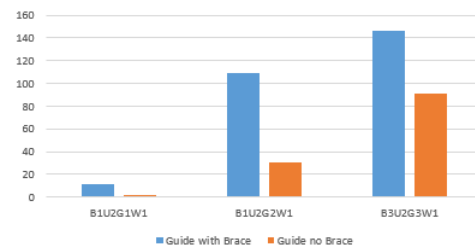


Figure 6.37: Load of the variation in impact location of guide with brace vs. guide without brace

### 6.6.2. CONCLUSION COR

The results show a relation between the CoR and the estimated equivalent loads. The CoR has a strong correlation to the stiffness of the structure in the case of the guide with brace. The change in CoG of the module has a large effect on CoR and equivalent loads for the guide with brace but it has a very small impact at the guide without brace. It seems that a higher CoG has more effect than a lower CoG. The change in deviation shows exactly what was to be expected, a larger deviation gives a smaller CoG but a larger load in a linear relation. The weight of the module does not seem to make large differences on the CoR although higher weights obviously cause larger loads. The damping material that was installed on the guides almost make no difference in equivalent loads or CoR. It is recommended to do further research on the change in CoG and the effects on the CoR.



# 7

## CONCLUSIONS AND RECOMMENDATIONS

### 7.1. CONCLUSIONS

The goal of this thesis was to determine the effect of energy transfer between guides and bumpers on the magnitude of the impact loads during offshore set-down. The first thing that could be concluded from the results, is that the deformation due to the pulse loads is linear elastic. This means that almost all energy goes back into the motion of the module. This corresponds to the high CoR values and the known fact that steel has a very low damping factor.

The shape of the impact was based on literature that concluded that the shape of the impact would be similar to half a sinus. The results of the experiment show that for all cases studies where the impact is dominated by one contact phase, the impact has a parabolic shape. With the fitting tool of MATLAB, the correlation between this shape and a quadratic curve was computed. For all cases apart from the cases where the response is not dominated by the deformation of the structure, but by the multiple collisions during the impact, there is a correlation higher than 0.979 to a quadratic curve. This means that the impact can be assumed to be linearly elastic in the cases where global deformation is dominant to the deformation that is dominated by what are assumed to be the shorter collisions between the steel structures. This conclusion is based on the results from the strain measurements.

As one can see from the results of the CoR computations, the CoR is lower in the case study where the module hits the guide at brace height. It is expected that that energy is transferred into local vibrations of the module and guide due to the higher stiffness of the guides at this location. The CoR is also lower than 0.9 when the bumper changes to a position above the CoG of the module or to a position below the CoG of the module. In these case studies, this response still has a high correlation with a linear elastic response. This could mean that the energy has been transferred to a different form than to the swinging motion of the module. It can be transferred to rotational energy of the module. Further research would be needed to conclude this.

From the strain measurements of the case study where the module hits the guide at brace height can be concluded that more strain is observed in the brace than below or above the impact location. With the energy balance it is possible to see which members of a steel structure receive higher volumes of energy. Based on these results it is possible to determine, when damping should be applied and in which members the damping should be applied.

The impulse loads were computed using an analytical model. In this analytical model, the damping ratio can be adjusted. Based on a number of frequency spectra, the best fit for this analytical model, was a damping ratio of 0.00002. Further research should determine the best fit for the damping ratio. Due to difficulties in transforming data from the frequency domain back in to the time domain, the computed pulse load based were compromised. These load curves shows a dominant shape on which the relevant loads are displayed. The reason for this dominant shape is probably a mathematical error that occurs when the pulse load (half a sinus) is transformed to the Fourier domain. By filtering out this dominant shape, a more accurate load curve can be computed. Data will be lost by applying a filter to the data. The applied load based on the curvature give a filtered load that lies between -200 and 400 newtons. The fact that the load has a negative value is due to the influences of the filtered data. The computed load based on the accelerations, lie between -100 and 150

newton.

The energy balance shows that almost all energy that is transferred into the structure, is transferred back to the module. This corresponds to the elastic behaviour that was concluded and the high CoR values. When the energy balance is properly adjusted so that it gives fully reliable values, it can show in which direction of the structure most of the energy flows. If this method is further elaborated, it is possible to base the design of the guides on energy transfer instead of on the computation of loads.

In the end there are three important conclusions; the first one is that the impulse loads can be assumed to be linear elastic. Based on these experiments a more accurately description of impulse loads can be used as an input for models, for both duration and shape. The second one is that based on these experiments, at least 97% of the energy is transferred back into motions of the module, the effect of energy transfer during impulse loads between the guides and bumper in this experiment has little to no effect on the magnitude of the loads and the third one is that this method will not give an accurate estimation of the loads.

## 7.2. RECOMMENDATIONS

It is important to state that the results derived from this research are speculations based on a scaled experiment. Conclusions on the magnitude of the load can not be based on this report, they can only be used as a guide for further research.

The loads that are calculated are part of the dominant shape that was not expected. Further research is recommended to find out how this dominant shape is computed and how it can be excluded from the loads. Once the loads are more reliable, it is possible to combine the loads based on the accelerations with the loads based on the strains and a more accurately conclusion can be drawn on the magnitude of the loads.

Only a few case studies were computed to estimate the applied loads due to the late discovery of an error in the model. It is recommended to compute the pulse loads for all case studies, so that a better comparison for the pulse load can be made.

To be able to compare the pulse loads to the static horizontal loads that are currently used as a criteria for the design of the guides and bumpers, the experiment should be scaled back to the demands for a full scale structure. The first step is to compare the deviation of the module in the experiment to the maximum allowable deviation in full scale. This will give an impression on the difference between the statically determined loads and the impulse loads that were determined during this research. The second step is to scale the wire of the experiment to the wire of the thialf for a the scaled weight. This will give an idea of the external energy that the full scale model can inflict on the guides. Comparing this with the computed external energy will give an idea of the scaling of energy between a full scale model and a scaled experiment. Together with full scale data, this will give new insides on the possibilities of this method.

One of the values that was used to estimate the loads, is the damping ratio. The damping ratio determines the response function and thus the estimated loads. For this research the damping ratio was set to 0.00002, based on a best fit using empirical data. From the measured data it is possible to determine the damping ratio for each of the case studies. The damping ratio was based on empirical data, but the damping could be computed using the measurements for each case study. With a more accurately calculated damping ratio, the estimated loads will probably be more accurate.

The results of this method should be compared to a finite element model to validate the use of the finite element model. With a finite element model, it is possible to use this method in all sorts of structures. The first step would be to test the same method on a full scale structure. According to this method, only two measurement points are necessary on a steel structure without junctions. This means that even on a full scale structure, only two accelerometers are needed to determine the loads. The results of a full scale test should than be compared to a finite element model of this full scale model. With reliable results and strain gauges at the measurement locations, it is possible to compute the energy balance for each structure. A comparison between the maximum accepted load and the external energy that is linked to this load, a maximum accepted external energy can be determined. With this maximum accepted energy, it is possible to say something about the maximum allowable motions and mass of the moving module.

# 8

## DISCUSSION

During this research, a number of assumptions have been made due to missing information. The first assumptions start at the experimental phase. In the analytical model, the guides are assumed to be clamped to the bottom. In the experimental set-up, the beams were welded to a steel plate that was screwed onto a 200 kg steel module. The guides can therefore not be assumed to be fully clamped. The second part of the set-up that could be improved are the sensors. The sensors measure up until certain frequencies. This means that it is possible that some of the higher frequencies have not been documented. This has been tested beforehand, and a decision had to be made on which frequencies have an engineering value and which frequencies have a scientific value. Based on this decision, frequencies over 7000 Hz were not taken into account in this research. The accelerometers can measure on a much lower maximum frequency range compared to the strain gauges. This means that the values based on the accelerometers are somewhat compromised. In the experiment, uni-axial sensors were used. This means that the accelerometers only measure the accelerations in the transverse direction. For the guide with brace, it was necessary to know the velocities in the longitudinal direction as well. This information was computed with the analytical model. Measurements would have been easily obtained by using multi-axial accelerometers.

The next step was analyzing the data. The data was analyzed and computed by using MATLAB. Within MATLAB the noise frequencies were canceled, which means you throw data away. This was necessary to get clean results in the energy balance, but again this means that the data is somewhat compromised. One of the steps in MATLAB was to integrate the measured accelerations to compute the velocities. To integrate within MATLAB, the lower frequencies should be filtered, otherwise the velocities would go to infinity, since they are multiplied with increasing time steps. Once again, the data is compromised.

The pulse loads that are computed with the analytical model are based on a certain damping ratio. The damping ratio was set at 0.000002 which is an empirically found value. From the measurements, a damping value can be derived as well. The damping value in the analytical model should be similar to the damping values derived from the experiment. This is an improvement that can predict more accurate pulse loads. The energy balance was computed by taking the load from the analytical model, the velocities from the acceleration measurements, the curvature from the strain measurements and the rotational velocity from the analytical model as well. The values were all analyzed at one location (x), to validate the estimated loads, the values should be analyzed at several locations to be compared to one another. The last point of interest is that the results are only based on three case studies, while the data of 38 case studies are available. By comparing the loads and energy balances of a larger number of case studies, more accurate conclusions could be drawn. The set-up of the analytical model was done in the three weeks before the deadline of this research. More information can be subtracted from this model if more time was put in extracting information from this analytical model. The experimental phase went well and the results of this experiment are very clear and extremely repeatable. The damping ratio for the structure can be extracted easily and more information about pulse loads can be extracted from the measurements. For a more complex structure, an analytical model is difficult to make, therefore the comparison between this analytical model and a FE model is of great use. I have enjoyed doing this research, the guidance in both the experimental set-up, the execution and the analytical phase was more than I could wish for!



# A

## EXPERIMENTAL SET-UP

### A.1. MATERIAL

The first picture (A.1) shows the clamps that were used to clamp the cable and therefore to adjust the cable length of the module. For the case studies where the bumper height needed to change or the impact location varied, these clamps were used to hang the module in the correct position. The turnbuckles (figure A.2) were used to level the module once the module hung at the correct height.

### A.2. LOAD CURVE

The load curve was used to scale the length of the wires. As one can see in the figure below (A.3), if the crane carries a load of 1000 tonnes, the radius of the hoist is approximately 92 meters. The scaling of the module wire was based on the estimations of this load curve.

### A.3. UNITY CHECK

A unity check was performed to determine whether the guides or bumper would fail (no plastic deformation) due to the applied load. The applied load was taken as twice the maximum allowed load, so 20% of the dry weight as a statically applied horizontal load. The unity check determines whether the stresses as a result of the applied load, do not exceed the maximum allowed stress and the UC should not be higher than 1. As one can see in the last column, the UC is a lot smaller than 1 and no plastic deformation of the guides or bumper is expected.



Figure A.1: Clamping system of cable to adjust length of cable between test variations



Figure A.2: Turnbuckle used to adjust cable length

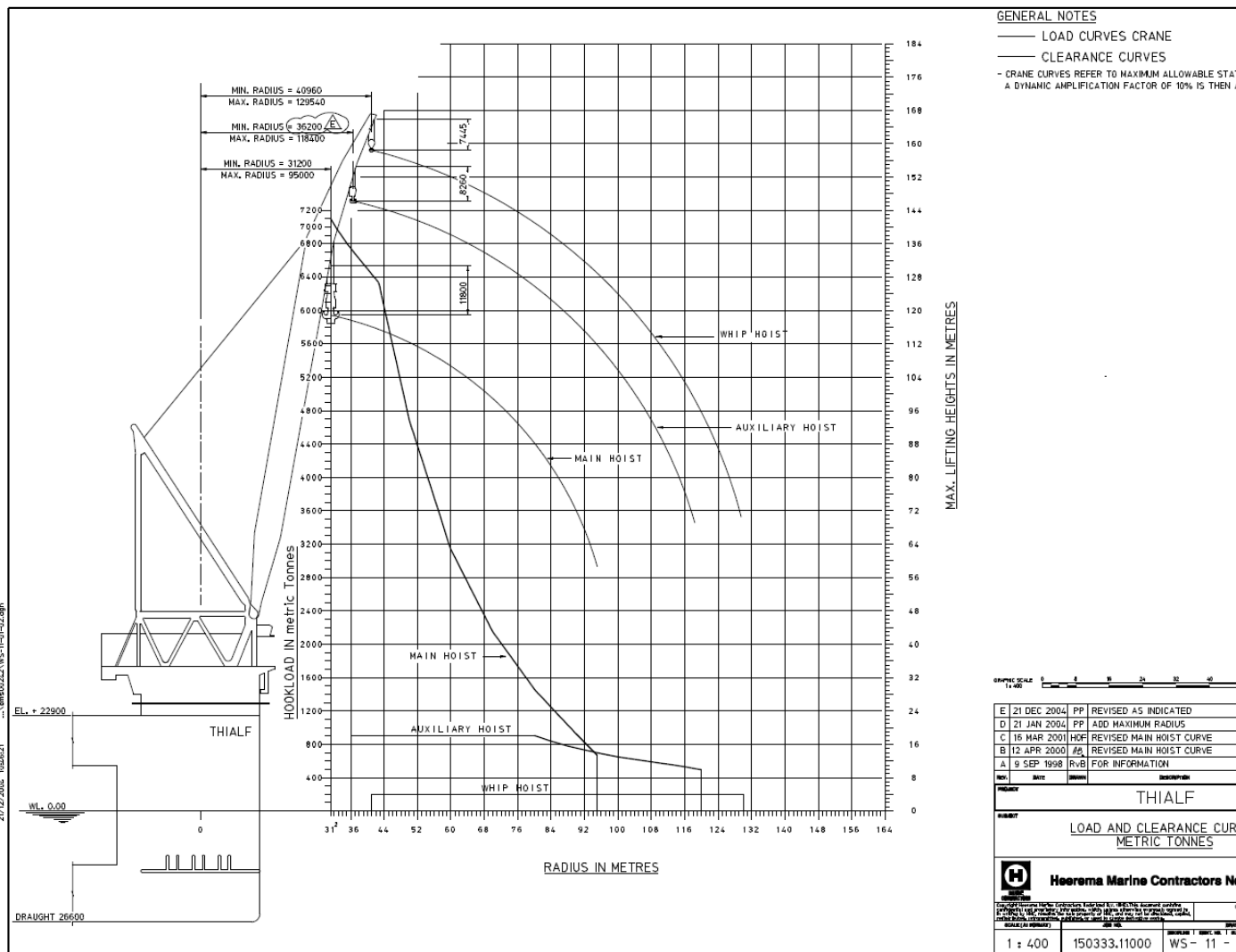


Figure A.3: Load and clearance curve Thialf

Length of Pipe (m)	Material	density (kg/m3)	length total module (m)	Do (m)	wall thickness (m)	Di (m)	Volume Pipe (m3)	mass module (kg)	Lenth pendulum (m)	Max hor motion (m)	Max height of drop (m)	Pot energy (N)	impact force	Eyield (N/mm2)
1	steel pipe	7850	27.95233	0.03	0.002	0.026	0.004918	38.6034	3.5	0.05	0.05	18.93497		235
0.7	steel pipe	7850	19.26116	0.03	0.0025	0.025	0.00416	32.65688	3.5	0.05	0.05	16.0182		235
0.7	steel koker	7850	19.36638	0.0269	0.00285	0.0212	0.00531	41.68099						235
Load case 1 (at top of guide/middle of bumper)	Fh (kN)	Fv (kN)	FL (kN)	Cross section area (mm2)	Moment of Inertia (mm4)	Section modulus (mm3)	Radius of Gyration (mm)	K	Slenderness <200	Compression stress (n/mm2)	Allowable stress = 0.566*Yield (AISC)	Unity check Compr/allow	Arm to Force (mm)	Moment Fh (Nmm)
"guide"	0.75	0.075	0.075	175.9291886	17329.02508	1155.268338	9.924717	1	100.7585	0.426308	133.01	0.003205	333	249750
"bumper" pipe	0.75	0.075	0.075	215.9844949	20586.02217	1372.401478	9.762812	1	71.70065	0.347247	133.01	0.002611	350	262500
"module" koker	0.75	0.075	0.075	274.17	26801.25987	1992.658727	9.887071	1	70.79953	0.273553	133.01	0.002057	350	262500
Bending stiffness EI (nmm2)														
"guide"	4072321													
"bumper" pipe	4837715													
"module" koker	6298296													
Bending stress FH (N/mm2)	Moment FL (Nmm)	Bending stress FL (N/mm2)	Length from top to brace (mm)	Rest length (mm)	Fshear Fh on brace point (kN)	Area under shear Ac	Final shear stress Fh (N/mm2)	Fshear Fl on brace point (kN)	Final shear stress Fl (N/mm2)	Combined stress due to all (N/mm2)	Unity check stress comb/0.6 6*yield			
216.1835408	24975	21.61835	333	666	1.125	87.96459	12.78924	0.1125	1.278924	218.4003	1.408126 <1?			
191.2705605	26250	19.12706	0	700	0.375	107.9922	3.472471	0.0375	0.347247	192.3204	1.239977 <1?			
131.733546	26250	13.17335	0	700	0.375	137.085	2.735529	0.0375	0.273553	132.4772	0.854141 <1?			

Figure A.4: Unity check for the guides and bumper



# B

## EXPERIMENTAL TESTS

### B.1. MEASUREMENTS

In this section, the differences between measurements will be shown. The first measurements are shown from the guide with brace and the guide without brace. The impact location for both these guides is 2 cm from the top.

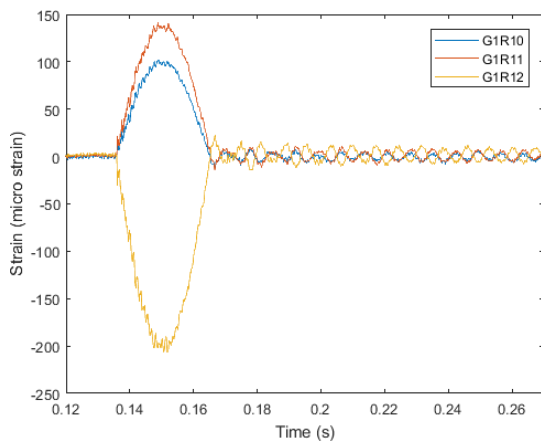


Figure B.1: Measurements of the three strains at the top of the guide without brace

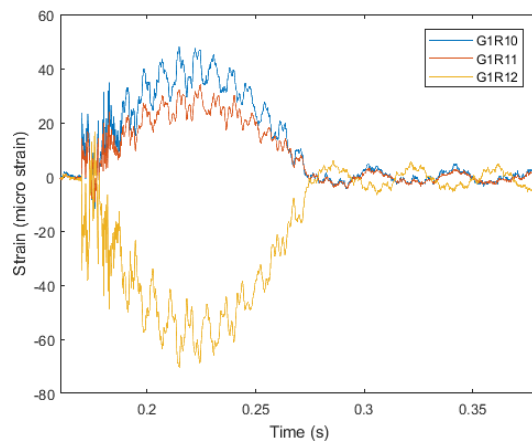


Figure B.2: Measurements of the three strains at the top of the guide with brace

The next figures show the difference between the guide with brace and without brace with the impact location below the brace, so at the lowest impact location. This location is 22 cm below the brace and 41 cm above the bottom of the guide.

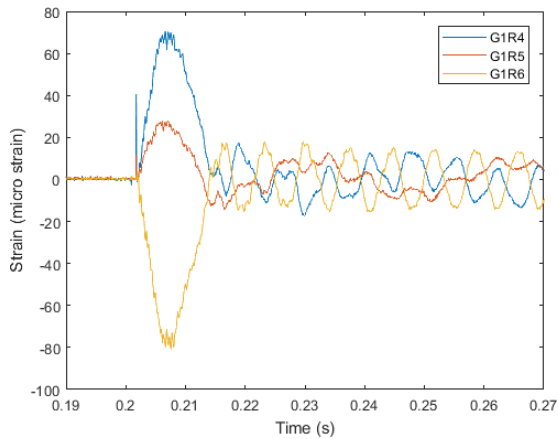


Figure B.3: Strain in the lowest sensors at the guide with impact at the lowest impact location, guide with brace

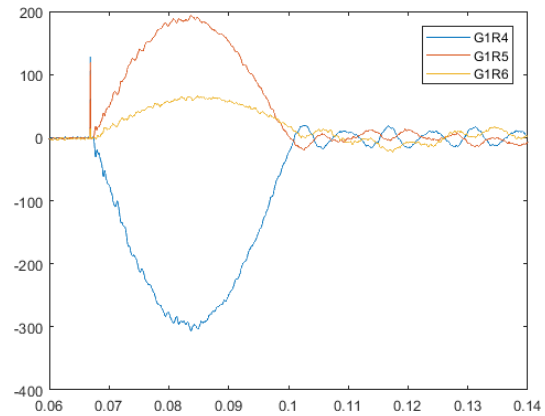


Figure B.4: Strain in the lowest sensors at the guide with impact at the lowest impact location, guide without brace

With the following picture (B.6) The strains above and below the impact load are compared to one another. The strain above the impact load seems to be a little higher, but this is due to the fact that the strain gauges are closer to the impact load than the strain gauges below the impact load. The frequencies of the vibration seem to be similar, but less consequent for the measurements below the impact (G1R4).

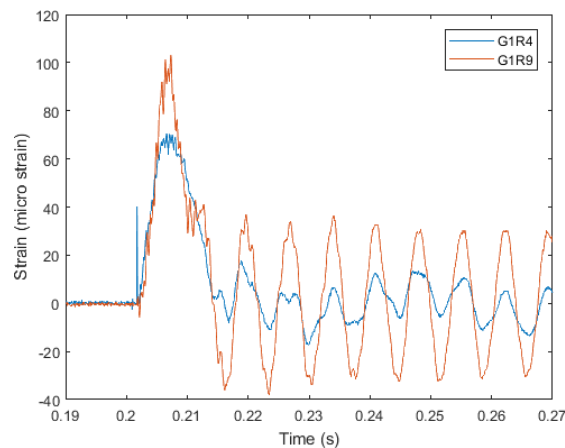


Figure B.5: Comparison maximum strain above and below impact at lowest impact location, G1R4 is below, G1R9 is above

The last picture shows the differences in strain with the impact at brace height. The maximum strains above the impact (G1R12) is compared with the maximum strain below the impact (G1R9) and the maximum strain in the brace (G1R3). One can see that the strains in the brace start later than the strains above and below the impact. This indicates that the strain waves have more difficulty with traveling around the beam (transverse to the brace) than in the longitudinal direction of the beam. The free vibrations in the brace are larger than the free vibrations above and below the impact. This indicates that more energy goes into the brace part during impact than above and below the impact.

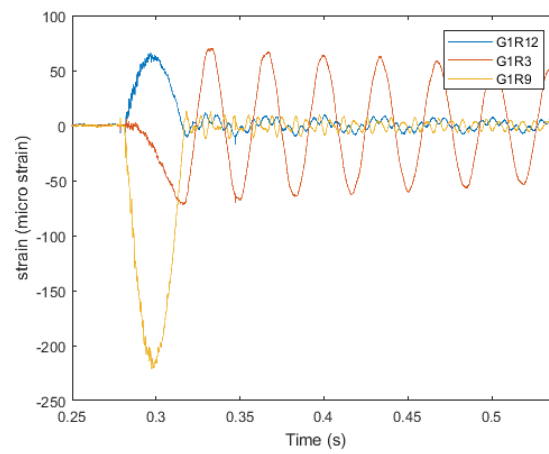


Figure B.6: Comparison maximum strain above, below and at brace for impact at brace height. G1R3 is at brace height, G1R9 is below and G1R12 is above.

## B.2. CASE STUDIES

This section shows all the different case studies with their exact values, locations etc. See figure

Variation	Nbr of Tests	Height Bumper	Distance start point (cm)	Impact location Guide	Weight (kg)	Location extra Weight	Pendulum Height (cm)	Height module rest (cm)	Height back module (cm)	Gap between guide and module (cm)	Material Type
B1U1G1W1-Wbr	15	Middle	15.5	Top (2 cm from top)	32.66		207	95.6	97.9	3.6	
B1U2G1W1-Wbr	20	Middle	12	Top (2 cm from top)	32.66		207	95.6	97.4	3.6	
B1U3G1W1-Wbr	20	Middle	9.3	Top (2 cm from top)	32.66		207	95.6	96.8	3.6	
B2U2G1W1-Wbr	20	Bottom	12	Top (2 cm from top)	32.66		183	119.5	121.5	3.6	
B2U3G1W1-Wbr	20	Bottom	9.3	Top (2 cm from top)	32.66		183	119.5	120.9	3.6	
B3U1G1W1-Wbr	12	Top (7.8 from	15.5	Top (2 cm from top)	32.66		230.7	71.1	72.9	3.2	
B3U2G1W1-Wbr	20	Top (7.8 from	12	Top (2 cm from top)	32.66		230.7	71.1	72.6	3.2	
B3U3G1W1-Wbr	15	Top (7.8 from	9.3	Top (2 cm from top)	32.66		230.7	71.1	73.3	3.2	
B1U2G1W1M1-Wbr	10	Middle	12	Top (2 cm from top)	32.66		206.8	95.4	97	3.2	Tape Pipe insulatio
B1U2G1W1M2-Wbr	10	Middle	12	Top (2 cm from top)	32.66		206.8	95.4	97	3.2	n
B1U2G1W2-Wbr	10	Middle	12	Top (2 cm from top)	36.9	Bottom left brace in the middle	206.8	95.4	97	3.2	
B1U2G1W3-Wbr	10	Middle	12	Top (2 cm from top)	41.17	Bottom left brace in the middle and bottom right brace middle	206.8	95.4	97	3.2	
B1U2G1W4-Wbr	10	Middle	12	Top (2 cm from top)	36.93	on top back middle brace	206.8	95.4	97	2.9	
B1U2G1W5-Wbr	10	Middle	12	Top (2 cm from top)	36.93	on top left brace middle	206.8	95.4	97	3	
B1U2G1W6-Wbr	10	Middle	12	Top (2 cm from top)	41.17	On top left brace middle and on bottom left brace middle	206.8	95.4	97	3.2	
B1U2G2W1-Wbr	10	Middle	12	Brace Height	32.66		237.3	64.8	66.4	3.2	
B1U3G2W1-Wbr	10	Middle	9.3	Brace Height	32.66		237.3	64.8	65.9	3.2	
B3U2G3W1-Wbr	10	Bottom	12	Bottom half 22 cm beneath welding, 41 cm from bottom	32.66		237.3	64.8	66.4	3.2	
B3U3G3W1-Wbr	10	Bottom	9.3	Bottom half 22 cm beneath welding, 41 cm from bottom	32.66		237.3	64.8	65.9	3.2	
B1U1G1W1-Nobr	10	Middle	15.5	Top (2 cm from top)	32.66		206.8	95.4	97.7	3.2	
B1U2G1W1-Nobr	10	Middle	12	Top (2 cm from top)	32.66		206.8	95.4	97.15	3.2	
B1U3G1W1-Nobr	10	Middle	9.3	Top (2 cm from top)	32.66		206.8	95.4	96.7	3.2	
B2U2G1W1-Nobr	10	Bottom	12	Top (6 cm from top)	32.66		185.1	117.3		3.4	
B2U3G1W1-Nobr	10	Bottom	9.3	Top (6 cm from top)	32.66		185.1	117.3	118.75	3.4	
B3U1G1W1-Nobr	10	Top (8.4 from	15.5	Top (2 cm from top)	32.66		230.9	71.6	73.8	3.6	
B3U2G1W1-Nobr	10	Top (8.4 from	12	Top (2 cm from top)	32.66		230.9	71.6	73.3	3.6	
B3U3G1W1-Nobr	10	Top (8.4 from	9.3	Top (2 cm from top)	32.66		230.9	71.6	72.15	3.6	
B1U2G1W1M1-Nobr	10	Middle	12	Top (2 cm from top)	32.66		206.8	95.4	97.15	3.2	Tape Pipe insulatio
B1U2G1W1M2-Nobr	10	Middle	12	Top (2 cm from top)	32.66		206.8	95.4	97.15	3.2	n
B1U2G1W2-Nobr	10	Middle	12	Top (2 cm from top)	36.94	Bottom left brace in the middle	206.8	95.4	97.15	3.2	
B1U2G1W3-Nobr	10	Middle	12	Top (2 cm from top)	41.17	Bottom left brace in the middle and bottom right brace middle	206.8	95.4	97.15	3.2	
B1U2G1W4-Nobr	10	Middle	12	Top (2 cm from top)	36.94	on top back middle brace	206.8	95.4	97.15	3.2	
B1U2G1W5-Nobr	10	Middle	12	Top (2 cm from top)	36.94	on top left brace middle	206.8	95.4	97.15	3.2	
B1U2G1W6-Nobr	10	Middle	12	Top (2 cm from top)	41.17	On top left brace middle and on bottom left brace middle	206.8	95.4	97.15	3.2	
B1U2G2W1-Nobr	10	Middle	12	Middle (32.6 from Top)	32.66		236.8	65.5	66.9	3.6	
B1U3G2W1-Nobr	10	Middle	9.3	Middle (32.6 from Top)	32.66		236.8	65.5	66.38	3.6	
B3U2G3W1-Nobr	10	Bottom(7.5 cr	12	Bottom (41.8 cm from bottom and 58.2 from top)	32.66		236.8	65.5	66.9	3.6	
B3U3G3W1-Nobr	10	Bottom(7.5 cr	9.3	Bottom (41.8 cm from bottom and 58.2 from top)	32.66		236.8	65.5	66.5	3.6	
B3U1G3W1-Nobr	11	Bottom(7.5 cr	15.5	Bottom (41.8 cm from bottom and 58.2 from top)	32.66		236.8	65.5		3.6	

Figure B.7: All cases studies for guide with and guide without brace

# C

## ANALYTICAL MODEL

### C.1. MODAL ANALYSIS GUIDE IN PYTHON

Using Sympy and Jupyter Notebooks

```
In [1]: from sympy import *
        from numpy import linalg
        import math
        import numpy as np
        import pandas as pd
        init_printing()
```

First we define which symbols to use for space, time and radial frequency.

```
In [2]: x, t, ω = symbols('x, t, ω')
```

#### C.1.1. GENERAL

##### BENDING VIBRATIONS

The governing differential equation for bending vibrations is as follows:

$$\rho A \frac{\partial^2 w}{\partial t^2} + EI \frac{\partial^4 w}{\partial x^4} + \alpha EI \frac{\partial^5 w}{\partial t \partial x^4} = 0$$

It can be rewritten into the frequency domain as:

$$-\omega^2 \rho A \times \tilde{w} + EI(1 + \alpha I \omega) \frac{d^4 \tilde{w}}{dx^4}$$

where:

$$\tilde{w}(\omega, x) = C(\omega) \times \exp(\lambda x)$$

The roots of the equation can be found by substituting the expression into the differential equation.

$$(-\omega^2 \rho A + EI(1 + \alpha I \omega) \lambda^4) \times C(\omega) \times \exp(\lambda x) = 0$$

Where the only non-trivial solution is found in:

$$-\omega^2 \rho A + EI(1 + \alpha I \omega) \lambda^4 = 0$$

Thus, the roots can be found:

$$\lambda = \pm \sqrt{\pm \sqrt{\frac{\omega^2 \cdot \rho A}{EI(1 + \alpha I \omega)}}}$$

### LONGITUDINAL VIBRATIONS

The differential equation for longitudinal vibrations is:

$$\rho A \frac{\partial^2 u}{\partial t^2} - EA \frac{\partial^2 u}{\partial x^2} - \alpha EA \frac{\partial^3 u}{\partial t \partial x^2} = 0$$

And in the frequency domain:

$$-\omega^2 \rho A \times \tilde{u} - EA(1 + \alpha I \omega) \frac{d^2 \tilde{u}}{dx^2} = 0$$

where:

$$\tilde{u}(\omega, x) = C(\omega) \times \exp(\beta x)$$

Substituting into the differential equation:

$$(-\omega^2 \rho A - EA(1 + \alpha I \omega)) \times C(\omega) \times \exp(\beta x) = 0$$

Here, the only non-trivial solution needs to comply with:

$$-\omega^2 \rho A - EA(1 + \alpha I \omega) \times \beta = 0$$

The roots are:

$$\beta = \pm I \times \left( \frac{\omega}{c} \cdot \sqrt{\frac{1}{(1 + \alpha I \omega)}} \right)$$

#### C.1.2. MODEL DESCRIPTION

The guide is subdivided into three sections: 1. Vertical section with length L1, between foundation and joint. 2. Vertical section with length L2, between joint and top. 3. Diagonal section with length L3, between foundation and joint.

Assumptions \* Axial and Bending motions for the vertical sections. \* Axial and Bending motions for the diagonal section. \* Local coordinate system for vertical beam with x pointing up and x=0 at the joint. \* Local coordinate system for diagonal beam with x pointing away from the brace and x=0 at the joint. \* Units are kg, N, m and s.

Note that in Python, index counting starts at 0 instead of 1.

#### C.1.3. MODEL PROPERTIES

Here, all model details are defined

Define the beam properties.

```
In [3]: d1 = 0.03 #m
        t1 = 0.0025 #m
        d3 = 0.0269 #m
        t3 = 0.00285 #m
        L1, L2, L3 = (0.667, 0.333, 0.871)
        theta = math.radians(50)
```

Define the material properties

```
In [4]: E = 210e9 #N/m**2
        rho = 7850 #kg/m**3
        c = sqrt(E/rho) # m/s
```

Calculate required beam properties from d, t, rho and E.

```
In [5]: class Section:
        def __init__(self, rho, E, d, t):
            self.r = d/2
            self.ri = self.r - t
            self.A = pi * (self.r**2 - self.ri**2)
```

```

self.I = pi/4 * (self.r**4 - self.ri**4)
self.rhoA = rho * self.A
self.EI = E * self.I
self.EA = E * self.A

```

```

sect1 = Section(rho, E, d1, t1)
sect3 = Section(rho, E, d3, t3)

```

Define damping coefficient

```

In [6]: # Assumed 0.00002
alpha = 0.00002

```

Define roots as a function of radial frequency for vertical (1) and diagonal section (3)

```

In [7]: gamma1 = (omega ** 2 * sect1.rhoA / (sect1.EI * (1 + I * omega))) ** 0.25
gamma3 = (omega ** 2 * sect3.rhoA / (sect3.EI * (1 + I * omega))) ** 0.25

```

```

In [8]: beta = omega/c * (1 / (1 + alpha * I * omega)) ** 0.5

```

#### C.1.4. GENERAL EXPRESSIONS

Define the constants to be used in the general expressions of the beam sections.

```

In [9]: C11, C12, C13, C14 = symbols('C11, C12, C13, C14')
C15, C16 = symbols('C15, C16')
C21, C22, C23, C24 = symbols('C21, C22, C23, C24')
C25, C26 = symbols('C25, C26')
C31, C32, C33, C34 = symbols('C31, C32, C33, C34')
C35, C36 = symbols('C35, C36')

```

Write the general expression for lateral displacement of a one dimensional beam for section 1.

```

In [10]: W1 = C11 * exp(I*gamma1*x) + C12 * exp(-I*gamma1*x) + C13 * exp(gamma1*x) + C14 * exp(-gamma1*x)
Phi1 = diff(W1, x)
M1 = -sect1.EI * diff(W1, x, x)
V1 = -sect1.EI * diff(W1, x, x, x)

```

Write the general expression for axial displacement of a one dimensional beam for section 1.

```

In [11]: U1 = C15 * exp(I*beta*x) + C16 * exp(-I*beta*x)
N1 = sect1.EA * diff(U1, x)

```

Similar for section 2.

```

In [12]: W2 = C21 * exp(I*gamma1*x) + C22 * exp(-I*gamma1*x) + C23 * exp(gamma1*x) + C24 * exp(-gamma1*x)
Phi2 = diff(W2, x)
M2 = -sect1.EI * diff(W2, x, x)
V2 = -sect1.EI * diff(W2, x, x, x)

```

```

In [13]: U2 = C25 * exp(I*beta*x) + C26 * exp(-I*beta*x)
N2 = sect1.EA * diff(U2, x)

```

And section 3.

```

In [14]: W3 = C31 * exp(I*gamma3*x) + C32 * exp(-I*gamma3*x) + C33 * exp(gamma3*x) + C34 * exp(-gamma3*x)
Phi3 = diff(W3, x)
M3 = -sect3.EI * diff(W3, x, x)
V3 = -sect3.EI * diff(W3, x, x, x)

```

```

In [15]: U3 = C35 * exp(I*beta*x) + C36 * exp(-I*beta*x)
N3 = sect3.EA * diff(U3, x)

```

### C.1.5. BOUNDARY CONDITIONS

No displacement or rotation or normal force at  $x = -L1$  for section 1.

```
In [16]: eq1 = expand(W1.subs(x, -L1))
         eq2 = expand(Φ1.subs(x, -L1))
         eq3 = expand(U1.subs(x, -L1))
```

A real, unit shear force at for section 2 and no bending moment or axial displacement at  $x = L2$  for section 2.

```
In [17]: eq4 = expand(M2.subs(x, L2))
         eq5 = expand(V2.subs(x, L2) - 1)
         eq6 = expand(N2.subs(x, L2))
```

No displacement and rotation at  $x = -L3$  for section 3.

```
In [18]: eq7 = expand(U3.subs(x, -L3))
         eq8 = expand(W3.subs(x, -L3))
         eq9 = expand(Φ3.subs(x, -L3))
```

Displacement continuity at the joint.

The angle between the horizontal and the diagonal brace is assumed  $\theta$ .

```
In [19]: eq10 = expand(W1.subs(x, 0) - W2.subs(x, 0))
         eq11 = expand(W1.subs(x, 0) - U3.subs(x, 0) * cos(θ))
         eq12 = expand(W1.subs(x, 0) - W3.subs(x, 0) * sin(θ))
         eq13 = expand(U1.subs(x, 0) - U3.subs(x, 0) * sin(θ))
```

Rotation continuity at the joint.

```
In [20]: eq14 = expand(Φ1.subs(x, 0) - Φ2.subs(x, 0))
         eq15 = expand(Φ1.subs(x, 0) - Φ3.subs(x, 0))
```

Moment continuity at the joint.

```
In [21]: eq16 = expand(M1.subs(x, 0) - M2.subs(x, 0) + M3.subs(x, 0))
```

Force balance at the joint, in vertical and horizontal directions respectively.

```
In [22]: eq17 = expand(N2.subs(x, 0) - N1.subs(x, 0) - V3.subs(x, 0) * sin(θ) - N3.subs(x, 0) * cos(θ))
         eq18 = expand(V2.subs(x, 0) - V1.subs(x, 0) + V3.subs(x, 0) * cos(θ) - N3.subs(x, 0) * sin(θ))
```

Generate a list of all equations:

```
In [23]: eqns = [eq1, eq2, eq3, eq4, eq5, eq6, eq7, eq8, eq9, eq10, eq11, eq12, eq13, eq14, eq15, eq16, eq17, eq18]
```

Rewrite into matrix form.

```
In [24]: A = linear_eq_to_matrix(eqns, (C11, C12, C13, C14, C15, C16, C21, C22, C23, C24, C25, C26, C27, C28, C29, C30, C31, C32, C33, C34, C35, C36, C37, C38, C39, C40, C41, C42, C43, C44, C45, C46, C47, C48, C49, C50, C51, C52, C53, C54, C55, C56, C57, C58, C59, C60, C61, C62, C63, C64, C65, C66, C67, C68, C69, C70, C71, C72, C73, C74, C75, C76, C77, C78, C79, C80, C81, C82, C83, C84, C85, C86, C87, C88, C89, C90, C91, C92, C93, C94, C95, C96, C97, C98, C99, C100, C101, C102, C103, C104, C105, C106, C107, C108, C109, C110, C111, C112, C113, C114, C115, C116, C117, C118, C119, C120, C121, C122, C123, C124, C125, C126, C127, C128, C129, C130, C131, C132, C133, C134, C135, C136, C137, C138, C139, C140, C141, C142, C143, C144, C145, C146, C147, C148, C149, C150, C151, C152, C153, C154, C155, C156, C157, C158, C159, C160, C161, C162, C163, C164, C165, C166, C167, C168, C169, C170, C171, C172, C173, C174, C175, C176, C177, C178, C179, C180, C181, C182, C183, C184, C185, C186, C187, C188, C189, C190, C191, C192, C193, C194, C195, C196, C197, C198, C199, C200, C201, C202, C203, C204, C205, C206, C207, C208, C209, C210, C211, C212, C213, C214, C215, C216, C217, C218, C219, C220, C221, C222, C223, C224, C225, C226, C227, C228, C229, C230, C231, C232, C233, C234, C235, C236, C237, C238, C239, C240, C241, C242, C243, C244, C245, C246, C247, C248, C249, C250, C251, C252, C253, C254, C255, C256, C257, C258, C259, C260, C261, C262, C263, C264, C265, C266, C267, C268, C269, C270, C271, C272, C273, C274, C275, C276, C277, C278, C279, C280, C281, C282, C283, C284, C285, C286, C287, C288, C289, C290, C291, C292, C293, C294, C295, C296, C297, C298, C299, C300, C301, C302, C303, C304, C305, C306, C307, C308, C309, C310, C311, C312, C313, C314, C315, C316, C317, C318, C319, C320, C321, C322, C323, C324, C325, C326, C327, C328, C329, C330, C331, C332, C333, C334, C335, C336, C337, C338, C339, C340, C341, C342, C343, C344, C345, C346, C347, C348, C349, C350, C351, C352, C353, C354, C355, C356, C357, C358, C359, C360, C361, C362, C363, C364, C365, C366, C367, C368, C369, C370, C371, C372, C373, C374, C375, C376, C377, C378, C379, C380, C381, C382, C383, C384, C385, C386, C387, C388, C389, C390, C391, C392, C393, C394, C395, C396, C397, C398, C399, C400, C401, C402, C403, C404, C405, C406, C407, C408, C409, C410, C411, C412, C413, C414, C415, C416, C417, C418, C419, C420, C421, C422, C423, C424, C425, C426, C427, C428, C429, C430, C431, C432, C433, C434, C435, C436, C437, C438, C439, C440, C441, C442, C443, C444, C445, C446, C447, C448, C449, C450, C451, C452, C453, C454, C455, C456, C457, C458, C459, C460, C461, C462, C463, C464, C465, C466, C467, C468, C469, C470, C471, C472, C473, C474, C475, C476, C477, C478, C479, C480, C481, C482, C483, C484, C485, C486, C487, C488, C489, C490, C491, C492, C493, C494, C495, C496, C497, C498, C499, C500, C501, C502, C503, C504, C505, C506, C507, C508, C509, C510, C511, C512, C513, C514, C515, C516, C517, C518, C519, C520, C521, C522, C523, C524, C525, C526, C527, C528, C529, C530, C531, C532, C533, C534, C535, C536, C537, C538, C539, C540, C541, C542, C543, C544, C545, C546, C547, C548, C549, C550, C551, C552, C553, C554, C555, C556, C557, C558, C559, C560, C561, C562, C563, C564, C565, C566, C567, C568, C569, C570, C571, C572, C573, C574, C575, C576, C577, C578, C579, C580, C581, C582, C583, C584, C585, C586, C587, C588, C589, C590, C591, C592, C593, C594, C595, C596, C597, C598, C599, C600, C601, C602, C603, C604, C605, C606, C607, C608, C609, C610, C611, C612, C613, C614, C615, C616, C617, C618, C619, C620, C621, C622, C623, C624, C625, C626, C627, C628, C629, C630, C631, C632, C633, C634, C635, C636, C637, C638, C639, C640, C641, C642, C643, C644, C645, C646, C647, C648, C649, C650, C651, C652, C653, C654, C655, C656, C657, C658, C659, C660, C661, C662, C663, C664, C665, C666, C667, C668, C669, C670, C671, C672, C673, C674, C675, C676, C677, C678, C679, C680, C681, C682, C683, C684, C685, C686, C687, C688, C689, C690, C691, C692, C693, C694, C695, C696, C697, C698, C699, C700, C701, C702, C703, C704, C705, C706, C707, C708, C709, C710, C711, C712, C713, C714, C715, C716, C717, C718, C719, C720, C721, C722, C723, C724, C725, C726, C727, C728, C729, C730, C731, C732, C733, C734, C735, C736, C737, C738, C739, C740, C741, C742, C743, C744, C745, C746, C747, C748, C749, C750, C751, C752, C753, C754, C755, C756, C757, C758, C759, C760, C761, C762, C763, C764, C765, C766, C767, C768, C769, C770, C771, C772, C773, C774, C775, C776, C777, C778, C779, C780, C781, C782, C783, C784, C785, C786, C787, C788, C789, C790, C791, C792, C793, C794, C795, C796, C797, C798, C799, C800, C801, C802, C803, C804, C805, C806, C807, C808, C809, C810, C811, C812, C813, C814, C815, C816, C817, C818, C819, C820, C821, C822, C823, C824, C825, C826, C827, C828, C829, C830, C831, C832, C833, C834, C835, C836, C837, C838, C839, C840, C841, C842, C843, C844, C845, C846, C847, C848, C849, C850, C851, C852, C853, C854, C855, C856, C857, C858, C859, C860, C861, C862, C863, C864, C865, C866, C867, C868, C869, C870, C871, C872, C873, C874, C875, C876, C877, C878, C879, C880, C881, C882, C883, C884, C885, C886, C887, C888, C889, C890, C891, C892, C893, C894, C895, C896, C897, C898, C899, C900, C901, C902, C903, C904, C905, C906, C907, C908, C909, C910, C911, C912, C913, C914, C915, C916, C917, C918, C919, C920, C921, C922, C923, C924, C925, C926, C927, C928, C929, C930, C931, C932, C933, C934, C935, C936, C937, C938, C939, C940, C941, C942, C943, C944, C945, C946, C947, C948, C949, C950, C951, C952, C953, C954, C955, C956, C957, C958, C959, C960, C961, C962, C963, C964, C965, C966, C967, C968, C969, C970, C971, C972, C973, C974, C975, C976, C977, C978, C979, C980, C981, C982, C983, C984, C985, C986, C987, C988, C989, C990, C991, C992, C993, C994, C995, C996, C997, C998, C999, C1000, C1001, C1002, C1003, C1004, C1005, C1006, C1007, C1008, C1009, C1010, C1011, C1012, C1013, C1014, C1015, C1016, C1017, C1018, C1019, C1020, C1021, C1022, C1023, C1024, C1025, C1026, C1027, C1028, C1029, C1030, C1031, C1032, C1033, C1034, C1035, C1036, C1037, C1038, C1039, C1040, C1041, C1042, C1043, C1044, C1045, C1046, C1047, C1048, C1049, C1050, C1051, C1052, C1053, C1054, C1055, C1056, C1057, C1058, C1059, C1060, C1061, C1062, C1063, C1064, C1065, C1066, C1067, C1068, C1069, C1070, C1071, C1072, C1073, C1074, C1075, C1076, C1077, C1078, C1079, C1080, C1081, C1082, C1083, C1084, C1085, C1086, C1087, C1088, C1089, C1090, C1091, C1092, C1093, C1094, C1095, C1096, C1097, C1098, C1099, C1100, C1101, C1102, C1103, C1104, C1105, C1106, C1107, C1108, C1109, C1110, C1111, C1112, C1113, C1114, C1115, C1116, C1117, C1118, C1119, C1120, C1121, C1122, C1123, C1124, C1125, C1126, C1127, C1128, C1129, C1130, C1131, C1132, C1133, C1134, C1135, C1136, C1137, C1138, C1139, C1140, C1141, C1142, C1143, C1144, C1145, C1146, C1147, C1148, C1149, C1150, C1151, C1152, C1153, C1154, C1155, C1156, C1157, C1158, C1159, C1160, C1161, C1162, C1163, C1164, C1165, C1166, C1167, C1168, C1169, C1170, C1171, C1172, C1173, C1174, C1175, C1176, C1177, C1178, C1179, C1180, C1181, C1182, C1183, C1184, C1185, C1186, C1187, C1188, C1189, C1190, C1191, C1192, C1193, C1194, C1195, C1196, C1197, C1198, C1199, C1200, C1201, C1202, C1203, C1204, C1205, C1206, C1207, C1208, C1209, C1210, C1211, C1212, C1213, C1214, C1215, C1216, C1217, C1218, C1219, C1220, C1221, C1222, C1223, C1224, C1225, C1226, C1227, C1228, C1229, C1230, C1231, C1232, C1233, C1234, C1235, C1236, C1237, C1238, C1239, C1240, C1241, C1242, C1243, C1244, C1245, C1246, C1247, C1248, C1249, C1250, C1251, C1252, C1253, C1254, C1255, C1256, C1257, C1258, C1259, C1260, C1261, C1262, C1263, C1264, C1265, C1266, C1267, C1268, C1269, C1270, C1271, C1272, C1273, C1274, C1275, C1276, C1277, C1278, C1279, C1280, C1281, C1282, C1283, C1284, C1285, C1286, C1287, C1288, C1289, C1290, C1291, C1292, C1293, C1294, C1295, C1296, C1297, C1298, C1299, C1300, C1301, C1302, C1303, C1304, C1305, C1306, C1307, C1308, C1309, C1310, C1311, C1312, C1313, C1314, C1315, C1316, C1317, C1318, C1319, C1320, C1321, C1322, C1323, C1324, C1325, C1326, C1327, C1328, C1329, C1330, C1331, C1332, C1333, C1334, C1335, C1336, C1337, C1338, C1339, C1340, C1341, C1342, C1343, C1344, C1345, C1346, C1347, C1348, C1349, C1350, C1351, C1352, C1353, C1354, C1355, C1356, C1357, C1358, C1359, C1360, C1361, C1362, C1363, C1364, C1365, C1366, C1367, C1368, C1369, C1370, C1371, C1372, C1373, C1374, C1375, C1376, C1377, C1378, C1379, C1380, C1381, C1382, C1383, C1384, C1385, C1386, C1387, C1388, C1389, C1390, C1391, C1392, C1393, C1394, C1395, C1396, C1397, C1398, C1399, C1400, C1401, C1402, C1403, C1404, C1405, C1406, C1407, C1408, C1409, C1410, C1411, C1412, C1413, C1414, C1415, C1416, C1417, C1418, C1419, C1420, C1421, C1422, C1423, C1424, C1425, C1426, C1427, C1428, C1429, C1430, C1431, C1432, C1433, C1434, C1435, C1436, C1437, C1438, C1439, C1440, C1441, C1442, C1443, C1444, C1445, C1446, C1447, C1448, C1449, C1450, C1451, C1452, C1453, C1454, C1455, C1456, C1457, C1458, C1459, C1460, C1461, C1462, C1463, C1464, C1465, C1466, C1467, C1468, C1469, C1470, C1471, C1472, C1473, C1474, C1475, C1476, C1477, C1478, C1479, C1480, C1481, C1482, C1483, C1484, C1485, C1486, C1487, C1488, C1489, C1490, C1491, C1492, C1493, C1494, C1495, C1496, C1497, C1498, C1499, C1500, C1501, C1502, C1503, C1504, C1505, C1506, C1507, C1508, C1509, C1510, C1511, C1512, C1513, C1514, C1515, C1516, C1517, C1518, C1519, C1520, C1521, C1522, C1523, C1524, C1525, C1526, C1527, C1528, C1529, C1530, C1531, C1532, C1533, C1534, C1535, C1536, C1537, C1538, C1539, C1540, C1541, C1542, C1543, C1544, C1545, C1546, C1547, C1548, C1549, C1550, C1551, C1552, C1553, C1554, C1555, C1556, C1557, C1558, C1559, C1560, C1561, C1562, C1563, C1564, C1565, C1566, C1567, C1568, C1569, C1570, C1571, C1572, C1573, C1574, C1575, C1576, C1577, C1578, C1579, C1580, C1581, C1582, C1583, C1584, C1585, C1586, C1587, C1588, C1589, C1590, C1591, C1592, C1593, C1594, C1595, C1596, C1597, C1598, C1599, C1600, C1601, C1602, C1603, C1604, C1605, C1606, C1607, C1608, C1609, C1610, C1611, C1612, C1613, C1614, C1615, C1616, C1617, C1618, C1619, C1620, C1621, C1622, C1623, C1624, C1625, C1626, C1627, C1628, C1629, C1630, C1631, C1632, C1633, C1634, C1635, C1636, C1637, C1638, C1639, C1640, C1641, C1642, C1643, C1644, C1645, C1646, C1647, C1648, C1649, C1650, C1651, C1652, C1653, C1654, C1655, C1656, C1657, C1658, C1659, C1660, C1661, C1662, C1663, C1664, C1665, C1666, C1667, C1668, C1669, C1670, C1671, C1672, C1673, C1674, C1675, C1676, C1677, C1678, C1679, C1680, C1681, C1682, C1683, C1684, C1685, C1686, C1687, C1688, C1689, C1690, C1691, C1692, C1693, C1694, C1695, C1696, C1697, C1698, C1699, C1700, C1701, C1702, C1703, C1704, C1705, C1706, C1707, C1708, C1709, C1710, C1711, C1712, C1713, C1714, C1715, C1716, C1717, C1718, C1719, C1720, C1721, C1722, C1723, C1724, C1725, C1726, C1727, C1728, C1729, C1730, C1731, C1732, C1733, C1734, C1735, C1736, C1737, C1738, C1739, C1740, C1741, C1742, C1743, C1744, C1745, C1746, C1747, C1748, C1749, C1750, C1751, C1752, C1753, C1754, C1755, C1756, C1757, C1758, C1759, C1760, C1761, C1762, C1763, C1764, C1765, C1766, C1767, C1768, C1769, C1770, C1771, C1772, C1773, C1774, C1775, C1776, C1777, C1778, C1779, C1780, C1781, C1782, C1783, C1784, C1785, C1786, C1787, C1788, C1789, C1790, C1791, C1792, C1793, C1794, C1795, C1796, C1797, C1798, C1799, C1800, C1801, C1802, C1803, C1804, C1805, C1806, C1807, C1808, C1809, C1810, C1811, C1812, C1813, C1814, C1815, C1816, C1817, C1818, C1819, C1820, C1821, C1822, C1823, C1824, C1825, C1826, C1827, C1828, C1829, C1830, C1831, C1832, C1833, C1834, C1835, C1836, C1837, C1838, C1839, C1840, C1841, C1842, C1843, C1844, C1845, C1846, C1847, C1848, C1849, C1850, C1851, C1852, C1853, C1854, C1855, C1856, C1857, C1858, C1859, C1860, C1861, C1862, C1863, C1864, C1865, C1866, C1867, C1868, C1869, C1870, C1871, C1872, C1873, C1874, C1875, C1876, C1877, C1878, C1879, C1880, C1881, C1882, C1883, C1884, C1885, C1886, C1887, C1888, C1889, C1890, C1891, C1892, C1893, C1894, C1895, C1896, C1897, C1898, C1899, C1900, C1901, C1902, C1903, C1904, C1905, C1906, C1907, C1908, C1909, C1910, C1911, C1912, C1913, C1914, C1915, C1916, C1917, C1918, C1919, C1920, C1921, C1922, C1923, C1924, C1925, C1926, C1927, C1928, C1929, C1930, C1931, C1932, C1933, C1934, C1935, C1936, C1937, C1938, C1939, C1940, C1941, C1942, C1943, C1944, C1945, C1946, C1947, C1948, C1949, C1950, C1951, C1952, C1953, C1954, C1955, C1956, C1957, C1958, C1959, C1960, C1961, C1962, C1963, C1964, C1965, C1966, C1967, C1968, C1969, C1970, C1971, C1972, C1973, C1974, C1975, C1976, C1977, C1978, C1979, C1980, C1981, C1982, C1983, C1984, C1985, C1986, C1987, C1988, C1989, C1990, C1991, C1992, C1993, C1994, C1995, C1996, C1997, C1998, C1999, C2000, C2001, C2002, C2003, C2004, C2005
```

Write to DataFrame, add radial frequencies as index column and rename columns to constants named in general expressions.

```
In [27]: df = pd.DataFrame(_)  
         df['radial frequencies'] = pd.Series(w_range)  
         df = df.rename(columns={0: 'C11', 1: 'C12', 2: 'C13', 3: 'C14', 4: 'C15', 5: 'C16',  
                                6: 'C21', 7: 'C22', 8: 'C23', 9: 'C24', 10: 'C25', 11: 'C26',  
                                12: 'C31', 13: 'C32', 14: 'C33', 15: 'C34', 16: 'C35', 17: 'C36'})  
         df = df.set_index('radial frequencies')
```

Export to csv file named 'constants.csv'

```
In [28]: with open('constants_B1U2G1.csv', 'w') as f:  
         f.write(df.to_csv())
```



# D

## RESULTS

### D.1. FREQUENCIES

The loads were calculated in the frequency domain. Below one can find the frequency spectra of the measurements and the response functions that was used to calculate the applied loads.

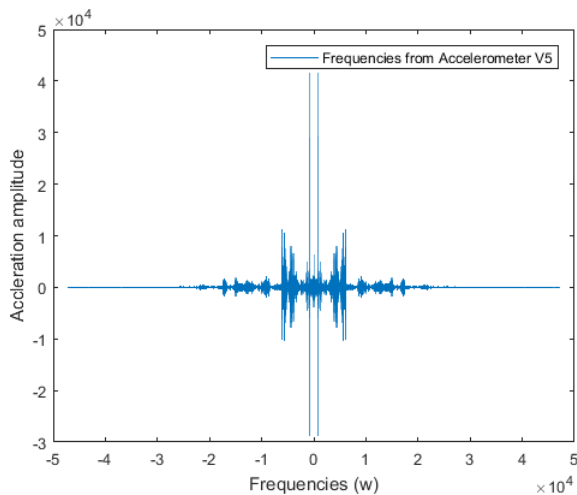


Figure D.1: Frequencies of the accelerations at V5

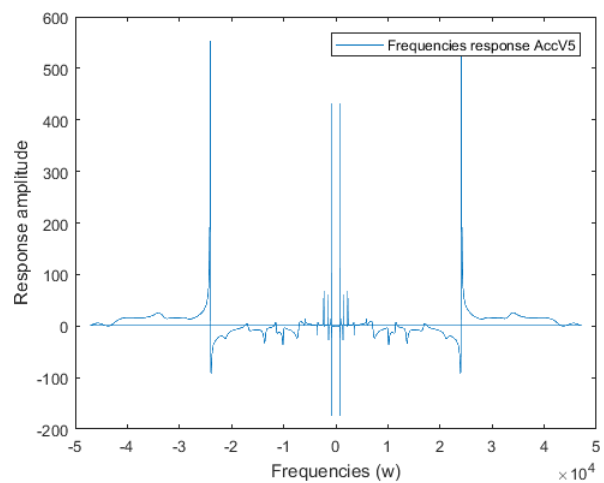


Figure D.2: Frequencies of the response function for accelerations

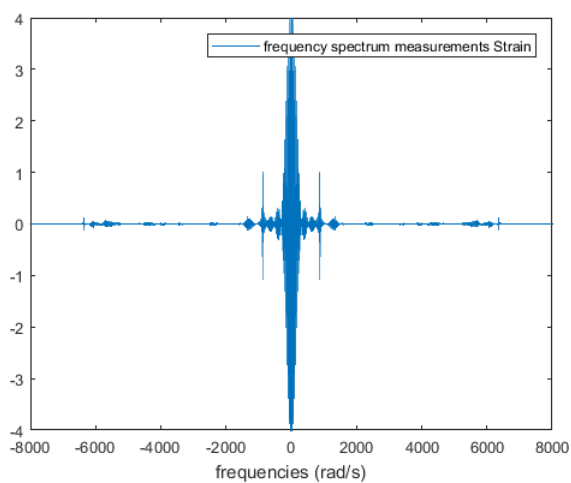


Figure D.3: Frequency spectrum of measured strain

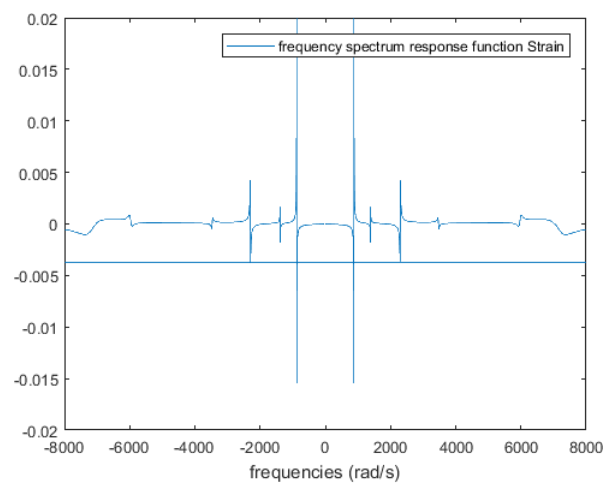


Figure D.4: Frequency spectrum of Response function for strains based on unit load 1

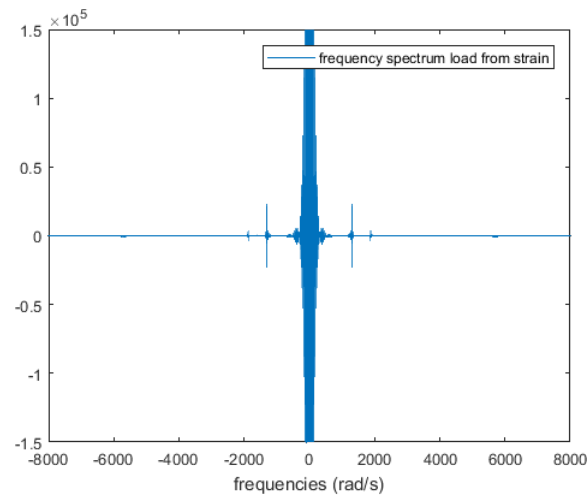


Figure D.5: Load in frequency spectrum based on curvature

## D.2. LOAD RESULTS

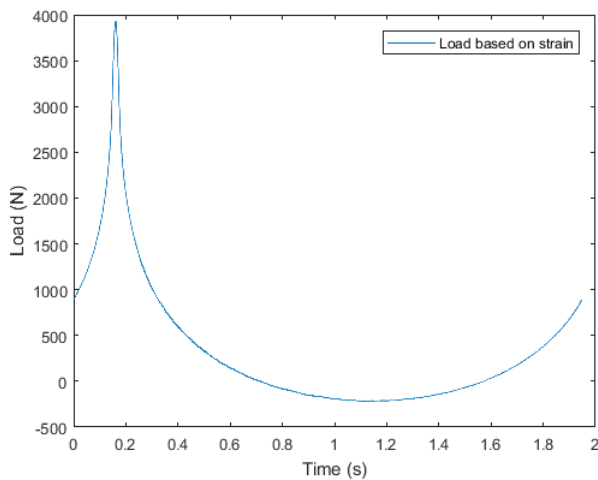


Figure D.6: Example of computed loads based on curvature non filtered

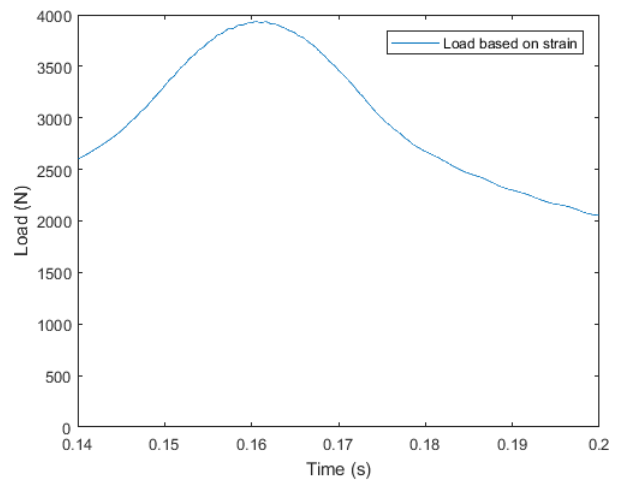


Figure D.7: Example of computed loads non filtered, zoomed in on impact

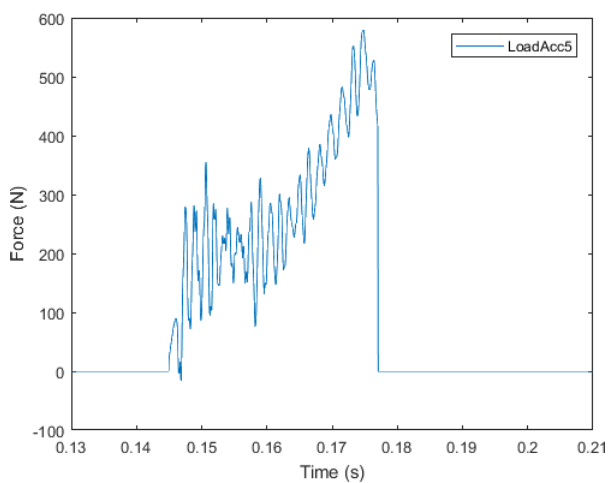


Figure D.8: Computed load case B1U2G1W1 at accelerometer V5, impact location top of guide 1

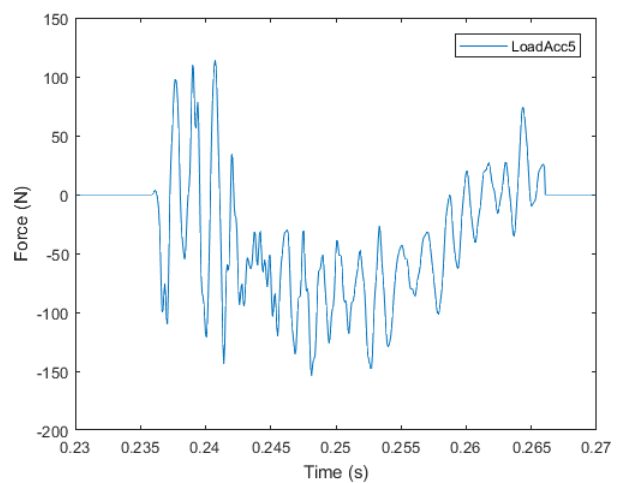


Figure D.9: Computed load case B1U3G1W1 at accelerometer V5, impact location top of guide 1

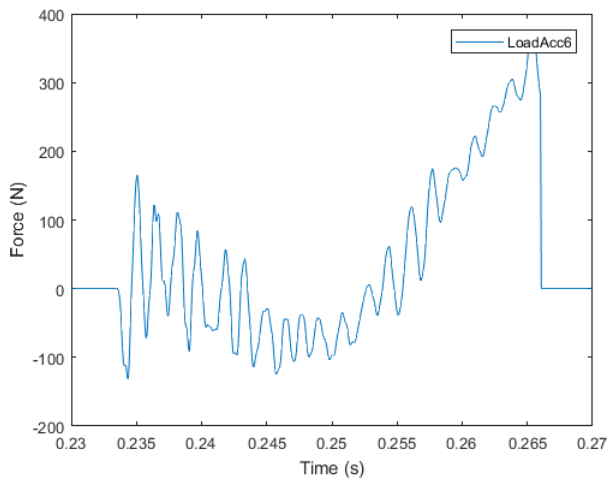


Figure D.10: Computed load case B1U2G1W1 at accelerometer V6, impact location top of guide 1

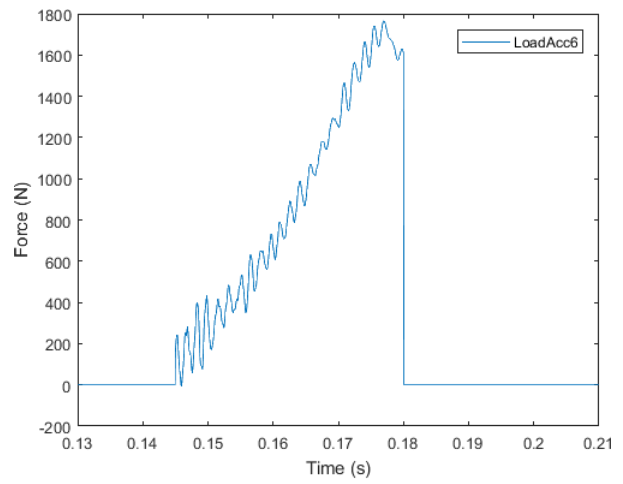


Figure D.11: Computed load case B1U3G1W1 at accelerometer V6, impact location top of guide 1

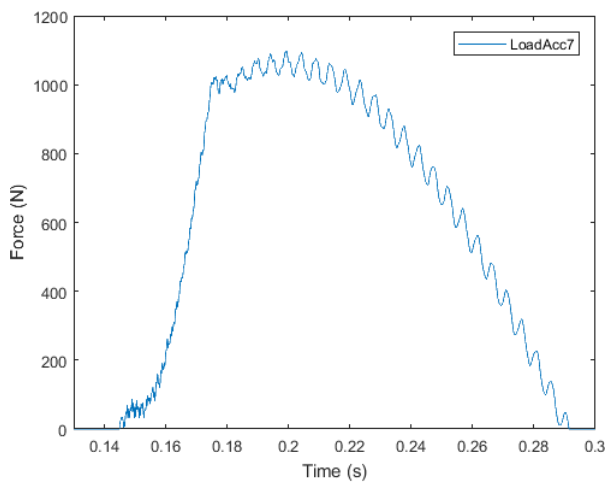


Figure D.12: Computed load case B1U2G1W1 at accelerometer V7, impact location top of guide 1

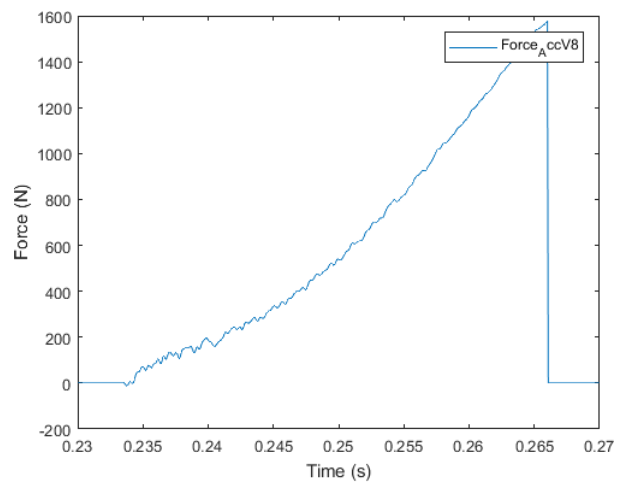


Figure D.13: Computed load case B1U2G1W1 at accelerometer V8, impact location top of guide 1

### D.3. ENERGY BALANCE RESULTS

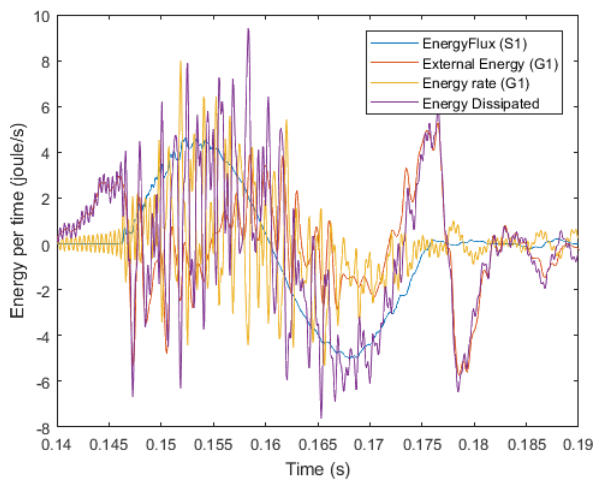


Figure D.14: A combination of the energy dissipated, energy flux and external energy of guide 1, module deviation 15.5 cm

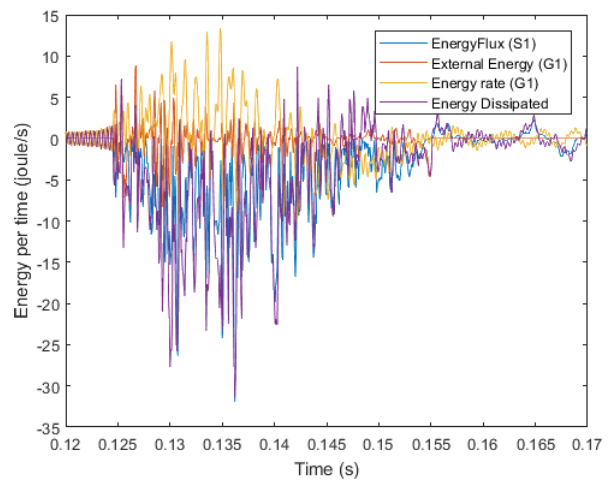


Figure D.15: A combination of the energy dissipated, energy flux, external energy and dissipated energy of guide 1, module deviation 15.5 cm

## D.4. CoR

the following sections will show the results of the CoR and the estimated load for all case study for the guide with and without brace. In each section only one parameter is changed, except for the impact location below the brace, the bumper height had to be adjusted to make this test case study. Each of the test cases was run at least ten times. The results are the averages taken over these ten runs per case study.

### D.4.1. RESULTS CoR AND LOAD, VARIATION IN IMPACT LOCATION

The first case study was the location of the impact on the guides; the top of the guide, at brace height and below the brace height and the bottom of the guide. Due to the limitations of the set-up, the impact location below the brace height and the bottom of the guide had to be combined with the bumper at its lowest position. The variation in impact location has effect on both magnitude of the load for the guide with brace as well as for the guide without brace. It was expected that the load at the brace height would be higher than the load between the brace and the bottom. The increase in load in relation to a lower stiffness at the lower impact location is expected to be caused by the different position of the bumper. This is probably the reason for the higher CoR at the lowest impact location. Based on these results the CoR depends on the stiffness of the structures as expected. The load increases if the stiffness increases as well, as was expected.

Case study: Impact Location	With Brace		No Brace	
	CoR	F (N)	CoR	F (N)
B1U2G1W1	0.95	11.05	0.97	2.17
B1U2G2W1	0.81	108.97	0.74	30.37
B3U2G3W1	0.55	145.90	0.92	90.68

Table D.1: Calculated load and CoR for the variations in impact location; top, brace height and low for the guide with and without brace

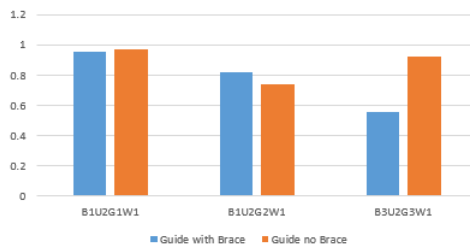


Figure D.16: CoR of the variation in impact location of guide with brace vs. guide without brace

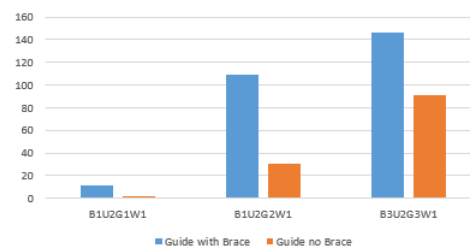


Figure D.17: Load of the variation in impact location of guide with brace vs. guide without brace

### D.4.2. RESULTS CoR AND LOAD, VARIATION IN BUMPER HEIGHT MODULE

The second case study was the position of the bumper on the module. The bumper was moved to the top of the module giving the module a CoG above the midpoint of the module and to the lowest point on the module, giving the module a CoG below the midpoint of the module. The results show that the effect of the position of the bumper and thus the CoG of the module has a larger effect on the guide with brace than the guide without brace. The higher/lower CoG causes instability in the movement of the module during its swing, increasing the velocity and thus the applied load. The higher stiffness of the guide with brace increases the effect of this positioning of the bumper.

case study: Bumper Height	With Brace		No Brace	
	CoR	F (N)	CoR	F (N)
B1U2G1W1	0.95	11.05	0.97	2.17
B2U2G1W1	0.77	58.05	0.95	4.65
B3U2G1W1	0.55	104.94	0.92	4.84

Table D.2: Calculated load and CoR for the variation in bumper height; middle, low and high for the guide with and without brace

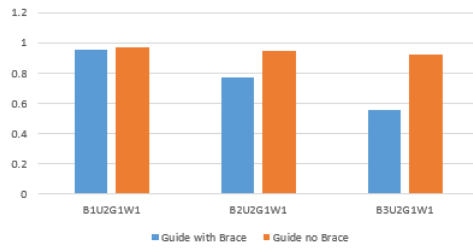


Figure D.18: CoR of the variation in bumper height of guide with brace vs. guide without brace

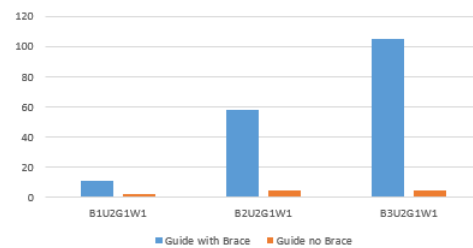


Figure D.19: Load of the variation in bumper height on guide with brace vs. guide without brace

### D.4.3. RESULTS CoR AND LOAD, VARIATION IN DEVIATION MODULE

The third case study was the displacement of the module. The displacement of the module increases the load and CoR linearly for both the guide with and without brace. The increase is stronger for the guide with brace. It is assumed this is due to the higher stiffness of the guide with brace versus the guide without brace.

Case study: Deviation	With Brace		No Brace	
	CoR	F (N)	CoR	F (N)
B1U1G1W1	0.97	8.47	0.99	1.50
B1U2G1W1	0.95	11.05	0.97	2.17
B1U3G1W1	0.92	14.79	0.95	2.77

Table D.3: Calculated load and CoR for the variations in deviation; 9.3, 12 and 15.5 cm for the guide with and without brace

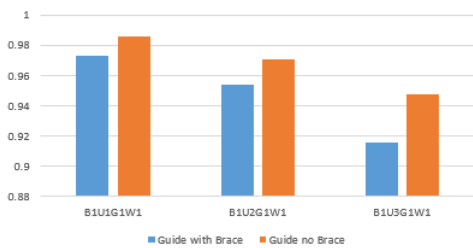


Figure D.20: CoR of the variation in deviation, guide with brace vs. guide without brace

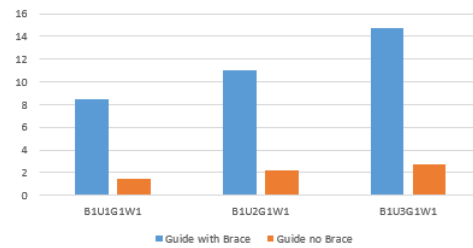


Figure D.21: Load of the variation in deviation on guide with brace vs. guide without brace

### D.4.4. RESULTS CoR AND LOAD, VARIATION IN ADDED WEIGHT AND CoG OF MODULE

The fourth case study is the added weight and change in CoG of the module.

Variation: Weight and CoG	With Brace		No Brace	
	CoR	F (N)	CoR	F (N)
B1U2G1W1	0.95	11.05	0.97	2.17
B1U2G1W2	0.93	15.20	0.97	1.97
B1U2G1W3	0.95	12.17	0.96	3.20
B1U2G1W4	0.96	14.07	0.98	1.85
B1U2G1W5	0.86	34.56	0.97	2.46
B1U2G1W6	0.81	47.27	0.94	4.79

Table D.4: Calculated load and CoR for the variations in added weight and its locations (variation of CoG of module)

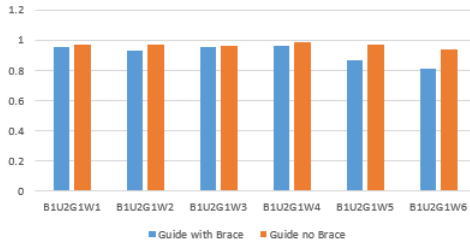


Figure D.22: CoR of the variation in added weight on the module on guide with brace vs. guide without brace

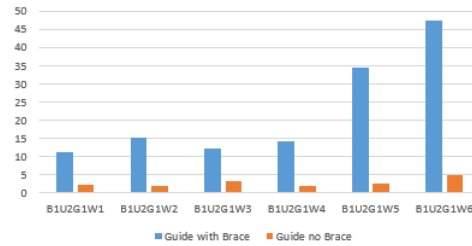


Figure D.23: Load of the variation in added weight on the module on guide with brace vs. guide without brace

#### D.4.5. RESULTS CoR AND LOAD, VARIATION IN ADDED MATERIAL ON THE GUIDES

The last variation is the added material to the guides. In the first case, tape was attached to the guides. The second case was a piece of pipe insulation that covered the guides. The strain measurements of the guide with brace with pipe insulation had stronger vibrations during the impact, which made it impossible to determine the duration of the impact and therefore, the CoR and the applied loads could not be calculated for this test case. At the guide without brace once can see that the CoR decreases and the loads increase. The decrease in CoR is an expected result due to damping material, but the increase in load is an unexpected result. The loads seemed to increase due to a longer duration of the impact with the use of damping materials; B1U2G1W1 has a duration of 0.1021 seconds, B1U2G1W1M1 a duration of 0.1024 and B1U2G1W1M2 a duration of 0.141 seconds. For the guide with brace the results are opposite to the results of the guide without brace; the CoR increases with the use of tape, and the load decreases. The duration of the impact for the first cases is a little longer than the duration of the impact in the second case (0.033 and 0.0319 seconds).

Variation: Material	With Brace		No Brace	
	CoR	F (N)	CoR	F (N)
B1U2G1W1	0.95	11.05	0.971	2.17
B1U2G1W1M1	0.98	3.58	0.967	2.38
B1U2G1W1M2	0.00	0.00	0.946	2.91

Table D.5: Calculated load and CoR for the variations in damping material; tape and pipe insulation for the guide with and without brace

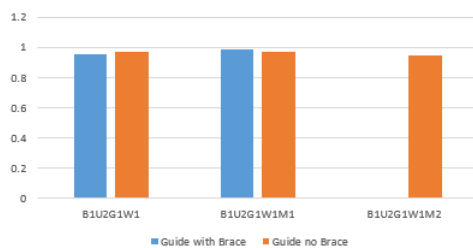


Figure D.24: CoR of the variation in adjusted material on guide with brace vs. guide without brace

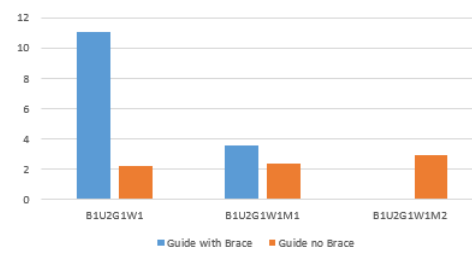


Figure D.25: Load of the variation in adjusted material on guide with brace vs. guide without brace

# BIBLIOGRAPHY

- [1] A.C.W.M. Klaver E.C. 1.Spijkers J.M.J., Vrouwenvelder. *Structural Dynamics; Part 1: Structural Vibrations. Lecture Notes CT 4140*. Structural Dynamics. Delft University of Technology, 2015.
- [2] Alessio. Impact loads during set-down on barges. *Impact loads*, 40:84–86, 2009.
- [3] N.P. Autar. Modeling impact in offshore guide and bumpers. *Impact loads*, 126:84–86, 2013.
- [4] C. Barclay. Design of guidance systems for lifting and placement. *Impact loads*, 66:1–66, 2017.
- [5] E. de Boer. Impact loads in offshore reel exchange. *Impact loads*, 173:104–106, 2012.
- [6] Wright C. Introduction to impact loading, 2012. URL <https://pdhonline.com/courses/s164/s164content.pdf>.
- [7] W. Goldsmith. *Impact: The Theory and Physical Behaviour of Colliding Solids Dover Publications*. 1960. ISBN ISBN 0-486-42004-3.
- [8] S. S Gómez. Identification of energy dissipation in structural joints by means of the energy flow analysis. *Journal of Vibration and Acoustics*, 8:1–8, 2018.
- [9] Y. Hurmuzlu. *An energy based coefficient of restitution for planar impacts of slender bars with massive external surfaces*. 1998.
- [10] P. J. Maas. Structural analysis of impact on guides & bumpers. *Impact loads*, pages 84–86, 2001.
- [11] IHS Markit. Ihs markit: 600 offshore projects slated for disposal over five years, 2016. URL <https://www.offshoreenergytoday.com/220801-2/>.
- [12] A. V. Metrikine. *Dynamics, Slender Structures and Introduction to Continuum mechanics; Module: Dynamics of Mechanical Systems and Slender Structures: Lecture Notes CT 4145*. Structural Dynamics. Delft University of Technology, 2015.
- [13] Offshore Energy Today. Ake breaks world record with arkutun dagi topside load out, 2014. URL <https://www.offshoreenergytoday.com/ake-breaks-world-record-with-arkutun-dagi-topside-load-out/>.